

**PHOTOACOUSTIC AND PHOTOTHERMAL
DEFLECTION STUDIES ON CERTAIN SELECTED
PHOTONIC MATERIALS**

NIBU A GEORGE

**THESIS SUBMITTED
IN PARTIAL FULFILMENT OF THE REQUIREMENTS
FOR THE DEGREE OF
DOCTOR OF PHILOSOPHY**

**INTERNATIONAL SCHOOL OF PHOTONICS
COCHIN UNIVERSITY OF SCIENCE AND TECHNOLOGY
COCHIN - 682022, INDIA**

MAY 2001

*"I have heard articulate speech produced by sunlight: I have heard a ray of the sun laugh and cough and sing! I have been able to hear a shadow, and I have even perceived by ear the passage of a cloud across the sun's disc...
...Can imagination picture what the future of this invention is to be..."*

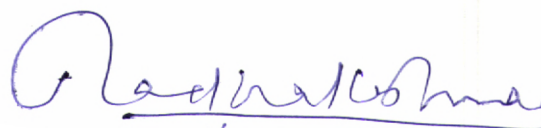
Alexander Graham Bell (1880)

Certificate

Certified that the research work presented in the thesis entitled "*Photoacoustic and photothermal deflection studies on certain selected photonic materials*" is based on the original work carried out by Mr. Nibu A George under my guidance in the International School of Photonics, Cochin University of Science and Technology. I also certify that no part of the thesis has been included in any other thesis submitted previously for the award of any degree.

Cochin-22

14 May, 2001



Prof. P Radhakrishnan

Dr. P. RADHAKRISHNAN,
PROFESSOR
INTERNATIONAL SCHOOL OF PHOTONICS
COCHIN UNIVERSITY OF
SCIENCE AND TECHNOLOGY
COCHIN - 682 022

Declaration

I hereby declare that the research work presented in the thesis entitled "*Photoacoustic and photothermal deflection studies on certain selected photonic materials*" is based on the original work carried out by me in the International School of Photonics, Cochin University of Science and Technology. I also declare that no part of the thesis has been included in any other thesis submitted previously for the award of any degree.

Cochin-22

14 May, 2001



Nibu A George

Contents

<i>Obligations</i>	i
<i>Preface</i>	iii
1. Introduction	1
1.1. Photo-induced processes.....	2
1.1.1. Detection methods.....	3
1.2. Photonic materials.....	8
<i>References</i>	10
2. Photoacoustics and photothermal deflection: General theoretical approach	12
2.1. Historical developments.....	13
2.2. Photoacoustic effect in condensed media.....	14
2.2.1. Rosencwaig-Gersho theory.....	14
2.2.2. Open photoacoustic cell configuration.....	19
2.3. Photothermal deflection: Mirage effect.....	21
<i>References</i>	26
3. Photoacoustic and photothermal deflection studies on III-V compounds	28
3.1. Introduction.....	29
3.2. Significance of thermal diffusivity.....	30
3.3. III-V compounds.....	31
3.4. Heat conduction in semiconductors.....	32
3.5. Photoacoustic investigation of heat diffusion in n-type InP.....	34
3.5.1. Theoretical outline.....	34
3.5.2. Experimental details.....	36
3.5.3. Design and fabrication of an open photoacoustic cell.....	37
3.5.4. InP sample.....	39
3.5.5. Results and discussion.....	39
3.6. Photothermal deflection studies on GaAs multilayers.....	43
3.6.1. Theoretical outline.....	43
3.6.2. Photothermal deflection set-up.....	45
3.6.3. GaAs thin film sample specifications.....	48
3.6.4. Results and discussion.....	49

3.7. Conclusions.....	61
<i>References</i>	62
4. Photoacoustic evaluation of thermal effusivity of transparent liquids and liquid crystals.....	67
4.1. An introduction to liquid crystal phases.....	68
4.1.1. Liquid crystalline phases.....	69
4.1.2. Liquid crystalline polymers.....	71
4.1.3. Liquid crystal mixtures.....	72
4.1.4. Induced alignment in liquid crystals.....	73
4.2. Thermal effusivity.....	73
4.3. Theoretical outline.....	74
4.4. Experimental details.....	75
4.4.1. Design and fabrication of an open photoacoustic cell.....	76
4.4.2. Experimental procedure.....	78
4.5. Results and discussion.....	79
4.5.1. Thermal effusivity of water and glycerol.....	79
4.5.2. Thermal effusivity of liquid crystalline polymers.....	82
4.5.3. Thermal effusivity of 7OCB and 8OCB.....	85
4.5.4. Thermal effusivity of nematic liquid crystal mixtures.....	90
4.6. Conclusions.....	92
<i>References</i>	94
5. Photoacoustic analysis of phase transitions in liquid crystals.....	97
5.1. Phase transitions.....	98
5.1.1. Phase transitions in liquid crystals.....	98
5.2. Experimental details.....	100
5.3. Results and discussion.....	102
5.3.1. Phase transitions in 7OCB and 8OCB.....	102
5.3.2. Phase transitions in nematic liquid crystal mixtures.....	105
5.3.3. Analysis of the PA signal profile using R-G theory.....	109
5.4. Conclusions.....	113
<i>References</i>	114
6. Photoacoustic investigations on photostability of Rhodamine 6G doped PMMA.....	117
6.1. Importance of dye doped polymers.....	118
6.2. Methods to measure dye photodegradation.....	120

6.2.1. Optical methods.....	121
6.2.2. Photothermal methods.....	122
6.3. Experimental details.....	123
6.3.1. Preparation of rhodamine 6G doped PMMA samples.....	123
6.3.2. Recording of photoacoustic spectra.....	124
6.3.3. Experimental setup used to study the dye photodegradation.....	126
6.4. Results and discussion.....	127
6.5. Conclusions.....	134
<i>References</i>	136
7. Summary and conclusions	139

Obligations

In fact, the contents of this thesis are not mere results of my few years research in ISP, rather it is the essence of knowledge I gradually acquired during my entire academic career. In this proud moment, it is my great pleasure to say that the basic, but the greatest lessons that I have ever learned is from my parents. Since then, thousands of people, including my teachers, colleagues, friends and even strangers have directly or indirectly influenced me in achieving this goal and I thankfully remember each of them in this occasion.

Prof. P.Radhakrishnan, my Ph.D. supervisor and guide, has took lot of efforts in shaping my research work and in framing the thesis. Apart from the academic guidance, his constant encouragement and strictness have helped me a lot in completing my research within a reasonable time-period. I greatly owe him for all his contributions in arriving at this thesis.

The intellectual discussions I had with Prof. C.P.G.Vallabhan have been an asset to my knowledge. The influence of his criticism in developing my career and personality, both in academic point of view and in personal regard, is so strong that I will never forget him.

Right from the beginning, Prof. V.P.N.Nampoori and Prof. V.M.Nandakumaran have always been there with a pleasant smile and moral support, especially during my tough days of research. It is my happiness to extend hearty thanks to them for all their suggestions and help. Though my experience with Prof. R.Pratap is very short, his enthusiasm and smartness even at this age has always been an inspiration to me.

Prof. A.K.George provided me a variety of liquid crystal samples, for which I am extremely thankful to him. I also extend my sincere thanks to Prof. Wolter and Dr. Haverkort for providing me the semiconductor samples.

During my initial stage of research, my senior colleagues Harilal, Bindhu, Riju, Ajith, Santhosh, Jayan and Lynta helped me a lot in driving my research in the right direction. I am sure that they will be happy to hear that I have reached the destination safely and successfully.

Despite the tight time schedule during her ultra-short visits to ISP, my colleague, Bindu.V spent most of her time to quarrel with me, which made my boring lab-life an active one. This young mother has always been a good friend to me.

It is my pleasure to mention here the name of Aneesh, who has been my colleague and good friend for long time. Jyothi and Saritha have also spent some ever-memorable and joyful moments with me. I am extremely thankful to Thomas and Jyotsna for spending some of their precious time with me. I will never forget the happy and wonderful moments they shared with me. Also, they are my major source of academic discussions.

I will never forget my experiences with my colleagues Pravitha and Indic. I am also thankful to my colleagues Prasanth and Sajan. I am fortuitous enough to work with veteran colleagues, Achamma teacher and Suresh sir, and they are always good to me. Though it is very hard to remember all those jokes and comments made by Jibu, my colleague and friend, I will always remember him for making my leisure so joyful.

During the course of my research, I have been able to interact with various batches of M.Tech. students of ISP. I would like to thank each of them for their cooperation and help. Also, I would like to thank all my friends in various departments of CUSAT for their help and cooperation and for extending a warm friendship to me.

I extend my sincere thanks to the non-teaching staff of ISP for their timely help and assistance. The technical staff of USIC have helped me a lot in bringing my ideas into practical shape. The library staff of physics department have also helped me at various instants. Financial assistance provided by CUSAT is gratefully acknowledged.

It will not be appropriate if I have forgotten those who raised challenging barriers in front of me, which really energized me to conquer more and more heights.

Finally, I would like to thank all those who added flavours to my campus life in CUSAT.

Superior to all, there is a power who controls all of us, without whose blessings and kindness we cannot achieve anything in this world.

Nibu A George

Preface

The emergence of lasers in the early sixties has not only revolutionized the field of optics and communication but also paved new ways in the field of material characterization. Material studies using photothermal techniques possess certain unique characteristics and advantages over conventional methods. The most important aspect of photothermal techniques is their ability to perform noncontact and nondestructive measurement. Photoacoustics, photothermal deflection, thermal lens, photothermal radiometry and photopyroelectric methods are some of the commonly used and powerful techniques for the thermal and optical characterization of materials using lasers.

In this thesis the applications of photoacoustic and photothermal deflection techniques for the thermal and optical characterization of different photonic materials, namely, semiconductors, liquid crystals and dye-doped polymers are discussed.

In **Chapter 1** a general overview of the various photothermal based material characterization techniques is given. Special emphasis is given to photoacoustic (PA) and photothermal deflection (PTD) techniques as these two methods are used for the studies that are included in this thesis. The PA effect is basically the conversion of optical energy into acoustical perturbation when a modulated light beam interacts with a sample kept in an air-tight cavity. A part or most of the energy absorbed will be liberated in the form of heat and the flow of heat from the sample to the coupling fluid is responsible for the acoustic pulse generation. The quantity of heat liberated and the time taken to produce the acoustic perturbation depend on the optical and thermal properties of the sample under investigation. Hence, a variety of optical and thermal parameters of materials can be studied using this nondestructive testing method.

In PTD, instead of keeping the sample in an airtight cell, it will be kept in a fluid which produces a change of index of refraction with temperature. The energy liberated as a result of the absorption of light produces a refractive index gradient in the fluid close to the sample surface. Another laser beam (probe beam) passing through this gradient will get deflected and the strength of the deflection and its phase are functions of thermal and optical properties of the specimen. An easily measurable thermal parameter using this technique is the thermal diffusivity. It is defined as the ratio of the thermal conductivity to the product of specific heat capacity and density of the sample. The thermal diffusivity is a very important thermal parameter, which essentially measures the amount of heat diffused through the material in unit time.

The use of lasers in modern communication technology and in many other similar fields necessitates the development of new materials for different kinds of applications. Materials that find some kind of application in this field are generally classified as photonic materials. This family of materials consists of a large variety, ranging from polymers, glasses, liquid crystals, ceramics, semiconductors to photonic band gap materials. In order to use these materials effectively in any application, a thorough knowledge of their optical and thermal properties is necessary. Lasers themselves can do this job in a perfect nondestructive manner and the laser based material characterization has already been established as a potential tool in this area.

Chapter 2 discusses the different theoretical models that are used for the studies described in the following sections. In 1976, Rosencwaig and Gersho formulated the basic theoretical model for the photoacoustic effect. Their theoretical analysis is essentially a one-dimensional heat flow model, by treating the sample as a distributed heat source. In subsequent years, several modifications and extensions to this theory are suggested by a number of researchers. Among these, the one suggested by McDonald and Wetsel, considering thermo-elastic bending of the sample, has great significance in many of the experimental conditions. However, all such modifications are valid only in certain specific cases and these refinements have not changed the basic results of R-G theory in most of the experimental situations.

One major renaissance in the field of PA technique is the emergence of open photoacoustic cell (OPC) configuration. Thermal and optical characterization of materials in solid or liquid states have become more simple, accurate and sensitive in OPC configuration. Both front surface and rear surface illuminations of the sample are possible in this approach. If the sample is in solid form, it can be directly mounted on the OPC and from the signal amplitude or phase dependence on the modulation frequency of the excitation beam, one can easily evaluate the thermal parameters such as the thermal diffusivity of the sample. In contrast, when the sample is a non-absorbing liquid, the sample can be used as a backing material to another thermally thin and absorbing solid sample whose thermal parameters are known.

Even though the concept of light beam deflection by thermally induced changes in the index of refraction of a medium has been known for a long time, only in 1979 Boccara *et.al* demonstrated the use of photothermal beam deflection method in material characterization. However, the initial attempts made by many people to give a quantitative explanation to this effect by making use of the one-dimensional heat flow model formulated by Rosencwaig and Gersho failed in many experimental conditions, especially when the pump-beam is focused to small spot size. In such situations, a three-dimensional heat flow model is required to give a satisfactory explanation. Details of the three-dimensional model are included in this chapter.

Chapter 3 deals with the photoacoustic and photothermal deflection studies on certain III-V compounds. An open photoacoustic cell configuration is used to evaluate the thermal diffusivity of the compound semiconductor InP. For this purpose an open photoacoustic cell is designed and fabricated and the details of the cell is also discussed in this chapter.

Photothermal beam deflection studies on n-type and p-type GaAs multilayers grown on semi-insulating GaAs substrates are also included in this chapter. An argon ion laser is used to heat up the sample and the refractive index gradient generated in the coupling fluid, close to the sample surface, is detected using a low power He-Ne laser. The thermal diffusivity of thin films as well as substrate of each sample is evaluated independently.

In **Chapter 4** the thermal effusivity values in different phases of liquid crystalline polymers, cyano-biphenyl liquid crystals and nematic liquid crystal mixtures, measured using an open photoacoustic cell configuration, are discussed. The thermal effusivity is defined as the square root of the product of the thermal conductivity, specific heat capacity and density. It is actually a measure of sample's thermal impedance or in other words it is the sample's ability to exchange heat with the ambient. The effects of molecular structure, orientation etc on the thermal effusivity values of these materials are also discussed.

In **Chapter 5** the phase transition studies performed in a variety of liquid crystals are discussed. The liquid crystals studied include the cyano-biphenyl liquid crystals such as 7OCB and 8OCB, and commercially available nematic liquid crystal mixtures. For this purpose the PA signal amplitude is recorded as a function of temperature. The effect of bulk light scattering on the photoacoustic signal strength and the difference in the signal amplitude profile during first order and second order phase transitions are some of the interesting results that are discussed in this chapter. The specific heat capacity profile during transitions between different phases of all these materials are derived from the photoacoustic signal amplitude data and the various aspects of the signal profile are also discussed.

Chapter 6 describes the use of laser induced photoacoustic technique in the study of photobleaching of Rhodamine 6G doped polymethyl methacrylate. The fact that the photoacoustic signal is directly proportional to the absorbed amount of energy is made use of in this investigation. Dye-doped polymer samples are prepared at various dye concentrations for the photostability measurements. The role of laser power, concentration of the dye, modulation frequency and wavelength of the laser beam on the dye photodecomposition rate are presented in this chapter.

Finally, the thesis is concluded with an overall assessment of the work and a general conclusion.

Paper published in International Journals:

1. Open-cell photoacoustic investigation of the thermal effusivity of liquid crystals,
Nibu A George, C P G Vallabhan, V P N Nampoore, A K George and P Radhakrishnan,
Optical Engineering (In press).
2. Photoacoustic evaluation of the thermal effusivity in the isotropic phase of certain comb-shaped polymers,
Nibu A George, C P G Vallabhan, V P N Nampoore, A K George and P Radhakrishnan,
J. Physics: Condensed Matter, 13 (2001) 365-371
3. Use of photoacoustic effect for the detection of phase transitions in liquid crystal mixtures,
Nibu A George, C P G Vallabhan, V P N Nampoore, A K George and P Radhakrishnan,
J. Physics D: Applied Physics, 33 (2000) 3228-3232
4. Photoacoustic investigation of the effect of excess lead oxide on thermal diffusivity of PLZT ceramic,
N A George, T Paul, P Radhakrishnan, V P N Nampoore, C P G Vallabhan and M T Sebastian,
J. Materials Science Letters, 19 (2000) 499-501
5. Photoacoustic study on photobleaching of Rhodamine 6G doped in poly methyl methacrylate,
Nibu A George, B Aneeshkumar, P Radhakrishnan and C P G Vallabhan,
J. Physics D: Applied Physics, 32 (1999) 1745-1749
6. Physical and optical properties of phthalocyanine doped inorganic glasses,
G A Kumar, J Thomas, **N A George**, N V Unnikrishnan, P Radhakrishnan, V P N Nampoore and C P G Vallabhan,
J. Materials Science, 35(10) 2539 (2000).
7. Optical absorption studies of free (H₂Pc) and rare earth (RePc) phthalocyanine doped borate glasses,
G A Kumar, J Thomas, **N A George**, B A Kumar, P Radhakrishnan, V P N Nampoore, C P G Vallabhan and N V Unnikrishnan,
Physics and Chemistry of Glasses, 41(2) 89 (2000).
8. Spectral studies of naphthalocyanine (Nc) and rare earth phthalocyanine (RePc) molecules in an inorganic glassy borate matrix,
G A Kumar, J Thomas, **N A George**, V P N Nampoore, P Radhakrishnan, C P G Vallabhan and N V Unnikrishnan,
Physics and Chemistry of Glasses, 41(4) 199 (2000).

Papers communicated/ to be communicated to Journals:

9. Photoacoustic evaluation of the thermal effusivity of the liquid crystals 7OCB and 8OCB,
Nibu A George, C P G Vallabhan, V P N Nampoore, A K George and P Radhakrishnan,
Applied Physics B: Lasers and Optics, (Communicated)
10. Photoacoustic study of phase transitions in liquid crystals 7OCB and 8OCB,
Nibu A George, V P N Nampoore, C P G Vallabhan, A K George and P Radhakrishnan,
J. Physics: Condensed Matter, (Communicated)
11. Photoacoustic studies on n-type Indium Phosphide,
Nibu A George, C P G Vallabhan, V P N Nampoore and P Radhakrishnan
Optical Engineering, (Communicated)
12. Photothermal deflection studies on GaAs multilayers,
Nibu A George, C P G Vallabhan, V P N Nampoore and P Radhakrishnan
Applied Physics B: Lasers and Optics, (to be communicated)
13. Studies on fluorescence efficiency and photodegradation of Rhodamine 6G doped PMMA
using thermal lens technique,
Achamma Kurian, **Nibu A George**, Binoy Paul, V P N Nampoore and C P G Vallabhan,
J. Photochemistry and Photobiology, (Communicated the Revised Version)

Papers presented in Conferences/ Symposia:

14. Photoacoustic study on photobleaching of Rhodamine 6G doped in poly methyl
methacrylate,
Nibu A George, B Aneeshkumar, P Radhakrishnan and C P G Vallabhan,
International Conference on Optics and Optoelectronics, (IRDE, Dehradun, India),
Dec 9-12, 1998
15. Investigations on the photobleaching of Rhodamine 6G doped in poly methyl methacrylate
using photoacoustic technique,
Nibu A George, B Aneeshkumar, P Radhakrishnan and C P G Vallabhan,
National Laser Symposium, (IIT Kanpur, India), Dec 14-16, 1998
16. Photoacoustic study of phase transitions in liquid crystals,
Nibu A George, A K George, V P N Nampoore, P Radhakrishnan and C P G Vallabhan,
National Seminar on High Power Lasers, (CUSAT, Cochin, India), Feb 26-27, 1999

17. Photoacoustic monitoring of nematic to isotropic transition in the liquid crystal BL001,
Nibu A George, A K George, V P N Nampoore, P Radhakrishnan and C P G Vallabhan,
International Conference on Laser Devices and Materials, (Defense Science Centre, New Delhi, India), Dec 8-10, 1999
18. Photoacoustic evaluation of the thermal effusivity of the liquid crystals 7OCB and 8OCB,
Nibu A George, A K George, V P N Nampoore, C P G Vallabhan and P Radhakrishnan,
National Laser Symposium (Defense Science Centre, New Delhi) Dec 13-15, 2000
19. Use of photoacoustic effect for the detection of phase transitions in polymer dispersed liquid crystal mixtures,
Nibu A George, C P G Vallabhan, A K George, V P N Nampoore and P Radhakrishnan,
National Laser Symposium (Defense Science Centre, New Delhi) Dec 13-15, 2000
20. Photoacoustic evaluation of thermal diffusivity of Indium Phosphide,
Nibu A George, C P G Vallabhan V P N Nampoore and P Radhakrishnan,
National Conference on Materials Science (M.G University, Kottayam) Mar. 23-24, 2001

Chapter 1

Introduction

The present chapter gives a general introduction to the subject matter contained in this thesis. It includes a short description of the photo-induced changes that occur during photon-matter interaction, with special emphasis to the nonradiative processes taking place in condensed matter and the associated detection schemes. The chapter concludes with pointing out the significance of the materials that are selected for the present investigations. The role of photothermal methods in the investigations of photonic materials is also addressed.

1.1. Photo-induced processes

The absorption of photons by atoms or molecules will result in a series of processes or effects in a material [1-6]. The excited level may lose its energy by radiative processes, such as spontaneous or stimulated emission, and by nonradiative processes which mainly results in heat generation. If the photon energy is high enough, direct photochemical changes such as photo-decomposition, photo-ionisation etc. of the excited molecule may take place. Destructive changes such as vapourisation of the material and plasma generation may take place as a result of photon-matter interaction at very high power densities of the incident light. Chemical changes may be either reversible or irreversible. However, in the following sections only the nondestructive changes that occur in condensed matter, subsequent to the photon absorption, will be discussed.

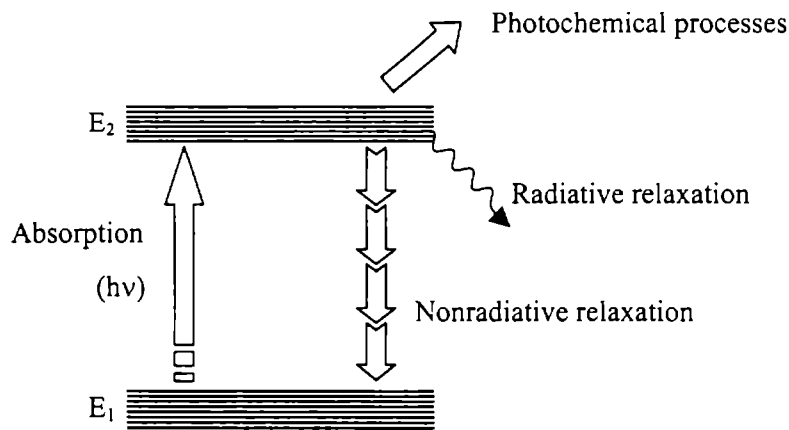


Figure 1: A schematic representation of various photo-induced processes in condensed matter.

Figure 1 shows the main channels of photoinduced changes that occur in a sample. Here E_1 and E_2 represent the energies of the lower and upper levels and $h\nu = E_2 - E_1$ is the energy of the absorbed photon. The absorbed power in the sample I_{abs} is determined in accordance with

$$I_{abs} = I[1 - \exp(-\alpha L)] \cong \alpha IL \quad (1)$$

with $\alpha L \ll 1$. Here, I and L are the incident light intensity and the sample length, respectively and α is the absorption coefficient.

Now, the absorbed energy will be liberated through radiative, nonradiative or chemical processes and each of these processes has specific quantum yield [2, 7,8]. If n_r , n_{nr} and n_{pc}

are the quantum yields of radiative, nonradiative and photochemical processes respectively, the total quantum yield of all the channels of de-excitation is given by

$$n_r + n_{nr} + n_{pc} = 1 \quad (2)$$

Accordingly, the intensity I_{abs} of the laser radiation absorbed will be distributed over all these channels,

$$I_{abs} = I_r + I_{nr} + I_{pc} \quad (3)$$

where $I_r = n_r I_{abs}$, $I_{nr} = n_{nr} I_{abs}$ and $I_{pc} = n_{pc} I_{abs}$ are the amount of energy liberated through the radiative, nonradiative and photochemical processes, respectively.

Measurement of the energy absorbed or that released through any of these relaxation channels facilitates the study of various properties and parameters of the sample.

1.1.1. Detection methods

Spectroscopy is the measurement and interpretation of electromagnetic radiation absorbed or emitted when the molecules, or atoms, or ions, of a sample move from one allowed energy state to another. In its broad sense, laser based spectroscopic techniques can be divided into three classes, (1) absorption method (2) radiative emission or photoluminescence measurements and (3) nonradiative emission or opto-calorimetric measurements. These methods can be employed independently or simultaneously, depending on the experimental set-up. It should be noted that each of these methods can be used only for some specific studies and for a complete characterization of the sample different approaches have to be employed.

The absorption method is the basic and the simplest approach and by using this technique information regarding the optical properties and composition of the sample can be obtained by varying different parameters such as the intensity, wavelength, polarization etc. of the light beam that passes through or gets reflected from the sample [8-11]. However, a variety of external parameters such as sample's surface quality, influence of stray light and many other problems related to the source, detector etc. have a pronounced effect on the accuracy of the conventional absorption measurements. The situation will be much more worse in the case of solids, powders etc, especially if the sample is highly scattering or reflecting. In such situations emission measurements (radiative/nonradiative) are more appropriate and will give more information regarding the sample.

Photoluminescence is a general term which includes both fluorescence and phosphorescence. Since the decay time of fluorescence is of the same order of magnitude as the lifetime of an excited state, its study can shed light into various complex and ultra-fast processes

taking place as a result of the light absorption in the sample [12-15]. Phosphorescence lifetime usually falls in the millisecond to several seconds range or even longer. Fluorescence is the most commonly employed method for the spectral studies of laser materials including organic dyes, crystals etc., semiconductors and many other similar materials. This method is applicable in the UV, visible and near IR spectral regions and the sensitivity of the fluorescence method is extremely high. But the basic requirement for employing this approach is that at least a part of the excitation energy should be liberated through the radiative channel, which is not always possible. Both absorption and luminescence techniques can be used for the optical characterization and for the structural studies, but they fail to give any information regarding many other significant characteristics such as the thermal properties of the sample.

The nonradiative relaxation of photoexcited states usually result in heating of the sample. Any kind of sample which absorbs energy will liberate at least a part of the excitation energy in this way and hence the methods to measure this nonradiative part is applicable for almost all types of samples. The liberated heat energy not only carries the information regarding the absorbed energy but also it contains details regarding the thermal properties of the sample. A group of such spectroscopic methods based on the measurement of photo-induced heating of the sample are called the *photothermal methods* [1,3-7,16-26]. Hence we can say that the basis of photothermal spectroscopy is the photo-induced changes in the thermal state of a sample.

The thermalisation of a sample or the medium as result of nonradiative relaxation not only results in a change in temperature of the sample but also it brings about changes in many other parameters such as density, pressure, refractive index etc. Hence, there exist a number of photothermal techniques depending on the mode of detection. Only the light energy absorbed contributes to the energy liberated in the form of heat. Scattered or reflected light will not contribute to the photothermal signals. Consequently, photothermal spectroscopy more accurately measures optical absorption in highly scattering solutions, in solids and at interfaces.

Various processes involved in photothermal spectroscopy are schematically shown in figure 2. Direct consequence of the nonradiative relaxation is a change in temperature of the sample or the coupling fluid which is in contact with the sample. This temperature change results in a change in the density of the sample or the coupling fluid. If the temperature change occurs in a faster time scale than the time required for the fluid to expand, then the rapid temperature change will result in a pressure change in the sample. The density change is primarily responsible for the refractive index change of the medium which can be probed by a variety of methods. Common detection techniques used in photothermal spectroscopy are listed in table I.

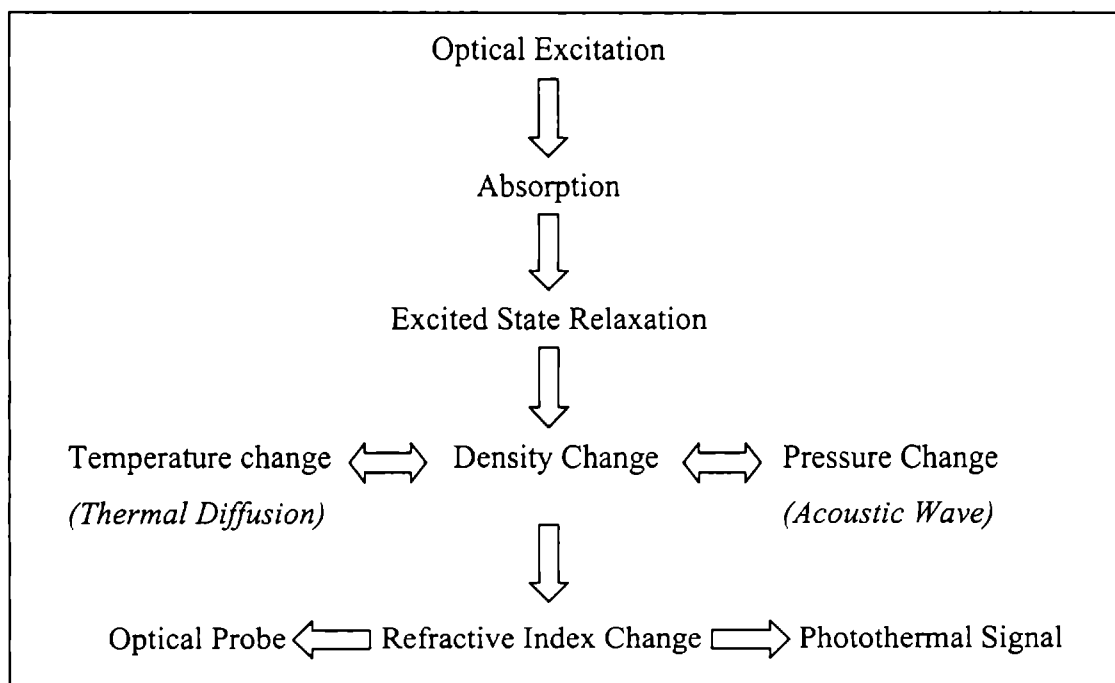


Figure 2: Basic processes responsible for the photothermal signal generation.

Table I: Common detection techniques used in photothermal spectroscopy.

Thermodynamic Parameter	Measured Property	Detection Technique
Temperature	Temperature	Calorimetry
	Infrared Emission	Photothermal Radiometry
Pressure	Acoustic Wave	Photoacoustic Spectroscopy
Density	Refractive Index	Photothermal Lens Photothermal Interferometry Photothermal Deflection Photothermal Refraction Photothermal Diffraction
	Surface Deformation	Surface Deflection

From the above table it is clear that there exists a variety of methods to monitor the thermal state of a sample. Direct calorimetric or thermometric methods use temperature transducers to measure the temperature change in the sample. For this purpose, thermocouples, thermistors, or pyroelectric devices can be used. Temperature changes can also be indirectly measured from the infrared emission since the infrared emission is directly related to the sample temperature. Although not very sensitive, photothermal radiometry has great potential in nondestructive analysis and testing of materials. Infrared cameras can be used for the thermal imaging of large samples.

Pressure transducers such as microphone, piezoelectric crystals etc. are commonly used to monitor the pressure waves associated with rapid sample heating. The branch of photothermal spectroscopy based on the pressure wave measurement is known as the optoacoustic or photoacoustic technique. More details regarding the photoacoustic technique are given in *chapter 2*.

Finally, there is another group of photothermal techniques based on the temperature dependent refractive index change and associated detection schemes (figure 3). The major difference between these group of methods and those previously explained is that in addition to the pump laser to produce photothermal effect, usually a probe laser is also used to monitor the refractive index changes. The probe-beam can be either passed through the sample under investigation or through a coupling fluid which is in contact with the sample. Though there are several methods to detect the temperature dependent refractive index change, all these methods rely on a few basic principles of light propagation, namely, optical path-length change, diffraction and refraction.

Photothermal interferometry directly measures the refractive index change by making use of the associated optical path-length change. In this experimental configuration, usually both pump and probe passes through the sample and the sample should be optically transparent at the probe-beam wavelength. Thermal lens technique is based on the probe-beam focusing or defocusing resulting from a spatially varying refractive index generated within the sample. Here also, the sample should be optically transparent at the probe beam wavelength. This method is usually employed in the study of liquid samples. Photothermal deflection essentially measures the refractive index gradient generated in a coupling fluid within which the solid sample is immersed. Spatial gradient in refractive index results in a change in the propagation direction of the probe-beam. Details of this technique are given in *chapter 2*. Photothermal refraction is essentially a combined effect of deflection and lensing.

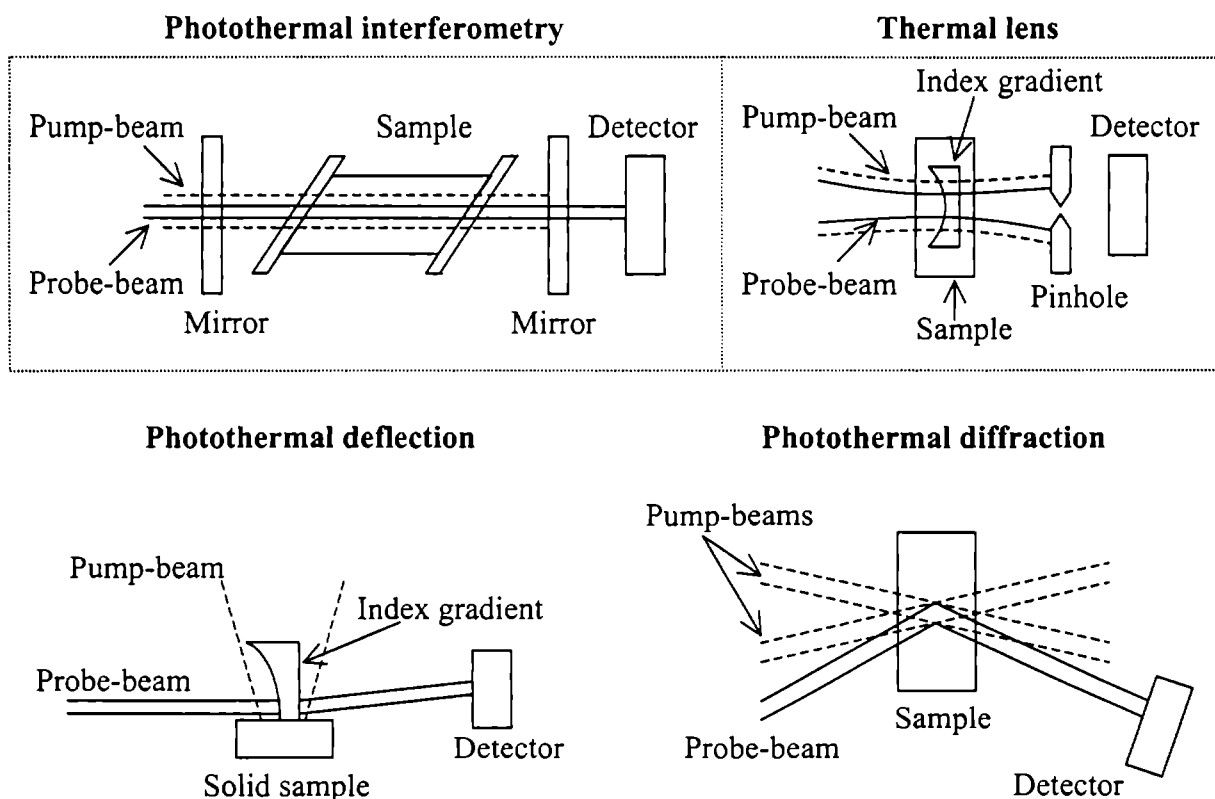


Figure 3: Different photothermal techniques based on the measurement of refractive index change.

In the case of solid samples, localized heating may result in the thermal expansion of the irradiation site, which in turn introduces a deformation to the sample surface. The amount of surface deformation is determined by the thermal properties of the sample. In photothermal surface deflection technique, a probe-beam is allowed to incident at an angle to the sample surface. Any deformation introduced to the sample surface will result in a change in the reflected beam position at the detector. However, this type of measurement is possible only with solid samples which possess a good surface quality. Photothermal diffraction technique is based on the probe-beam diffraction due to a periodic index of refraction (grating) generated when two pump-beams cross each other inside or at the surface of a sample. The grating will diffract light at an angle according to Bragg's law. This method is widely used for studies in the ultra-short time scales.

Two types of pumping mechanisms can be used for the excitation of the sample. They are the pulsed laser excitation and modulated continuous-wave (cw) laser excitation. Pulsed excitation produces transient signals of large amplitude immediately after the excitation and it decays as the sample approaches thermal equilibrium through heat diffusion. Usually the transient signals last for few microseconds in gas phase and several milliseconds in condensed

matter. By performing the transient waveform analysis, one can obtain a variety of sample properties. Now, if the excitation is carried out using a periodically modulated cw laser then the signal will also be periodic, the magnitude and phase of which are functions of modulation frequency. The frequency dependent phase-shift information is essentially equivalent to that contained in the time-dependent signal transients obtained from pulsed excitation.

Photothermal effect based techniques have a lot of applications in material and chemical analysis. Its applications in biological and medical fields are clearly established [3-7, 16-26]. The important aspect of photothermal spectroscopy which makes it a unique approach in various applications is its flexibility to perform in different experimental configurations. On the other hand conventional optical absorption spectroscopy and luminescence studies require some specific experimental configurations and basic requirements, which limits, to some extent, their widespread use in material studies.

1.2. Photonic materials

Photonics can be defined as the science and technology of the generation, manipulation, transport, detection, and use of light and other forms of radiant energy whose quantum unit is the photon. Vast range of devices are coming under this definition, including light sources such as lamps and lasers, devices such as polarisers, amplifiers, electro-optic devices, which modify the nature of light, light detectors etc. Over and above this, there exists a very fundamental and most important section in photonics technology, which is the *materials science*. Nowadays, photonics finds applications in a variety of fields including communication, sensing, display, imaging, medical, defence and industrial applications. But, for the effective use of this modern technology in any of these potential applications, suitable materials are necessary from the generation to manipulation, detection and display of light. For example, semiconductors will do the job of both generation and detection of light and organic materials such as dyes in the liquid or solid forms are suitable as sources of light. Liquid crystals are the most suitable materials in the display technology, in addition to their use in optical computing and data storage. In addition to the above listed materials, there are hundreds of different types of materials which find some kind of application in the photonic technology. All those materials which are directly related to the photonic technology are generally termed as photonic materials, analogues to the electronic materials in electronics.

Being the technology of generation and harnessing of light, the immense market potential of photonics has attracted the attention of industries. Consequently, a variety of new

photonic materials suitable for different applications have been developed by them. But, mere development of a new material with some specific features will not be sufficient for its effective use in any of the applications. Rather, a complete characterisation of materials is necessary for a comparative study of different materials to identify the most appropriate one. Photonic materials, being directly related to the generation or detection of photons, optical techniques are the most suitable for their characterisation. But, we have seen in the previous section that simple absorption studies and luminescence studies have some kind of limitations in many situations. However, photothermal methods, which is essentially an optical method, can be employed for any sample since at least a part of the excitation energy will be liberated through nonradiative channels. Moreover, among the different photothermal configurations, appropriate method can be chosen depending on the specifications and properties of the sample.

References

1. Kliger.D.S (Edit.), *Ultrasensitive laser spectroscopy*, (Academic Press, New York) 1983.
2. Mukherjee.K.K.R, *Fundamentals of photochemistry*, (New Age International Publishers, New Delhi) 1978.
3. Winefordner.J.D (Edit.), *Chemical analysis: A series of monographs on analytical chemistry and its applications*, (John Wiley & Sons, Inc.) 1996.
4. Hieftje.G.M, Travis.J.C and Lytle.F.E (Eds.), *Lasers in chemical analysis*, (Humana: Clifton, New Jersey) 1981.
5. Bindhu.C.V, *Studies on laser induced photothermal phenomena in selected organic compounds and fullerenes*, (Ph.D. thesis, Cochin University of Science and Technology) 1998.
6. Kumar.A.V.R, *Applications of laser induced photoacoustic effect for the study of gases and solids*, (Ph.D. thesis, Cochin University of Science and Technology) 1992.
7. Zharov.V.P and Letokhov, *Laser optoacoustic spectroscopy*, (Springer-Verlag, Berlin) 1986.
8. Bauman.R.P, *Absorption spectroscopy*, (John Wiley & Sons, New York) 1962.
9. Olsen.E.D, *Modern optical methods of analysis*, (McGraw Hills, New York) 1975.
10. Jaffe.H.H and Orchin.M, *Theory and applications of ultraviolet spectroscopy*, (John Wiley & Sons, New York) 1962.
11. West.W (Edit.), *Chemical applications of spectroscopy*, Vol. IX, Part I (John Wiley & Sons, New York) 1968.
12. Guilbault.G.G, *Practical fluorescence: theory, methods and technique*, (Marcel Dekker, New York) 1973.
13. Hercules.D.M, *Anal.Chem.* 38, 29A (1966).
14. Wehry.E.L, *Modern fluorescence spectroscopy*, Vols. I-II (Plenum, New York) 1976.
15. Winefordner.J.D, Schulman.S.G and O'Haver.T.C, *Luminescence spectrometry in analytical chemistry*, (Wiley Interscience, New York) 1972.
16. Hess.P (Edit.), *Photoacoustic, photothermal and photochemical processes in Gases*, (Springer-Verlag, Berlin) 1989.
17. Hess.P and Pelzl.J (Eds.), *Photoacoustic and photothermal phenomena*, (Springer-Verlag, Berlin) 1988.
18. Luscher.E, Korpiun.P, Coufal.H and Tilgner.R, *Photoacoustic effect: principles and applications*, (Friedr.Vieweg & Sohn, Braunschweig) 1984.

19. Rosencwaig.A, *Photoacoustics and photoacoustic spectroscopy*, (John Wiley & Sons, New York) 1980.
20. Sell.J.A, *Photothermal investigations of solids and fluids*, (Academic Press, Boston) 1989.
21. Hess.P (Edit.) *Photoacoustic and photothermal processes at surfaces and thin films*, (Springer-Verlag, Berlin) 1989.
22. Mandelis.A (Edit.) *Photoacoustic and thermal wave phenomena in semiconductors*, (North Holland, New York) 1987.
23. Pao.Y-H (Edit.), *Optoacoustic spectroscopy and detection*, (Academic press, New York) 1977.
24. D. Bicanic (Edit.), *Proceedings of seventh international topical meeting on photoacoustic and photothermal phenomena*, 1991.
25. Badoz.J and Fournier.D (Eds.)*Photoacoustic and photothermal spectroscopy, J.de Phys., Colloque C6* (Les Editions de Physique, Les Ulis) 1983.
26. Eichler.H.J, Ghnter.P, and Pohl.D.W, *Laser-induced dynamic gratings*, (Springer-Verlag, New York) 1986.

Chapter 2

Photoacoustics and photothermal deflection: General theoretical approach

Photothermal methods are well developed from the experimental point of view and the theoretical foundations on which they rely are also substantially strong. Since the formulation of one-dimensional heat flow model by Rosencwaig and Gersho to explain the photoacoustic signal generation, a number of modifications and extended models have been reported in the literature. In the present chapter a brief discussion regarding the Rosencwaig-Gersho model and its extension to open photoacoustic cell configuration are presented. The three-dimensional heat flow model used to describe the photothermal deflection signal generation is also included in this chapter.

2.1. Historical developments

Among the different photothermal methods, the photoacoustic effect is credited with the first observed photothermal phenomena noticed in 1880 during Alexander Graham Bell's voyage for new inventions [1,2]. Though Bell has prophesied the scope of his novel observation, after the initial flurry of interest generated by his original work, experimentation with the photoacoustic effect is almost in a dormant state. After the advent of microphones, Viengerov is able to observe this effect in gaseous sample [3]. Still the growth of this new branch of spectroscopy is in a hopeless state due to many of the experimental limitations. The emergence of lasers in early sixties paved a new way in the photoacoustic spectroscopy of gaseous samples. But the applications of this technique have been efficiently extended to liquids and solids only after the successful formulation of a general theoretical model by Rosencwaig and Gersho in mid-seventies [4]. Subsequent developments in the theoretical aspects of photothermal phenomena are mere extensions or modifications of Rosencwaig-Gersho model. Though Bennett and Forman in 1976, and Aamodt *et.al.* in 1977 have modified the basic theoretical model by treating the acoustic wave transport in the gas using Navier-Stokes equations, the basic results of Rosencwaig-Gersho model remains the same [5,6]. Modification to the R-G theory by McDonald and Wetsel in 1978 by taking into account the contributions from thermally induced vibrations in the sample is somewhat intriguing [7]. By this time, a new form of photoacoustic configuration, namely the open photoacoustic cell has emerged [9]. Nowadays, the open cell photoacoustic technique is in widespread use for the thermal characterisation of solid and even liquid samples [10-20].

In fact, the concept of light beam deflection by thermally induced changes in the index of refraction of a medium has been known for a long time. However, only in 1979 Boccara *et.al* demonstrated the use of photothermal beam deflection method in material characterization [21]. Subsequent theoretical and experimental developments made by Jackson *et.al* in 1981, Aamodt *et.al* in 1981 and Grice *et.al* in 1983 have formed a strong basis to this technique [22-24]. Initially, people used the one-dimensional heat flow model formulated by Rosencwaig and Gersho to give a quantitative explanation to this effect. But, in many experimental conditions, such as when a focused pump-beam is used, this approach failed. In such situations, a three-dimensional heat flow model is required to give a satisfactory explanation and the details of this approach are included in this chapter.

2.2. Photoacoustic effect in condensed media

The photoacoustic technique is essentially a closed cavity detection of energy liberated by atoms or molecules through nonradiative de-excitation mechanism, subsequent to light absorption by a sample. When a solid sample placed inside an airtight cavity is irradiated with a modulated optical radiation, the energy liberated through nonradiative channels will result in the generation of thermal waves within the sample. The thermal waves diffused through the sample to the gas in the cavity will produce a periodic pressure fluctuation inside the cavity. This pressure variation can be detected using a microphone kept inside the cavity. If the sample to be analyzed is in the gaseous form, then the sample itself can act as the source of signal generation and the acoustic coupler to the microphone. In order to investigate a liquid sample, a piezoelectric transducer is usually used. The piezoelectric transducer kept in contact with the liquid sample will detect the acoustic pulse propagated through the liquid. In 1976 Rosencwaig and Gersho formulated a complete theoretical explanation to this effect in condensed media [4].

2.2.1. Rosencwaig-Gersho theory

The Rosencwaig-Gersho (R-G) theory is essentially a one-dimensional heat flow model, which is sufficient to describe the photoacoustic (PA) signal generation in condensed matter [4,8]. According to R-G theory, with a gas-microphone detection of PA signal, the signal depends on the generation of an acoustic pressure disturbance at the sample-gas interface. The generation of the surface pressure disturbance, in turn, depends on the periodic temperature at the sample-gas interface. Exact expressions for this temperature are derived in R-G theoretical model, but the transport of the acoustic disturbance in the gas is treated in an approximate heuristic manner, which is, however, valid in most experimental conditions.

The formulation of R-G model is based on the light absorption and thermal-wave propagation in an experimental configuration as shown in figure 1. Here the sample is considered to be in the form of a disc of thickness l . It is assumed that the back surface of the sample is in contact with a poor thermal conductor of thickness l_b and the front surface is in contact with a gas column of length l_g . It is further assumed that both gas and backing material are not light absorbing. Following are the parameters used in the R-G model which is being discussed below.

k : the thermal conductivity (cal/cm-s-°C)

ρ : the density (g/cm³)

C : the specific heat capacity(cal/g-°C)

$\alpha = k/\rho C$: the thermal diffusivity (cm^2/s)

$a = \sqrt{\omega/2\alpha}$ the thermal diffusion coefficient (cm^{-1})

$\mu = 1/a$: the thermal diffusion length (cm)

where $\omega = 2\pi f$, with f the modulation frequency of the incident light beam.

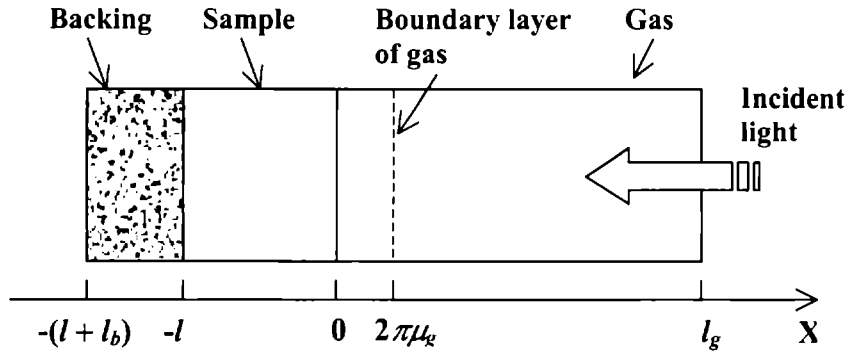


Figure 1: Schematic representation of photoacoustic experimental configuration.

When a sinusoidally modulated light beam of intensity I_0 is incident on a solid sample having an absorption coefficient β , the heat density generated at any point due to the light absorbed at this point can be represented by

$$\frac{1}{2} \beta I_0 e^{\beta x} (1 + \cos \omega t) \quad (1)$$

The thermal diffusion equation in the solid taking into account the distributed heat source, can be written as

$$\frac{\partial^2 \theta}{\partial x^2} = \frac{1}{\alpha} \frac{\partial \theta}{\partial t} - \frac{\beta I_0 \eta}{2k} e^{\beta x} (1 + e^{i\omega t}) \quad \text{for } -l \leq x \leq 0 \quad (2)$$

For the backing material and the gas, the heat diffusion equations are

$$\frac{\partial^2 \theta}{\partial x^2} = \frac{1}{\alpha_b} \frac{\partial \theta}{\partial t} \quad \text{for } -(l_b + l) \leq x \leq -l \quad (3)$$

$$\frac{\partial^2 \theta}{\partial x^2} = \frac{1}{\alpha_g} \frac{\partial \theta}{\partial t} \quad \text{for } 0 \leq x \leq l_g \quad (4)$$

where θ is the temperature and η is the light to heat conversion efficiency. Here, the subscripts b and g represent the backing and gas respectively. The real part of the complex valued solution $\theta(x, t)$ of equations (2)-(4) is the solution of physical interest and represents the temperature in the cell relative to ambient temperature as a function of position and time.

After imposing appropriate boundary conditions for the temperature and heat flux continuity, and neglecting convective heat flow in the gas at steady-state conditions, the explicit solution for the complex amplitude of the periodic temperature at the solid-gas boundary can be obtained as

$$\theta_o = \frac{\beta I_o}{2k(\beta^2 - \sigma^2)} \left[\frac{(r-1)(b+1)e^{\sigma l} - (r+1)(b-1)e^{-\sigma l} + 2(b-r)e^{-\beta l}}{(g+1)(b+1)e^{\sigma l} - (g-1)(b-1)e^{-\sigma l}} \right] \quad (5)$$

where

$$b = \frac{k_b a_b}{ka}, \quad g = \frac{k_g a_g}{ka}, \quad r = (1-i) \frac{\beta}{2a}, \quad \sigma = (1+i)a \quad (6)$$

The periodic heat flow from the solid to the surrounding gas produces a periodic temperature variation in the gas. The time dependent component of the temperature in the gas attenuates rapidly to zero with increasing distance from the surface of the solid. At a distance of $2\pi\mu_g$, where μ_g is the thermal diffusion length in the gas, the periodic temperature variation in the gas is effectively fully damped out. Thus there is a boundary layer of gas, which is only capable of responding thermally to the periodic temperature at the surface of the sample. This layer of gas expands and contracts periodically and thus can be thought of as acting as an acoustic piston on the rest of the gas column, producing an acoustic pressure signal that travels through the entire gas column. Assuming that the rest of the gas responds adiabatically to the action of the acoustic piston, the adiabatic gas law can be used to derive an expression for the complex envelope of the sinusoidal pressure variation Q as

$$Q = \frac{\gamma P_o \theta_o}{\sqrt{2} T_o l_g a_g} \quad (7)$$

with θ_o given by equation (5). γ , P_o and T_o are the ratio of heat capacities of air, ambient pressure and temperature, respectively.

Equation (7) can be used to evaluate the magnitude and phase of the acoustic pressure wave produced in the cell due to photoacoustic effect. However, a useful interpretation of the above equation is rather difficult in the present form. Hence, some special cases, according to the experimental conditions, have to be considered to get a clear physical insight. In fact, three lengths related to the sample, namely, the physical length l , the thermal diffusion length μ and the optical absorption length l_β ($= 1/\beta$) can be made use of in arriving at different special cases.

Optically transparent solids ($l_\beta > l$)

Case 1(a): Thermally thin solids ($\mu \gg l; \mu > l_\beta$)

We can set $e^{-\beta l} \cong 1 - \beta l$, $e^{\pm \sigma l} \cong 1$ and $|r| > 1$ in equation (7) and we obtain

$$Q \cong \frac{(1-i)\beta}{2a_g} \left(\frac{\mu_b}{k_b} \right) Y \quad (8)$$

$$\text{with } Y = \frac{\gamma P_o I_o}{2\sqrt{2} T_o l_g} \quad (9)$$

Now the acoustic signal is proportional to β and varies as f^{-1} . Moreover, the signal is now determined by thermal properties of the backing material.

Case 1(b): Thermally thin solids ($\mu > l; \mu < l_\beta$)

We can set $e^{-\beta l} \cong 1 - \beta l$, $e^{\pm \sigma l} \cong (1 \pm \sigma l)$ and $|r| < 1$ in equation (7) and we obtain

$$Q \cong \frac{(1-i)\beta}{2a_g} \left(\frac{\mu_b}{k_b} \right) Y \quad (10)$$

The acoustic signal now behaves in the same fashion as in the previous case.

Case 1(c): Thermally thick solids ($\mu < l; \mu \ll l_\beta$)

We can set $e^{-\beta l} \cong 1 - \beta l$, $e^{-\sigma l} \cong 0$ and $|r| \ll 1$ in equation (7) and we obtain

$$Q \cong -i \frac{\beta \mu}{2a_g} \left(\frac{\mu}{k} \right) Y \quad (11)$$

Now, only the light absorbed within the first thermal diffusion length contributes to the signal in spite of the fact that light is being absorbed throughout the length of the sample. Also since ($\mu < l$), the backing material does not have any contribution to the signal. Interestingly, the signal now varies as $f^{-1.5}$

Optically opaque solids ($l_\beta \ll l$)

Case 2(a): Thermally thin solids ($\mu \gg l; \mu \gg l_\beta$)

We can set $e^{-\beta l} \cong 0$, $e^{\pm \sigma l} \cong 1$ and $|r| \gg 1$ in equation (7) and we obtain

$$Q \cong \frac{(1-i)}{2a_g} \left(\frac{\mu_b}{k_b} \right) Y \quad (12)$$

Now the signal is independent of β , which is valid for a perfect black absorber such as carbon black. The signal will be much stronger compared to *case 1(a)* and varies as f^{-1} , but still depends on the thermal properties of the backing material.

Case 2(b): Thermally thick solids ($\mu < l; \mu > l_\beta$)

We can set $e^{-\beta l} \cong 0$, $e^{-\sigma l} \cong 0$ and $|r| > 1$ in equation (7) and we obtain

$$Q \cong \frac{(1-i)}{2a_g} \left(\frac{\mu}{k} \right) Y \quad (13)$$

Equation (13) is analogous to (12), but the thermal parameters of the backing material are now replaced with those of the sample. Again the signal is independent of β and varies as f^{-1}

Case 2(c): Thermally thick solids ($\mu \ll l; \mu < l_\beta$)

We can set $e^{-\beta l} \cong 0$, $e^{-\sigma l} \cong 0$ and $|r| < 1$ in equation (7) and we obtain

$$Q \cong -i \frac{\beta \mu}{2a_g} \left(\frac{\mu}{k} \right) Y \quad (14)$$

This is a very interesting and important case. Even though the solid is optically opaque, the photoacoustic signal is proportional to β as long as $\beta \mu < 1$. As in *case 1(c)*, the signal is independent of the thermal properties of the backing material and varies as $f^{-1.5}$

The different cases discussed so far can be made use of in the photoacoustic study of any kind of sample. One of the important predictions of the R-G theory is that the photoacoustic signal is always linearly proportional to the incident light intensity, irrespective of the sample properties and cell geometry. In *cases 2(a)* and *2(b)*, we have seen that the PA signal is independent of the optical absorption coefficient of the sample. For these cases, therefore, the only term in (12) and (13) that depends on the wavelength of the incident radiation is the light source intensity I_0 . Thus it is clear that the PA spectrum of an optically opaque sample ($\mu > l_\beta$) is simply the power spectrum of the light source.

2.2.2 Open photoacoustic cell configuration

Open photoacoustic cell (OPC) configuration is a modified and more convenient form of conventional photoacoustic configuration. In OPC, usually, solid sample will be mounted directly on top of the microphone, leaving a small volume of air in between the sample and the microphone [9-20]. It is an open cell detection configuration in the sense that the sample is placed on top of the detection system itself, as in the case of piezoelectric and pyroelectric detection. Consequently, this configuration is a minimum volume PA detection scheme and hence the signal strength will be much greater than the conventional PA configurations. The major advantage of this configuration is that samples having large area can be studied, whereas in conventional PA cells sample size should be small enough to be contained inside the PA cavity. A schematic representation of a typical OPC is shown in figure 2.

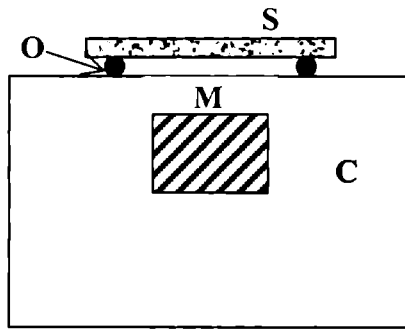


Figure 2: A general schematic representation of an open photoacoustic cell. Here S is the sample; O the o-ring; M the microphone and C the cell body.

R-G theory can be used to derive an expression for the periodic pressure variation inside the air chamber. Consider the OPC geometry shown in figure 3. Assume that the sample is optically opaque and whole energy is absorbed at the sample surface itself. Then, for the arrangement shown in figure 3, according to R-G theory, we can show that the periodic pressure variation in the air chamber is given by,

$$Q = \frac{\gamma P_o I_o (\alpha_g \alpha_s)^{1/2}}{2\pi T_o l_g k_s f} \frac{e^{j(\omega t - \pi/2)}}{\sinh(l_s \sigma_s)} \quad (15)$$

Now, if the sample is thermally thin (*i. e.*, $l_s \alpha_s \ll 1$), equation 15 reduces to

$$Q \cong \frac{\gamma P_o I_o \alpha_g^{1/2} \alpha_s}{(2\pi)^{3/2} T_o l_g l_s k_s} \frac{e^{j(\omega t - 3\pi/4)}}{f^{3/2}} \quad (16)$$

That is, the amplitude of the PA signal decreases as $f^{-1.5}$

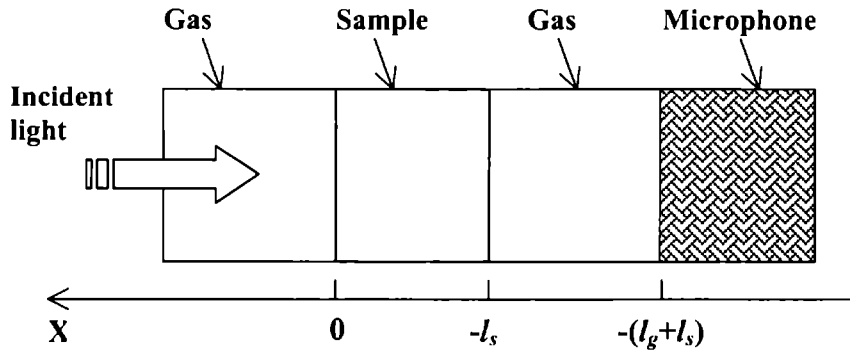


Figure 3: Schematic representation of the open photoacoustic cell geometry.

In contrary, at high modulation frequencies, such that the sample is thermally thick (*i. e.*, $l_s a_s \gg 1$), then

$$Q \cong \frac{\gamma P_o I_o (\alpha_g \alpha_s)^{1/2}}{\pi T_o l_g k_s} \frac{e^{-l_s \sqrt{\pi f / \alpha_s}}}{f} e^{j(\omega t - \pi/2 - l_s a_s)} \quad (17)$$

Equation (17) means that, for a thermally thick sample, the amplitude of the OPC signal decreases exponentially with the modulation frequency as $\left(\frac{1}{f}\right) \exp(-b\sqrt{f})$, where $b = l_s \sqrt{\pi / \alpha_s}$, whereas its phase decreases linearly with \sqrt{f} with a slope of b . Hence, the thermal diffusivity α_s of the sample can be easily evaluated from either signal amplitude plot or from the phase plot. However, a necessary condition to employ the OPC configuration is that the sample should be optically opaque at the incident wavelength. The OPC configuration can not only be used for the study of solid samples, but liquid samples can also be characterised using this configuration. Commonly used approach in the study of liquid samples using OPC configuration is by keeping the liquid in contact with a thermally thin solid sample, the thermal properties of which are known [18-20].

2.3. Photothermal deflection: Mirage effect

In 1979 Boccara *et.al* proposed and demonstrated the usefulness of photothermal beam deflection (mirage effect) method for monitoring the temperature gradient field close to a sample surface or within the bulk of a sample [21]. In subsequent years, many theoretical and experimental developments have been reported in [22-32]. The method is essentially based on the detection of refractive index gradient associated with the temperature gradient. As we have seen in the previous section, absorption of optical radiation results in the generation of thermal waves in the sample which heats up the gas or liquid above the surface. The heated gas deflects a probe laser passing through it. The probe-beam deflection can be monitored using a position-sensing detector. Figure 4 shows a schematic diagram of the passage of a probe-beam through a refractive index profile.

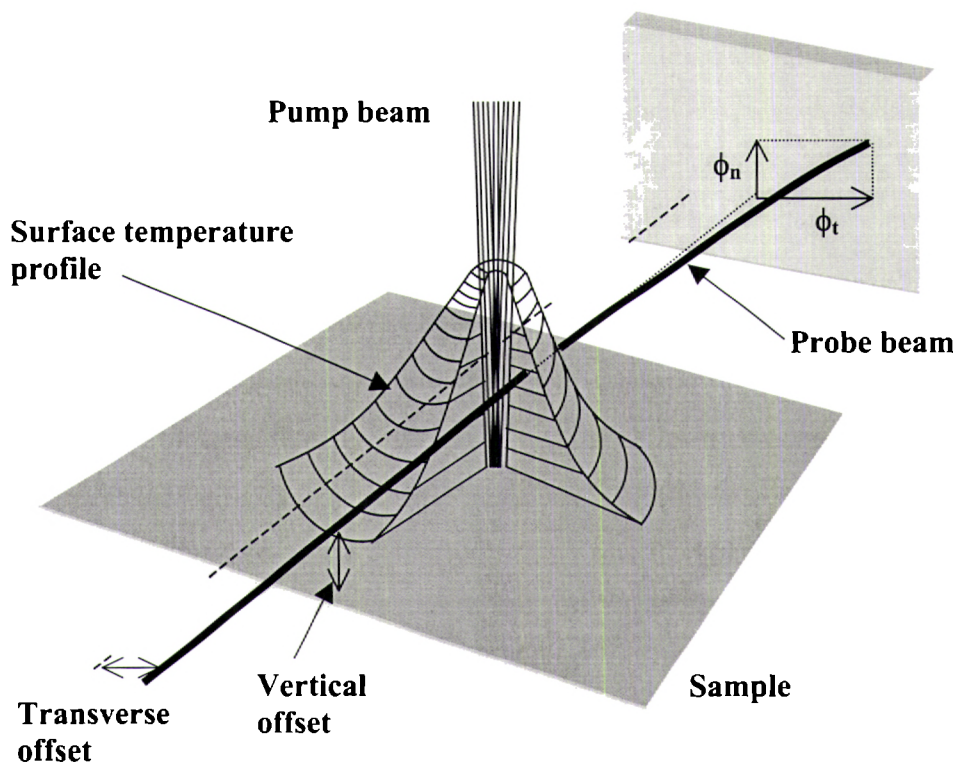


Figure 4: A schematic diagram of the passage of a probe-beam through a refractive index profile and the resulting normal and transverse components of the PTD signal.

For a Gaussian beam propagating through an inhomogeneous medium, most of the beam parameters can be deduced from the analysis of Casperson [33]. The propagation of a light beam through a spatially varying index of refraction is given by [34]

$$\frac{d}{ds} \left(n_o \frac{dr_o}{ds} \right) = \nabla_{\perp} n(r, t) \quad (18)$$

where r_o is the perpendicular displacement of the beam from its original direction, n_o is the uniform index of refraction, and $\nabla_{\perp} n(r, t)$ is the gradient of index of refraction perpendicular to the ray path. The above relation can be integrated over the ray path:

$$\frac{dr_o}{ds} = \frac{1}{n_o} \int_{path} \nabla_{\perp} n(r, t) ds \quad (19)$$

where s is the optical path length. Since the deviation is small, one can get the expression for the deflection $\theta(t)$ as

$$\frac{dr_o}{ds} = \theta(t) = \frac{1}{n_o} \frac{\partial n}{\partial T} \int_{path} \nabla_{\perp} T(r, t) ds \quad (20)$$

where $\nabla_{\perp} T(r, t)$ is the temperature gradient perpendicular to the ray path. The deflection $\theta(t)$ can be resolved into two components θ_n and θ_t . Where θ_n and θ_t are, respectively, the deflections normal and parallel to the sample surface and are given by

$$\theta_n = \frac{1}{n_o} \frac{dn}{dT} \int_{-\infty}^{+\infty} \frac{\partial T_f}{\partial z} dx \quad (21)$$

$$\text{and } \theta_t = \frac{1}{n_o} \frac{dn}{dT} \int_{-\infty}^{+\infty} \sin \alpha \frac{\partial T_f}{\partial r} dx \quad (22)$$

Now, we have to evaluate the temperature field in the sample and in the surrounding fluid. Though initially people used a one-dimensional heat flow model to evaluate the temperature field, it is found to vanish in most of the experimental conditions, especially when the excitation beam is focused. Hence, to get a complete general solution, we have to depend on a three-dimensional model. Consider an experimental configuration as shown in figure 5. The 3-D model used to describe the photothermal deflection is more complicated than the 1-D model used to explain the photoacoustic signal generation, since the thermal conduction in the solid and fluid has to be taken into account in the former case.

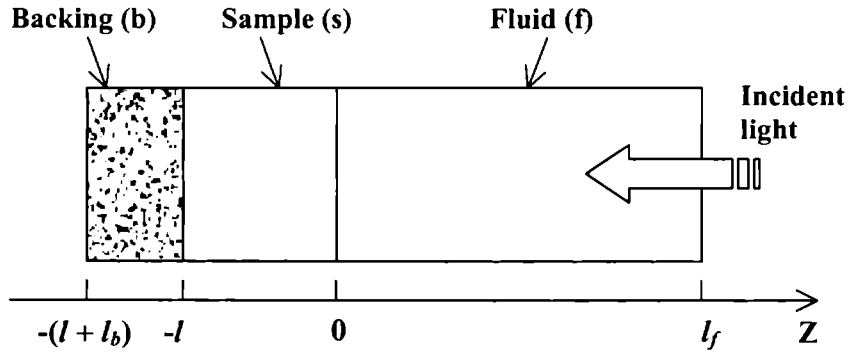


Figure 5: Schematic representation of experimental geometry used in 3-D model

Assume that the homogeneous sample is the only absorbing medium whereas the fluid and backing material are transparent. For simplicity, it is assumed that all the three regions extend infinitely in the radial direction, with the irradiated area usually being limited and small compared to the radial size of the sample. The heat diffusion equations in the three regions are

$$\frac{\partial^2 T_f}{\partial r^2} + \frac{1}{r} \frac{\partial T_f}{\partial r} + \frac{\partial^2 T_f}{\partial z^2} = \frac{1}{D_f} \frac{\partial T_f}{\partial t} \quad \text{for } 0 \leq z \leq l_f \quad (23)$$

$$\frac{\partial^2 T_s}{\partial r^2} + \frac{1}{r} \frac{\partial T_s}{\partial r} + \frac{\partial^2 T_s}{\partial z^2} = \frac{1}{D_s} \frac{\partial T_s}{\partial t} - A(r, t) e^{\alpha z} (1 + e^{j\alpha t}) \quad \text{for } -l \leq z \leq 0 \quad (24)$$

$$\frac{\partial^2 T_b}{\partial r^2} + \frac{1}{r} \frac{\partial T_b}{\partial r} + \frac{\partial^2 T_b}{\partial z^2} = \frac{1}{D_b} \frac{\partial T_b}{\partial t} \quad \text{for } -(l + l_b) \leq z \leq -l \quad (25)$$

Here, the suffixes f , s and b stands for fluid, sample and backing material, respectively. D is the thermal diffusivity and α is the optical absorption coefficient of the sample.

After introducing appropriate boundary conditions and making use of Hankel transform, one can arrive at the expressions for the modulated temperature field in the three regions as

$$T_f(r, z, t) = \int_0^\infty T_s(\lambda) \exp(-\beta_f z) \exp(j\alpha t) J_0(\lambda r) \lambda d\lambda \quad (26)$$

$$T_b(r, z, t) = \int_0^\infty W(\lambda) \exp(\beta_b(z + l) + j\alpha t) J_0(\lambda r) \lambda d\lambda \quad (27)$$

$$T_s(r, z, t) = \int_0^\infty [U(\lambda) \exp(\beta_s z) + V(\lambda) \exp(-\beta_s z) - E(\lambda) \exp(\alpha z)] \times \exp(j\alpha t) J_0(\lambda r) \lambda d\lambda \quad (28)$$

where

$$E(\lambda) = \frac{P\eta}{\pi k_s} \frac{\exp\left(\frac{-\lambda^2 a^2}{8}\right)}{\left(-\lambda^2 - j \frac{\omega}{D_s} + \alpha^2\right)} \quad (29)$$

$$\text{with } a^2 \exp\left(\frac{-\lambda^2 a^2}{8}\right) = \int_0^\infty \exp\left(-\frac{2r^2}{a^2}\right) J_0(r\lambda) r dr \quad (30)$$

$$\beta_i^2 = \lambda^2 + \frac{j\omega}{D_i} \quad (31)$$

$$T_s(\lambda) = -E(\lambda) + U(\lambda) + V(\lambda) \quad (32)$$

$$W(\lambda) = -E(\lambda) \exp(-\alpha l) + U(\lambda) \exp(-\beta_s l) + V(\lambda) \exp(\beta_s l) \quad (33)$$

$$U(\lambda) = \left[(1-g)(b-r) \exp(-\alpha l) + (g+r)(1+b) \exp(\beta_s l) \right] \frac{E(\lambda)}{H(\lambda)} \quad (34)$$

$$V(\lambda) = \left[(1+g)(b-r) \exp(-\alpha l) + (g+r)(1-b) \exp(-\beta_s l) \right] \frac{E(\lambda)}{H(\lambda)} \quad (35)$$

$$\text{with } g = \frac{k_f \beta_f}{k_s \beta_s}, \quad b = \frac{k_b \beta_b}{k_s \beta_s}, \quad r = \frac{\alpha}{\beta_s} \quad (36)$$

$$\text{and } H(\lambda) = (1+g)(1+b) \exp(\beta_s l) - (1-g)(1-b) \exp(-\beta_s l) \quad (37)$$

In photothermal deflection technique, measurements are carried out using a probe-beam propagating through a transparent fluid in contact with the sample surface. The temperature field along the probe-beam path is a function of both the surface temperature and the distance between sample-surface and the probe-beam.

The complex amplitude of the surface temperature can be obtained as

$$T_s(0, t) = \int_0^\infty E(\lambda) \left[\frac{- (1+b)(1-r) \exp(\beta_s l) + (1-b)(1+r) \exp(-\beta_s l)}{(1+g)(1+b) \exp(\beta_s l) - (1-g)(1-b) \exp(-\beta_s l)} \right] \times J_0(\lambda r) \lambda d\lambda \exp(j\omega t) \quad (38)$$

In the above expression, the term in the bracket describes the thermal response of the three media, namely, the sample, backing and the coupling fluid. Now, if the sample is thermally thick, then the surface temperature of the sample can be easily evaluated by replacing this term of the above expression by

$$\frac{(r-1)}{(g+1)} \quad (39)$$

and for thermally thin sample the term in the bracket becomes

$$\frac{(r - b)(1 - \exp(-al)) + \sigma_s l(rb - 1)}{(b + g)} \quad (40)$$

Based on expression (38), many people have carried out photothermal deflection measurements for the thermal and optical characterisation of solids [30-32, 35-48]. Among these, the thermal diffusivity of solids is one of the most widely studied thermal parameter. Salazar *et.al* analysed various theoretical and experimental conditions and arrived at certain expressions which describe a linear relationship of PTD signal phase with various parameters such as pump-probe offset, height of the probe-beam above the sample surface etc [31]. For $a = b = z = 0$, where a , b and z are the pump-beam spot size, probe-beam spot size and the probe-beam height above the sample surface, there exist a linear relationship between the phase of the transverse component of the probe-beam deflection and the pump-probe offset. Slope of the plot connecting the phase of the PTD signal and the pump-probe offset is given by

$$m = \frac{1}{\mu_s} = \sqrt{\pi f / \alpha_s} \quad (41)$$

Investigations discussed in the subsequent chapters are based on the theoretical models described in this chapter.

References

1. Bell.A.G, *Am.J.Sci.* **20**, 305 (1880).
2. Bell.A.G, *Philos.Mag.* **11**, 510 (1881).
3. Viengerov.M.L, *Dokl.Akad.Nauk SSSR* **19**, 687 (1938).
4. Rosencwaig.A and Gersho.A, *J.Appl.Phys.* **47**, 64 (1976).
5. Bennet.H.S and Forman.R.A, *Appl.Opt.* **15**, 2405 (1976)
6. Aamodt.L.C, Murphy.J.C and Parker.J.G, *J.Appl.Phys.* **48**, 927 (1977).
7. McDonald.F.A and Wetsel.G.C, *J.Appl.Phys.* **49**, 2313 (1978).
8. Rosencwaig.A, *Photoacoustics and photoacoustic spectroscopy*, (John Wiley & Sons, New York) (1980).
9. Kanstad.S.O and Nordal.P.E, *Opt.Comm.*, **26**, 367 (1978).
10. Perondi.L.F and Miranda.L.C.M, *J.Appl.Phys.* **62**, 2955 (1987).
11. Marquezini.M.V, Cella.N, Mansanares.A.M., Vargas.H and Miranda.L.C.M, *Meas.Sci. Technol.* **2**, 396 (1991).
12. Neto.A.P, Vargas.H, Leite.N.F and Miranda.L.C.M, *Phys.Rev.B* **40**, 3924 (1989).
13. Neto.A.P, Vargas.H, Leite.N.F and Miranda.L.C.M, *Phys.Rev.B* **41**, 9971 (1990).
14. Mansanares.A.M., Vargas.H, Galembeck.F, Buijs.J and Bicanic.D, *J.Appl.Phys.* **70**, 7046 (1991).
15. Nikolic.P.M, todorovic.D.M, Bojicic.A.J, Radulovic.K.T, Urosevic.D, Elzar.J, Blagojevic.V, Mihajlovic.P and Miletic.M, *J.Phys: Condens.Matter*, **8**, 5673 (1996).
16. Segundo.C.G, Muniz.M.V and Muhl.S, *J.Phys.D:Appl.Phys.* **31**, 165 (1998).
17. Marin.E, Vargas.H, Diaz.P and Riech.I, *Phys.Stat.Sol (a)*, **179**, 387 (2000)
18. Vasallo.,O.D, Valdes.A.C, Marin.E, Lima.J.A.P, Silva.M.G, Sthel.M, Vargas.H and Cardoso.S.L, *Meas.Sci.Technol.* **11**, 412 (2000).
19. Vasallo.,O.D and Marin.E, *J.Phys.D:Appl.Phys.* **32**, 593 (2000).
20. Lopez.B, Avalos.D.A, Alvarado.J.J, Angel.J, Sinencio.F.S, Falcony.C, Orea.F and Vargas.H, *Meas.Sci.Technol.* **6**, 1163 (1995).
21. Boccara.A.C, Fournier.D and Badoz.J, *Appl.Phys.Lett.* **36**, 130 (1979).
22. Jackson.W.B, Amer.N.M, Boccara.A.C and Fournier.D, *Appl.Opt.* **20**, 1333 (1981).
23. Aamodt.L.C and Murphy.J.C, *J.Appl.Phys.* **52**, 4903 (1981).
24. Grice.K.R, Inglehart.L.J, Favro.L.O, Kuo.P.K and Thomas.R.L, *J.Appl.Phys.* **54**, 6245 (1983).
25. Charbonnier.F and Fournier.D, *Rev.Sci.Instrum.* **57**, 1126 (1986).

26. Salazar.A, Lavega.A.S and Fernandez.J, *J.Appl.Phys.* **65**, 4150 (1989).
27. Cheng.J.C, Li.F.H, Guo.L and Zhang.S.Y, *Appl.Phys.A.* **61**, 441 (1995).
28. Salazar.A, Lavega.A.S and Fernandez.J, *J.Appl.Phys.* **74**, 1539 (1993).
29. Murphy.J.C and L.C.Aamodt, *J.Appl.Phys.* **51**, 4580 (1980).
30. M.Bertolotti, Voti.R.L, Liakhov.G and Sibilia.C, *Rev.Sci.Instrum.* **64**, 1576 (1993).
31. Salazar.A and Lavega.A.S. *Rev.Sci.Instrum.* **65**, 2896 (1994).
32. Kuo.P.K, Lin.M.J, Reyes.C.B, Favro.L.D, Thomas.R.L, Kim.D.S, Zhang.S, Inglehart.L.J, Fournier.D, Boccara.A.C and Yacoubi.N, *Can.J.Phys.* **64**, 1165 (1986).
33. Casperson.L.W, *Appl.Opt.* **12**, 2434 (1973).
34. Born.M and Wolf.E, *Principle of Optics* (Pergamon Press, Oxford) (1970).
35. M.Bertolotti, Liakhov.G, Voti.R.L, Paoloni.S and Sibilia.C, *J.Appl.Phys.* **83**, 966 (1998).
36. Havaux.M, Lorrain.L and Leblanc.M, *FEBS Letters* **250**, 395 (1989).
37. Machlab.H, McGahan.W.A, Woollam.J.A and Cole.K, *Thin.Sol.Film.* **224**, 22 (1993).
38. Bertolotti.M, Fabbri.L, Sibilia.C, Ferrari.A, Sparvieri.N and suber.G, *J.Phys.D: Appl.Phys.* **21**, S14 (1988).
39. Lavega.A.S, Salazar.A, Ocariz.A, Pottier.L, Gomez.E, Villar.L.M and Macho.E, *Appl.Phys.A* **65**, 15 (1997).
40. Salazar.A, Lavega.A.S and Fernandez.J, *J.Appl.Phys.* **69**, 1216 (1991).
41. Li.B.C and Gupta.R, *J.Appl.Phys.* **89**, 859 (2001).
42. Zhou.W.Y, Qian.S.F, Zhao.R.A, Wang.G, Qian.L.X, Li.W.Z and Xie.S.S, *Prog.Natu.Sci.*, **6**, S22 (1996).
43. Kimura.H, Matsuzawa.S, Tu.C.Y, Kitamori.T and Swada.T, *Anal.Chem.* **68**, 3063 (1996).
44. Commandre.M and Roche.P, *Appl.Opt.* **35**, 5021 (1996).
45. Zimering.B and Boccara.A.C, *Rev.Sci.Instru.* **67**, 1819 (1996).
46. Thomas.R.L, Inglehart.L.J, Lin.M.J, Favro.L.D and Kuo.P.K, In *Review of Progress in Quantitative Nondestructive Evaluation*, (Thompson.D.O and Chimenti.D.E (Eds.), Plenum, New York) Vol. **4B**, 859 (1985).
47. Thomas.R.L, Favro.L.D Kim.D.S, Kuo.P.K, Reyes.C.B and Zhang.S, In *Review of Progress in Quantitative Nondestructive Evaluation*, (Thompson.D.O and Chimenti.D.E (Eds.), Plenum, New York) Vol. **5B**, 1379 (1986).
48. Kuo.P.K, Reyes.C.B Favro.L.D, Thomas.R.L, Kim.D.S and Zhang.S, In *Review of Progress in Quantitative Nondestructive Evaluation*, (Thompson.D.O and Chimenti.D.E (Eds.), Plenum, New York) Vol. **5B**, 1519 (1986).

Photoacoustic and photothermal deflection studies on III-V compounds

The present chapter comprises of two sections. The first section discusses the investigation carried out on sulphur doped n-type InP wafer using an open photoacoustic cell. The thermal diffusivity of the sample is evaluated from the phase data associated with the photoacoustic signal as a function of the modulation frequency. Analysis is made on the basis of the Rosencwaig-Gersho theory and the results are compared with those from earlier reported photoacoustic studies on semiconductors. Results show that, under the present experimental conditions, the pure thermal-wave component is responsible for the photoacoustic signal generation from n-type InP sample. Results obtained from a dual-beam photothermal deflection studies on n-type and p-type GaAs thin films grown on a semi-insulating GaAs substrate are discussed in the second section.

3.1. Introduction

Absorption of intensity modulated optical radiation by a sample leads to periodic heat generation, thereby causing excitation of thermal waves in the sample. Thermal wave physics is emerging as a valuable tool in the study of thermal parameters of materials, especially in the semiconductor industry [1-17]. Among the various methods used to study these thermal waves, the gas-microphone photoacoustic (PA) technique and the dual-beam photothermal deflection (PTD) technique are the most commonly employed experimental approaches [15-26]. Apart from the pure spectroscopic studies in the very beginning, the PA method has now grown to a multipurpose analytical tool for the investigation of different thermal and optical properties of a variety of materials.

In many of the earlier reported papers, PA signal amplitude data as a function of the modulation frequency has been mainly used for the thermal diffusivity measurements in semiconductors [22-28]. Since the first report of Sablikov *et.al* regarding the use of PA technique for heat transport studies in semiconductors, researchers are using this approach for a variety of measurements [29]. But a major renaissance in this field was made by Dramicanin *et.al* [30], who analytically evaluated the expression for the distribution of the periodic thermal flux originating from three principal thermal sources namely, the instantaneous thermalisation component, nonradiative bulk recombination and non radiative surface recombination. Their model is very useful for the analysis of PA signal amplitude and phase at the front and rear surfaces of a semiconductor sample. Subsequently, in more recent years, carrier transport properties such as carrier diffusion coefficient, carrier recombination velocity and mean recombination time are evaluated together with the thermal diffusivity of a large number of semiconducting samples such as GaAs, CdTe, Si solar cells, CdInGaS₄, InSb, GaSb etc using the photoacoustic phase measurements [31-42].

Similar to the PA technique, PTD technique has also become mature both in the theoretical aspect as well as from the experimental point of view. The only difference between the PA and PTD techniques is in the mode of detection, but the basic mechanism of heat transport on which the two methods relies is the same [15,16]. Consequently, PA and PTD techniques can be used for similar type of studies, but each approach has its own advantages and disadvantages. Following the theoretical model developed by Sablikov *et.al* for the PA signal generation in semiconductors, Fournier *et.al* formulated a one-dimensional heat-flow model to describe the PTD signal generation in semiconductors, by taking into account the nonradiative recombination processes [43]. However, the contributions from the free carriers plays a

dominant role in the PA and PTD signal only under certain experimental conditions such as a particular frequency range, sample surface quality etc. Details of each experimental approach and the observed results are described in the respective sections.

3.2. Significance of thermal diffusivity

Centuries before, Jean Fourier (1768-1830) derived a basic law defining the propagation of heat in a one-dimensional homogeneous solid as [44-46]

$$\frac{dQ}{dt} = -kA \frac{dT}{dx} \quad (1)$$

The above equation is known as Fourier equation. Equation (1) implies that the quantity of heat dQ conducted in the x-direction of a uniform solid in time dt is equal to the product of the conducting area A normal to the flow path, the temperature gradient dT/dx along this path, and the thermal conductivity k of the conducting material.

Formal definition of thermal diffusivity arises when deriving an expression for a transient temperature field in a conducting solid from the Fourier equation. The equation describing the temperature field in a homogeneous, linear conducting solid with no internal heat source is

$$\nabla^2 T = \frac{1}{\alpha} \frac{\partial T}{\partial t} \quad (2)$$

where the thermal diffusivity α is given by

$$\alpha = \frac{k}{\rho C} \quad (3)$$

where k is the thermal conductivity, ρ is the density and C is the specific heat capacity of the material. The thermal diffusivity α is usually expressed in m^2s^{-1}

The thermal diffusivity is thus a derived quantity whose significance is evident from the above relationship. The reciprocal of thermal diffusivity, $1/\alpha$, expressed in sm^{-2} is a measure of the time required to heat-up a conducting material to some temperature level. Therefore, the ratio of heating times for two materials of the same thickness will be inversely proportional to their respective thermal diffusivity values. Obviously, α is a significant thermophysical parameter that determines the heat diffusion in bulk as well as thin film samples.

Being a widely used and important substrate material in the field of semiconductor technology, measurement of the thermal diffusivity and a detailed analysis of the heat diffusion processes in InP have great practical significance. The same is the case with GaAs since it is a

widely used compound semiconductor material in electronic and optoelectronic devices. Moreover, the bandgap of semiconductors, in general, decreases as the temperature increases [47-52]. These changes have very important consequences in electronic and optoelectronic devices. The variation in the operating temperature may alter the laser frequency in semiconductor lasers, and may alter the response of semiconductor modulators and detectors. Hence, a clear knowledge of the thermal transport properties such as the thermal diffusivity of these materials assumes importance.

3.3. III-V compounds

Most semiconductors of interest for electronics and optoelectronics have an underlying fcc lattice. If two atoms of the basis are different, the structure is called the zinc-blende structure and such semiconductor materials are usually known as compound semiconductors. Usually, the compound semiconductors are denoted by the position of the atoms in the periodic table, e.g. II-IV, III-V etc. GaAs and InP are examples of III-V compounds. Both these compounds are direct bandgap materials which ensures excellent optical properties as well as superior electron transport in the conduction band. The bandgap energy in GaAs is 1.43 eV and in InP it is 1.34 eV [47-49,54]. In the field of semiconductor research the main thrust is towards III-V compounds which are widely used in solid state electronics, in particular in the manufacturing of very important types of devices such as those used in optoelectronics, microwaves, high speed integrated circuits, high efficiency solar cells etc [53-59].

Bulk crystal growth techniques are mainly used to produce large size substrates on which the thin film devices are fabricated. These techniques are widely used in the growth of semiconductors such as Si, GaAs and to some extent InP. One of the commonly employed bulk growth method is the Czochralski technique [60-65]. But, in the case of GaAs and InP the Czochralski technique has problems arising from the very high pressures of As and P at the melting temperature of these compounds. Not only the chamber has to withstand such high pressures, but also the As and P leave the melt and condense on the side-walls. To avoid the second problem, usually the melt is covered with a molten layer of a second material (*e.g.* boron oxide) which floats on the surface. The technique is then referred to as Liquid Encapsulated Czochralski (LEC) method. Both InP and GaAs substrates used in the present investigations are grown by LEC method.

The substrates that result from the bulk grown semiconductor boules are almost never used directly for device fabrication. Invariably an epitaxial layer is grown over the substrate, which may be a few microns in thickness. The epitaxial growth techniques have a very slow growth rate which allows precise control over the dimensions in the growth direction. One such technique is the Molecular-Beam Epitaxy (MBE) which is essentially a refined form of vacuum evaporation [54, 60-62,66]. In this technique, elements are heated in crucibles called Knudsen cells or furnaces and directed beams of atoms or molecules are condensed onto a heated single-crystal substrate where they react chemically under ultra-high-vacuum conditions. The special merits of this technique are that thin films can be grown with precise control over their thickness, alloy composition and doping level. Using rapidly acting mechanical shutters, the composition can be changed abruptly, which permits novel structures to be prepared. MBE grown n-type and p-type GaAs double-layers on a semi-insulating GaAs wafer are used for the photothermal deflection studies.

3.4. Heat conduction in semiconductors

In general, two different mechanisms are responsible for heat conduction in a solid material. One is the heat conduction due to the charge carrier motion and is termed as electron or hole heat conductivity (k_e). The second mechanism is connected with the lattice vibrations [66-70]. The lattice atoms (or ions) oscillating around their respective equilibrium positions exchange energy with each other. When a temperature gradient is built up in a substance, this energy gradient proceeds in such a manner that energy is transmitted from an atom which oscillates more intensely to an atom which oscillates less intensely. Heat conductivity due to lattice vibrations is termed as lattice, or phonon, heat conductivity (k_L). The total heat conductivity may thus be described by the quantity k as

$$k = k_e + k_L \quad (4)$$

the value of k_L is related to the elastic properties of the solid and k_e to the charge carrier concentration. In dielectrics $k_L \gg k_e$ and in metals opposite is the case, *i.e.* $k_e \gg k_L$. In semiconductors the value of k_e strongly depends on the composition and on the temperature.

In the case of a semiconductor irradiated with an optical radiation of suitable energy, in addition to the above-described mechanisms, photogenerated carrier recombination will also contribute to the heat transport [22,30-43]. Free-carrier generation resulting from the light absorption occurs when the incident photon energy is greater than the band gap energy. The photon is absorbed in this process and the excess energy, $E_{ph} - E_g$, is added to the electron

and hole in the form of kinetic energy. Now, the nonradiative recombination of these carriers will result in the release of excess energy in the form of heat to the lattice. The recombination rate of majority carriers is equal to that of minority carriers since the steady state recombination involves equal number of holes and electrons. Therefore, the recombination rate of the majority carriers depends on the excess minority carrier density as the minority carriers limit the recombination rate. There exist different possible pathways for the nonradiative recombination [22,30-43]. Nonradiative band-to-band recombination depends on the density of available electrons and holes and is proportional to the product of the two densities. In this case the electrons carrying excess energy above the bandgap recombine with a hole and the energy equivalent to the bandgap energy will be liberated as a phonon. Usually this process takes place in the bulk of the material and is termed as the bulk recombination. Another nonradiative recombination process is the surface recombination. Surfaces and interfaces of semiconductors usually contain large number of recombination centers because of the abrupt termination of the crystal, which leaves a large number of electrically active dangling bonds. In addition, the surfaces and interfaces are likely to contain more impurities since they are exposed during the growth of the material. The surface recombination is also essentially an interband recombination process and the excess energy is ultimately transferred to the lattice as heat. Trap assisted recombination and Auger recombination are the other two recombination mechanisms. Apart from these interband nonradiative recombination processes there exists an instantaneous thermalisation component which arises from the intraband interaction of excited electrons with the lattice. This process is an after-effect of excitation of electrons to the higher levels in the conduction band. Such hot electrons will come back to the minimum of the conduction band by imparting the excess energy to the lattice. This thermalisation process usually takes place in ultra-short time scales (\sim picosecond) and hence known as the instantaneous thermalisation process [22,66-68]. In the subsequent section of this chapter experimental investigations of heat diffusion in n-type InP carried out by PA technique and PTD studies on GaAs multi-layers are presented.

Part A

3.5. Photoacoustic investigation of heat diffusion in n-type InP

3.5.1. Theoretical outline

The open photoacoustic cell (OPC) is a renewed form of conventional photoacoustic configuration [25,40,71-82]. OPC can be used in two different configurations for the thermal characterisation of solids. They are the heat transmission configuration and the reflection configuration. The reflection configuration is equivalent to the commonly employed front surface illumination mode in conventional photoacoustic cells. The heat transmission configuration is depicted in figure 1. For an optically opaque solid, the entire light is absorbed by the sample at $x = 0$ and the periodic heat is generated at the same place. Assuming that the heat flow into the gas (air) in contact with the front side of the solid is negligibly small, the thermal waves generated at $x = 0$ will penetrate through the sample to its rear surface. The heat thus reaching the sample-air interface at $x = -l_s$ will get attenuated after travelling a very small distance called the first thermal diffusion length in the air. The thermal diffusion length is given by $\mu = \sqrt{2\alpha/\omega}$, where α and ω are the thermal diffusivity of air and modulation frequency of the incident light, respectively. Consequently, this periodic heating process arising as a result of the periodic absorption of light at the interface at $x = 0$ results in an acoustic piston effect in the air column in between the sample and the microphone.

According to the one-dimensional heat flow model of Rosencwaig and Gersho, for the arrangement schematically shown in figure 1, the pressure fluctuation in the air inside the chamber is given by [17,83-85]

$$Q = \frac{\gamma P_o I_o (\alpha_g \alpha_s)^{1/2}}{2\pi l_g T_o k_s f \sinh(l_s \sigma_s)} e^{j(\omega t - \pi/2)} \quad (5)$$

where γ is the ratio of specific heat capacities of air, P_o and T_o are the ambient pressure and temperature, I_o is the radiation intensity, f is the modulation frequency, and l_i , k_i and α_i are the length, thermal conductivity and the thermal diffusivity of the medium. $i = g$ refers to the gas and $i = s$ refers to the solid sample. Also $\sigma_i = (1 + j)a_i$, where $a_i = (\pi f / \alpha)^{1/2}$ is the thermal diffusion coefficient of the medium i . In arriving at the above expression it is assumed that the sample is optically opaque and that the heat flux into the air in contact with the irradiated surface of the sample is negligible.

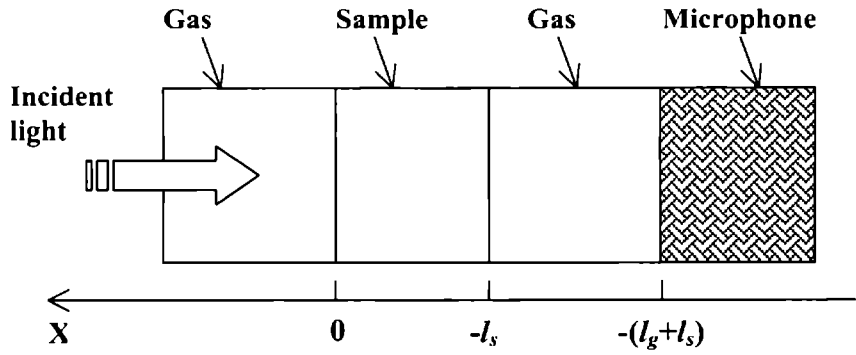


Figure 1: Schematic representation of an open photoacoustic cell configuration

For thermally thin sample (*i.e.* $l_s a_s \ll 1$), equation (5) reduces to

$$Q = \frac{\gamma P_o I_o \alpha_g^{1/2} \alpha_s}{(2\pi)^{3/2} T_o l_g l_s k_s} \frac{e^{j(\omega t - 3\pi/4)}}{f^{3/2}} \quad (6)$$

Above expression implies that the PA signal amplitude from a thermally thin sample under the heat transmission configuration varies as $f^{-1.5}$ and the phase is insensitive to the variation in the modulation frequency. On the contrary, for high modulation frequencies, when the sample is thermally thick (*i.e.* $l_s a_s \gg 1$), equation (5) becomes

$$Q = \frac{\gamma P_o I_o (\alpha_g \alpha_s)^{1/2}}{\pi T_o l_g k_s} \frac{\exp[-l_s (\pi f / \alpha_s)^{1/2}]}{f} e^{j(\omega t - \pi/2 - l_s a_s)} \quad (7)$$

Equation (7) suggests that for a thermally thick sample, the amplitude of the PA signal decreases exponentially with the modulation frequency according to $(1/f) \exp(-b\sqrt{f})$, with $b = l_s (\pi / \alpha_s)^{1/2}$ while the phase φ decreases linearly with $b\sqrt{f}$. Hence, the thermal diffusivity α_s can be evaluated either from the amplitude data or from the phase response with respect to the modulation frequency, provided the sample is optically opaque and thermally thick in the frequency region of interest. When the amplitude data is available, α_s can be obtained from the fitting coefficient b appearing as the argument of the exponent $(-b\sqrt{f})$. When the signal phase data is used, α_s can be obtained from the slope of the phase plot as a function of \sqrt{f} . However, in the case of thermally thick, disk-like solid samples the contribution from thermoelastic bending has also to be taken into account. This effect is essentially due to the temperature gradient existing along the direction of thickness, due to which the sample surface at higher temperature expands more than the other surface and

eventually the sample bends outwards [17,85-87]. In such situations the phase plot will no longer obey the linear relation with the square root of the modulation frequency. Details of the thermoelastic bending and the modifications to the phase relation with the modulation frequency are not discussed here since the sample under investigation (n-type InP) is free from this effect.

We have seen in the previous section that the charge carrier recombination (surface and bulk) is an important factor which contributes significantly to the heat conduction in a semiconductor. In such situations the expressions derived above for the amplitude and phase, obtained by taking only the dominant phonon contribution into account, are not adequate. Then, additional terms are required to accommodate the contributions from the surface as well as the bulk nonradiative recombination processes, and consequently, the above expressions will become more complex and nonlinear [29-30,32-39]. However, from the experimental observations described in the following sections, no such effects are observed for n-type InP sample and hence the corresponding theoretical model is not presented here.

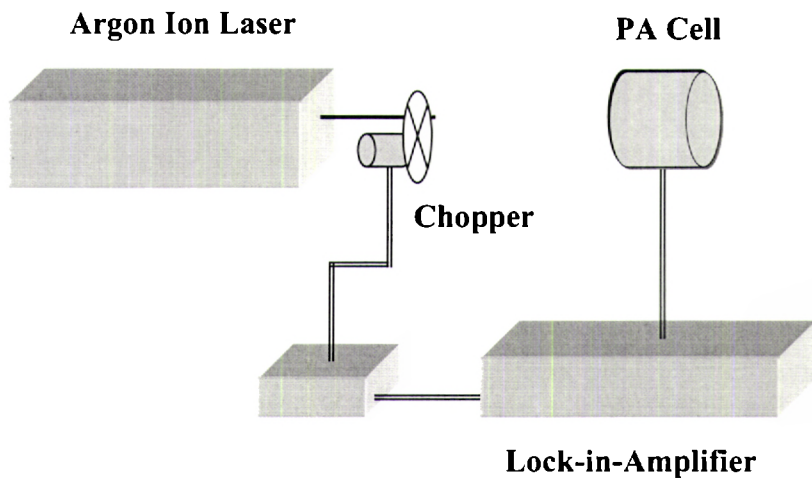


Figure 2: A schematic diagram of the experimental set-up

3.5.2. Experimental details

A schematic diagram of the experimental set-up based on the open photoacoustic cell (OPC) configuration is shown in figure 2. The OPC employed here has provision to illuminate the sample either from the rear side or from its front side. The design and fabrication details of the OPC are discussed in the next section. The rear side illumination or the so-called heat transmission configuration is used for the present investigations. The InP wafer is fixed to the top of the air chamber of OPC using vacuum grease at the edges and laser irradiation is made on its surface facing the ambient. Modulated optical radiation at 488nm from an argon ion laser

(Liconix 5000) is used as the source of excitation. The original laser beam has a $1/e^2$ diameter of 1.2mm and is used without further focusing to avoid lateral heat flow. The PA signal is produced in a small volume of air in between the sample and the microphone. The signal is detected using a highly sensitive electret microphone (Knowles BT 1834) kept in a side chamber. The phase of the signal as a function of modulation frequency of the laser beam is recorded using a dual phase digital lock-in-amplifier (Stanford Research Systems SR830). Three different laser power levels, 50mW, 100mW and 200mW, with a stability of $\pm 0.5\%$ are used for the investigations. Since one surface of the sample is highly polished and the other side is roughened, separate measurements are carried out with either face for laser irradiation.

3.5.3. Design and fabrication of an open photoacoustic cell

For the study of solid samples, a simple and sensitive OPC is designed and fabricated. In the case of a conventional OPC the sample is placed directly on top of the microphone, by leaving a small volume of gas in between the two [72,79,85,88]. Such OPCs can be employed only in the heat transmission configuration. However, the design of the OPC fabricated for the present studies allows one to illuminate the sample from both sides, *i.e.* it can be used either as an OPC or as a conventional photoacoustic cell. In order to achieve this goal the microphone is kept in a side chamber and is acoustically coupled to the main chamber through a small cylindrical cavity. The cross-sectional view of the cell is shown in figure 3. When the sample is irradiated through the glass window, it is known as the reflection configuration and in the transmission configuration irradiation has to be made at the outer surface of the sample.

The major building block of the cell is an acrylic (perspex) disk of thickness 1cm and diameter 5.5cm. The acoustic chamber is made by drilling a bore of diameter 3mm across the thickness at the centre of the disk. One end of this cylindrical hole is closed with an optical quality glass slide of thickness 1.4mm and the other end is left open. Another fine bore of diameter 1.5mm pierced at the middle of the main chamber and perpendicular to it serves as the acoustic coupler between the main chamber and the microphone. At a distance of 8mm from the main chamber the microphone is firmly glued to the orifice of the side tube. Shielded wires are used to take the electrical connections directly from the microphone. Entire system is then fixed inside a cylindrical hollow block of aluminium, leaving half the thickness of the acrylic disk outside the aluminium holder. Plate-like solid samples having uniform surface quality can be easily stick at the top of the sample chamber (open end) by using vacuum grease. On the other hand, if the sample is very thin and requires more tight contact, then another identical acrylic disk with a 3mm hole at the centre can be used to press the sample in between the two disks.

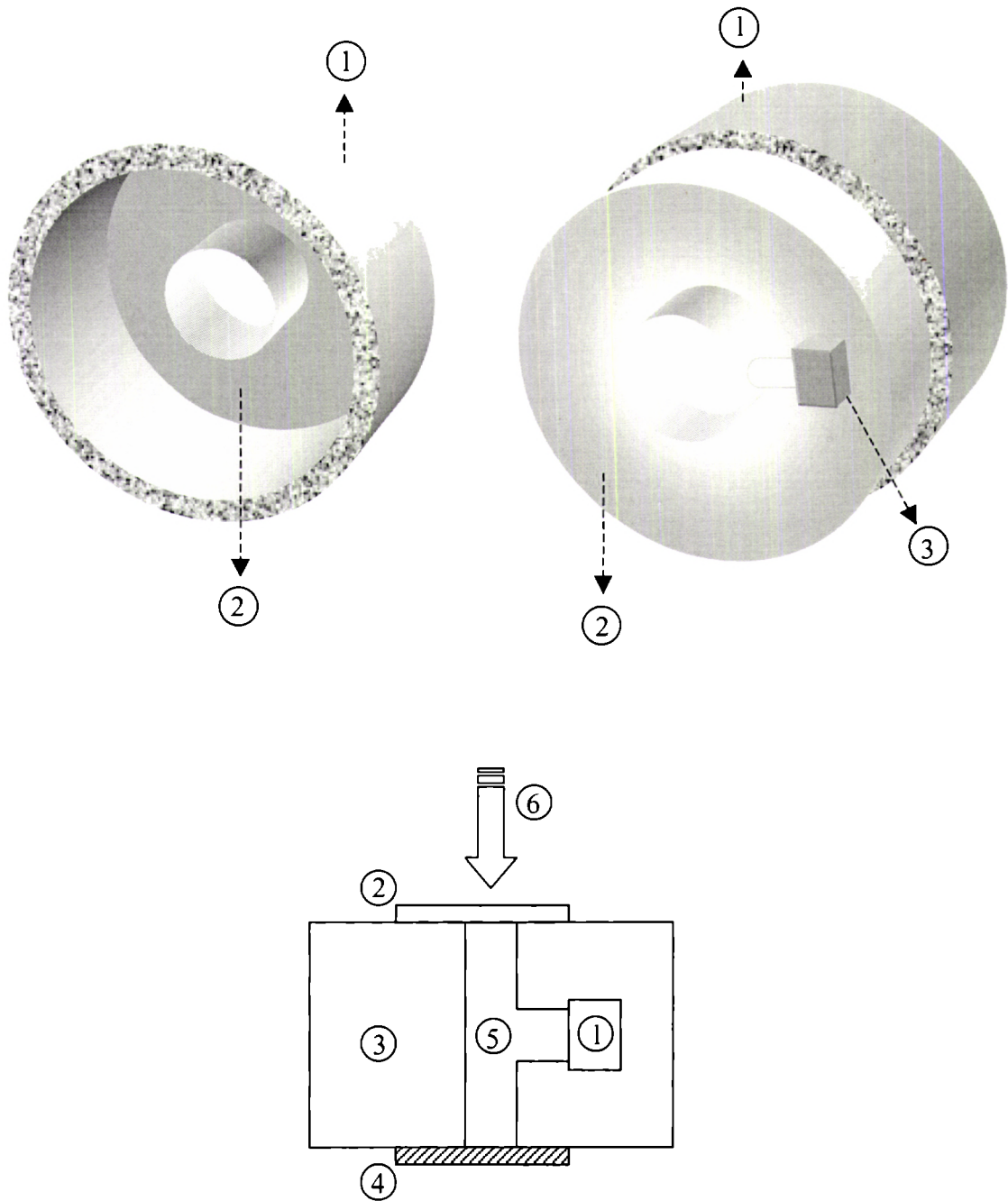


Figure 3: Cross-sectional view of the OPC. (**Top**); 1: aluminium case, 2: perspex body, 3: microphone. (**Bottom**); 1: microphone, 2: sample, 3: perspex body, 4: glass window, 5: gas chamber, 6: incident laser beam

3.5.4. InP sample

Sulphur doped n-type InP sample grown by liquid encapsulated Czochralski (LEC) method is obtained from Sumitomo electric industries (Japan). The opposite faces of the wafer have different surface qualities, one side is polished and etched whereas the other surface is pre-etched. The wafer has a thickness of 350 μm and has a carrier concentration of $4.0 \times 10^{18} /\text{cm}^3$. Square sample with dimensions 8mm by 8mm is used for the investigations.

3.5.5. Results and discussion

As indicated earlier, the heat conduction in semiconductors is mainly contributed by three factors. If the excitation energy is more than the band-gap energy of the semiconductor material, under certain experimental conditions, apart from the pure thermal wave component, the photogenerated carriers may also contribute to the heat transport in these materials. When a modulated optical radiation is incident on a semiconductor sample, the usually observed order of different thermal diffusion processes in the thermally thick regime of the sample is as follows. The pure thermal wave component dominates in the lower frequency range, followed by the heat transfer by bulk recombination process and finally the surface recombination mechanism [30,32-43].

Even though in many studies the amplitude behaviour is used for the evaluation of thermal diffusivity of solid disk like samples, the necessary condition for employing this approach is that the detector (microphone) should have flat response over the frequency range of interest. Otherwise, complicated normalisation procedures are required as reported by Nikolic *et.al* [30,34,89]. Figure 4 shows the variation of OPC signal amplitude as a function of square root of the modulation frequency. It is very clear from the plot that it no longer obeys a linear relationship as predicted by the theory. The exact reason for the deviation of the observed amplitude data from the theoretically predicted behaviour is not known. The microphone response may be a contributing factor. However, a change in response of the detector with frequency will not affect the phase data and hence the measurement of phase as a function of frequency seems to be a simpler and more reliable strategy. But, a major drawback of the phase method is that the phase plot may not obey a linear relationship as predicted by the theory when thermoelastic bending of the sample contributes significantly to the signal.

Figure 5 shows the variation of the PA signal phase with square root of the modulation frequency for the n-type InP sample. In this figure we can identify a linear portion that satisfies the equation (7). The deviation from the straight line fit in the low frequency region is obviously due to the fact that the sample is thermally thin in this regime. From the slope of the phase data in the thermally thick regime the thermal diffusivity of the sample is evaluated as $0.401 (\pm .005) \text{ cm}^2\text{s}^{-1}$. This measured value for the n-type InP is less than the thermal diffusivity $0.4569 \text{ cm}^2\text{s}^{-1}$ ($k = 0.68 \text{ Wcm}^{-1} \text{ K}^{-1}$, $\rho = 4.79 \text{ gmcm}^{-3}$, $C = 0.3107 \text{ Jgm}^{-1}\text{K}^{-1}$) of pristine InP [47,49,90-94]. The decrease in the experimentally observed value of thermal diffusivity of n-type InP can be explained in terms of the dominant phonon contribution or the pure thermal wave diffusion. Addition of the dopant adds to the scattering of the phonon which results in a reduction of the phonon mean free path and consequently a decreased thermal conductivity [47,49,51,66-68,94]. Observations discussed in the following sections also confirm this dominant phonon assisted heat diffusion mechanism in the InP sample under investigation.

This linear dependence of the phase data on the square root of the modulation frequency is an important result that has to be analysed in detail. First of all, this observation implies that the thermoelastic bending is not a contributing factor to the observed PA signal. The absence of thermoelastic bending in the present sample may be due to the fact that the InP sample has a moderately high thermal diffusivity. Then the heat generated at the irradiating surface gets transmitted quickly to the other side without leaving a considerable temperature gradient along the thickness of the specimen. Also, the thickness of the sample is sufficiently high to withstand such bending effects. But in the case of materials with low thermal diffusivity, the thermoelastic bending may dominate and in such cases appropriate corrections have to be incorporated in the calculation.

It is worthwhile to note here that in many OPC studies involving a variety of semiconductors, more complex phase behaviour with a minimum in the phase plot is reported [29,30,32-42]. This nonlinear behaviour of the phase data is attributed to bulk and surface recombination processes of photogenerated carriers in those materials. However, from figure 5 it is clear that for the present sample, the photogenerated excess carriers do not contribute to the OPC signal in any significant manner in the frequency range of investigation. This is again confirmed by recording OPC phase data for different incident laser powers, namely, 50mW, 100mW and 200mW. As can be seen from the figure, for all the pump powers the plots are exactly identical and have same slopes. This implies that the OPC signal is not influenced by the increased photogenerated carrier density at 200mW compared to that at 50mW.

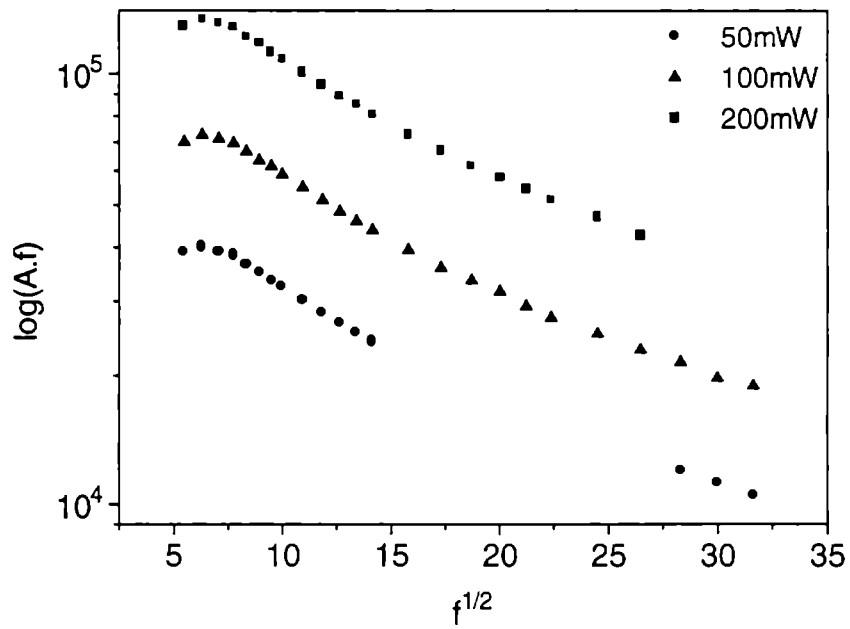


Figure 4: Semi-log plot connecting the OPC signal amplitude and \sqrt{f} for three different pump powers.

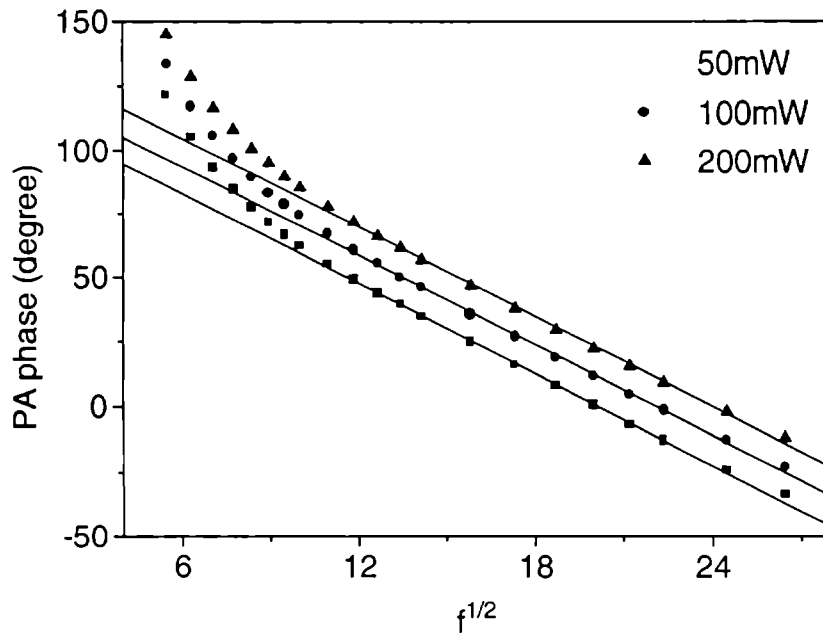


Figure 5: Variation of the OPC signal phase with \sqrt{f} for three different pump powers. Plots corresponding to different incident intensities are shifted from each other for the sake of clarity.

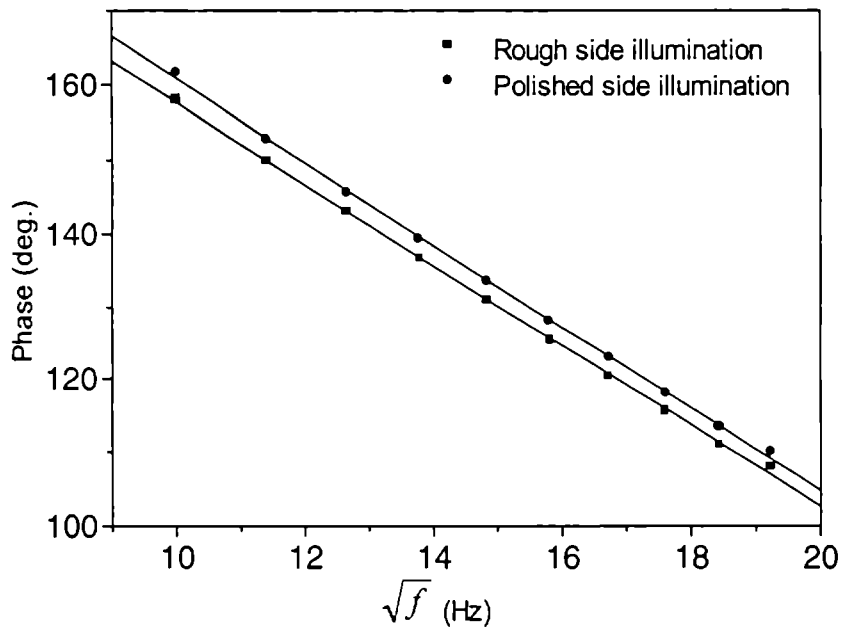


Figure 6: Variation of PA signal phase with \sqrt{f} for two different sample surface qualities.

Apart from this it is a well-known fact that the surface quality of semiconductor samples has a pronounced influence on the carrier recombination properties such as the surface recombination velocity [36,54,66-68]. In order to check whether the surface quality has any influence on the OPC phase data, two different experimental configurations are used. In the first case, the polished side of the sample is illuminated and the OPC signal is detected at the rough side and in second case the sample is turned up-side down and its rough side is illuminated and the signal is detected at the polished side. But the results obtained are again exactly identical as shown in figure 6. This again confirms that throughout the frequency range of investigations, the pure thermal wave component is the major contributing factor to heat diffusion in the present sample. If the free carriers are contributing to the OPC signal, then its influence should be visible within the frequency range of investigation [32-42].

Part B

3.6. Photothermal deflection studies on GaAs multilayers

3.6.1. Theoretical outline

The photothermal deflection (PTD) technique can be employed in different detection configurations for the investigation of solid samples [15,23,24,95]. Probe-beam deflection in the skimming configuration is one of the widely accepted and simple approaches among the PTD techniques. A schematic representation of the probe-beam skimming configuration is shown in figure 7. In this configuration, the solid disk-like sample is irradiated with a laser beam having suitable power density and the resultant refractive index gradient generated in the coupling fluid (usually a liquid) close to the sample surface is monitored using a low power probe-beam passing through this gradient. In this scheme it is assumed that the temperature distribution in the coupling fluid, very close to the sample surface, is the same as that inside the sample. The probe-beam propagating through the spatially varying refractive index gradient suffers a deflection from its normal path and the amount of deflection is determined by a number of thermal and optical parameters of the solid sample [96-107].

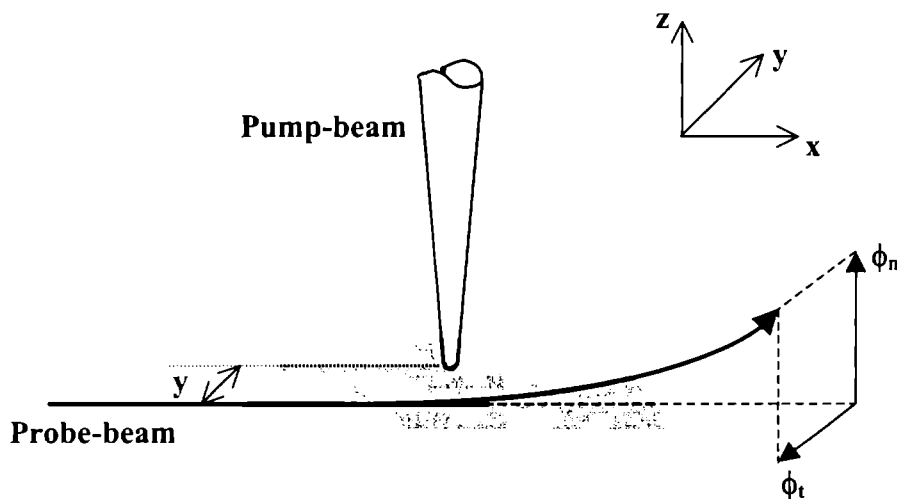


Figure 7: A schematic diagram of probe-beam skimming PTD configuration

The angle through which the probe-beam deflects from its trajectory, ϕ is given by [104-106]

$$\phi = \frac{1}{n} \frac{dn}{dT} \int_{path} \nabla_t T(r, t) ds \quad (8)$$

where "n" is the refractive index of the coupling fluid, "s" is the optical path length and ∇_t is gradient transverse to the propagation direction.

Let the probe-beam make a transverse offset "y" with respect to the pump-beam axis and a vertical offset "z" with respect to the sample surface. From figure 7, it is clear that we can split the effective deflection into two components, namely the lateral or transverse (ϕ_t) and the normal (ϕ_n) components and are given by [104]

$$\phi_t = \frac{1}{n} \frac{dn}{dT} \int_{-\infty}^{\infty} \frac{\partial T}{\partial y} dx \quad (9)$$

$$\phi_n = \frac{1}{n} \frac{dn}{dT} \int_{-\infty}^{\infty} \frac{\partial T}{\partial z} dx \quad (10)$$

The temperature field distribution, due to the pump-beam absorption, obtained by solving the heat diffusion equations in the sample as well as in the coupling fluid, leads to the evaluation of ϕ_t and ϕ_n as [106]

$$\phi_t = -\frac{1}{\pi n} \frac{dn}{dT} \int_0^{\infty} \sin(\delta y) A e^{-\beta_0 z} \delta d\delta \cdot e^{j\omega t} \quad \text{for } z > 0 \quad (11)$$

$$\phi_n = -\frac{1}{\pi n} \frac{dn}{dT} \int_0^{\infty} \cos(\delta y) A e^{-\beta_0 z} \beta_0 d\delta \cdot e^{j\omega t} \quad \text{for } z > 0 \quad (12)$$

where A is a complex integration constant, δ is the spatial Fourier transformed variable, $\beta_0 = \sqrt{\delta^2 + j\omega/D_0}$, D_0 being the thermal diffusivity of the coupling fluid.

Salazar *et.al* have analysed various theoretical and experimental conditions and arrived at certain expressions which describe a linear relationship of PTD signal phase as well as amplitude with various parameters such as pump-probe offset, height of the probe-beam above the sample surface etc [107]. For $a = b = z = 0$, where a , b and z are the pump-beam spot size, probe-beam spot size and the probe-beam height above the sample surface, there exists a linear relationship between the phase of the transverse component of the probe-beam deflection and the pump-probe offset. This linearity is found to be valid for three different configurations, (1) when the probe-beam is propagated through the same side of the sample where the pump-beam falls, (2) when the probe-beam passes through the opposite face of the sample and (3) when the probe-beam passes through the sample. The experimental configuration used in the present study is of type (1). Slope of the plot connecting the phase of the PTD signal and the pump-probe offset is given by

$$m = \frac{1}{\mu_s} = \sqrt{\pi f / \alpha_s} \quad (13)$$

Practically, the condition $a = b = z = 0$ cannot be achieved and a finite value of a , b and z may result in a change in the slope, especially when the sample has very low thermal diffusivity. But for samples having moderately high diffusivity the linear relationship will hold without any change in slope for finite values of a , b and z [107-109].

In the case of semiconductor samples, in addition to the above described pure thermal wave effect, electronic diffusion process and the carrier recombination process will also contribute to the PTD signal as in the case of photoacoustic effect. However, the additional terms arising from the carrier contributions come into the picture only at high modulation frequencies at which the pump-beam modulation time scale approaches the carrier lifetime [43]. But in the present investigation, the measurements are carried out at low modulation frequencies and hence the pure thermal wave approach is found to be sufficient for the analysis of the experimental results.

3.6.2. Photothermal deflection set-up

A dual-beam photothermal deflection technique is employed for the heat diffusion studies and for the evaluation of thermal diffusivity of n-type or p-type GaAs thin film double-layers grown on a semi-insulating GaAs substrate. Continuous wave laser emission at 488nm from a water-cooled argon ion laser (Liconix 5000) is used as the pump-beam. The original laser beam has a $(1/e^2)$ diameter of 1.2mm. In all the measurements a laser power of 50mW ($\pm 0.5\%$) is used. The excitation laser energy, 2.54eV, is very high compared to the band gap energy, 1.43eV, of GaAs and hence the sample is optically opaque at the excitation wavelength. Carbon tetrachloride (CCl_4) is used as the coupling fluid to the sample, which is the most suitable and commonly used coupling fluid in photothermal deflection studies. The significant parameters that make CCl_4 a potential coupling fluid in photothermal deflection technique are its low values of thermal conductivity, $k = 0.099 \text{ Wm}^{-1}\text{K}^{-1}$; specific heat capacity $C_p = 0.85 \text{ Jg}^{-1}\text{K}^{-1}$ and thermal diffusivity, $\alpha = 7.31 \times 10^{-4} \text{ cm}^2\text{s}^{-1}$. Another important parameter that favours the use of CCl_4 is its very high rate of change of refractive index with respect to temperature, $(dn/dT) = 6.12 \times 10^{-4} \text{ K}^{-1}$, compared to many other liquids [110-111]. The sample is placed horizontally at the bottom of a quartz cuvette having dimensions 10mm \times 10mm \times 40mm and CCl_4 is filled in the cuvette up to a height of about 10mm above the sample surface.

A schematic view of the experimental set-up is depicted in figure 8. The cuvette containing the sample is firmly fixed on a heavy stand. An argon ion laser beam is focussed on to the sample surface using a convex lens of focal length 20cm. The pump-beam spot size at the

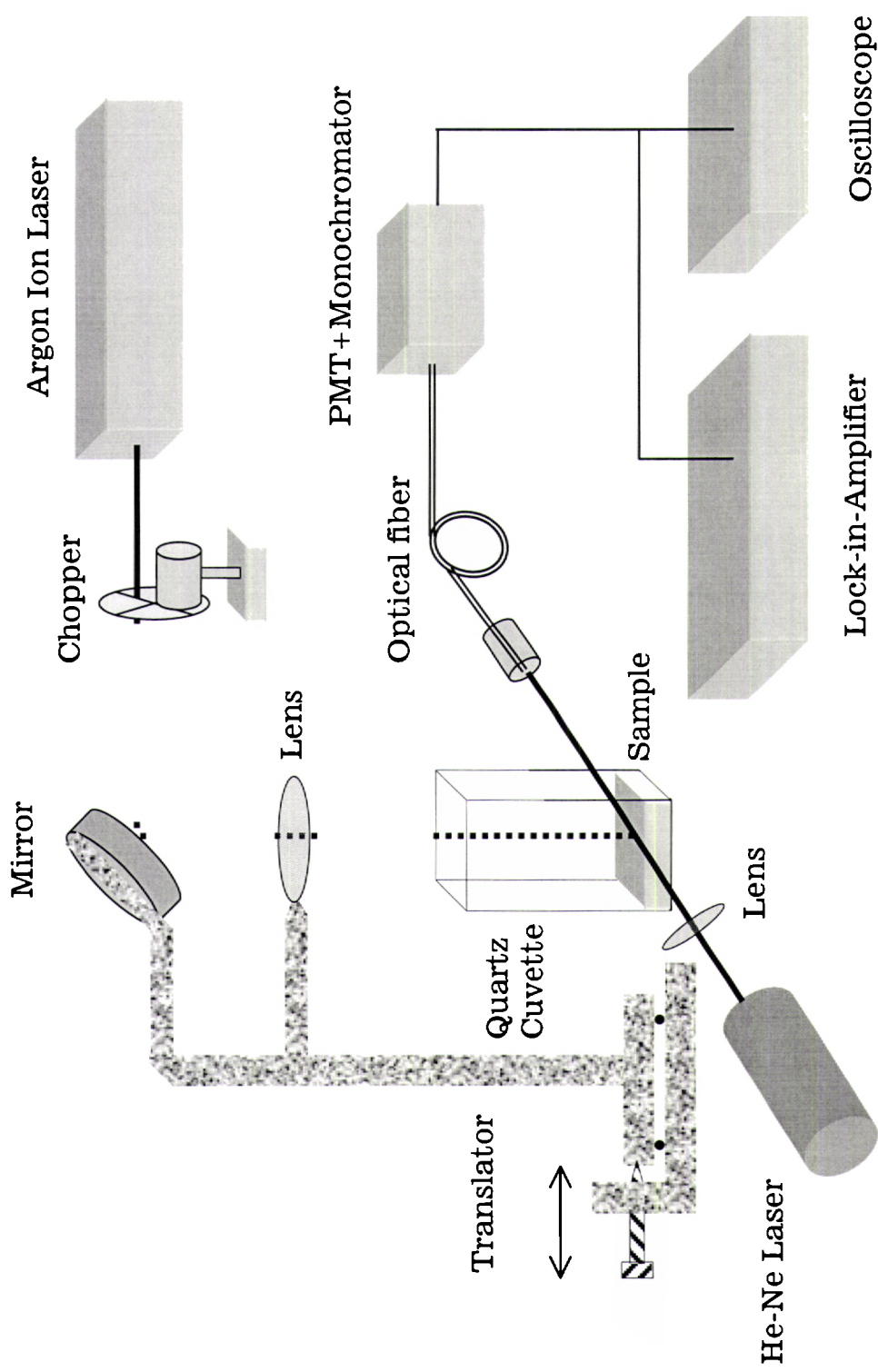


Figure 8: Schematic diagram of dual-beam photothermal deflection set-up

sample surface is estimated to be $102\mu\text{m}$. The mirror and the lens are fixed on an XY translator and the translator is positioned in such a way that the centre of the mirror, lens and the cuvette are in a vertical line, the Z-axis. Under this experimental arrangement, the pump-beam position on the sample can be accurately varied along the X-direction by simply moving the translator in the X-direction. The resolution of the translator scale is $10\mu\text{m}$. A mechanical chopper (Stanford Research systems SR540) is placed in the pump-beam path for modulating the pump-beam intensity at any desired frequency.


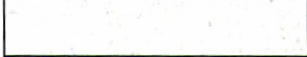

A low power (3mW) He-Ne laser emitting at 632.8nm is used as the probe-beam to detect the strength and profile of the refractive index gradient generated in the CCl_4 , very close to the pump-beam irradiation site at the sample surface. The probe laser beam with a gaussian profile and having a $(1/e^2)$ diameter of $800\mu\text{m}$ is focused using a double convex lens of focal length 10cm . The probe-beam spot size at the point where it crosses the pump-beam is estimated to be $101\mu\text{m}$. The probe laser is arranged in such a fashion that it just skims through the surface of the sample and it propagate in a direction (Y-axis) orthogonal to that of the pump-beam (Z-axis).

A plastic fiber having a circular core of diameter 1mm is used as position sensitive detector to monitor the periodic deflection suffered by the probe-beam. One end of the fiber is firmly fixed on an XYZ translator at a distance of 15cm from the sample. The other end of the fiber is coupled to a 0.25m monochromator (McPherson) tuned to the probe-beam wavelength. This ensures a perfect elimination of stray light, including the scattered pump-beam, from reaching the detector. A photomultiplier tube is coupled to the exit slit of the monochromator. The output of the photomultiplier tube is fed to a dual phase digital lock-in-amplifier, through an impedance matching circuit. A storage oscilloscope is also connected to the photomultiplier tube output in parallel to the lock-in-amplifier. This is done to optimise the position of the pump-beam, probe-beam, sample and the detector to ensure a perfect distortion free signal. The entire experimental set-up is laid out on a moderately vibration-isolated table to protect from the ambient vibrations. Whole measurements are carried out at a pump-beam modulation frequency of 10.6Hz and the probe-beam height above the sample surface is kept as minimum as possible to get non-diffracted (from the sample edge) signal. At high modulation frequencies the noise contribution from various background sources are observed to suppress the PTD signal and consequently accurate measurements are not possible in the high frequency region.

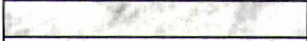
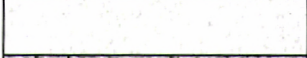

3.6.3. GaAs thin film sample specifications

Both n-type and p-type GaAs thin films grown on a semi-insulating GaAs substrate are used for the investigations. The thin films are grown by molecular beam epitaxy (MBE) method (Technical University of Eindhoven, The Netherlands). Each of the samples contains two epitaxial layers. The sample structure together with the specifications of each layer, including the growth conditions and dopants are given in figure 9.


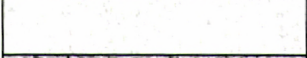

Sample 1

Si doped GaAs		$l = 0.25 \mu\text{m}, n = 3.6 \times 10^{14}/\text{cm}^3, T = 580 \text{ }^\circ\text{C}$
Si doped GaAs		$l = 10.00 \mu\text{m}, n = 3.6 \times 10^{14}/\text{cm}^3, T = 630 \text{ }^\circ\text{C}$
Semi-insulating GaAs		$l = 400.0 \mu\text{m}$

Sample 2

Si doped GaAs		$l = 0.20 \mu\text{m}, n = 2.0 \times 10^{16}/\text{cm}^3, T = 610 \text{ }^\circ\text{C}$
Si doped GaAs		$l = 2.80 \mu\text{m}, n = 2.0 \times 10^{16}/\text{cm}^3, T = 695 \text{ }^\circ\text{C}$
Semi-insulating GaAs		$l = 400.0 \mu\text{m}$

Sample 3

Si doped GaAs		$l = 0.20 \mu\text{m}, n = 2.0 \times 10^{18}/\text{cm}^3, T = 610 \text{ }^\circ\text{C}$
Si doped GaAs		$l = 1.80 \mu\text{m}, n = 2.0 \times 10^{18}/\text{cm}^3, T = 695 \text{ }^\circ\text{C}$
Semi-insulating GaAs		$l = 400.0 \mu\text{m}$

Sample 4




Be doped GaAs		$l = 0.20 \mu\text{m}, p = 2.0 \times 10^{18}/\text{cm}^3, T = 610 \text{ }^\circ\text{C}$
Be doped GaAs		$l = 1.80 \mu\text{m}, p = 2.0 \times 10^{18}/\text{cm}^3, T = 695 \text{ }^\circ\text{C}$
Semi-insulating GaAs		$l = 400.0 \mu\text{m}$

Figure 9: Structure and properties of the doped GaAs epitaxial layers on the semi-insulating GaAs substrate. Here, l corresponds to the thickness of each layer, n (p) represents the electron (hole) concentration and T is the substrate temperature at which the layers are grown.

3.6.4. Results and discussion

Photothermal deflection (PTD) measurements are carried out independently by irradiating either the thin film side or the substrate side of the samples. In PTD technique, there exist various experimental approaches to evaluate the thermal diffusivity of solids and the strategy used in the present investigation is the measurement of PTD signal phase as a function of pump-probe offset at a fixed modulation frequency in the probe-beam skimming configuration [15,105-106]. In order to achieve this goal the probe-beam as well as the position sensitive detector and the sample are firmly fixed at a particular position and the pump-beam irradiation site is varied from one side of the probe-beam to the other side. Typical variation of the signal phase with the pump-probe offset for *sample 3* when the semi-insulating GaAs substrate side is facing the pump-beam is shown in figure 10. The minimum in the phase plot corresponds to the zero offset or when the pump and probe beams cross each other. Figure 11 (a) and (b) projects the linear portion of figure 10 and from the slope of these plots the thermal diffusivity of the substrate is evaluated using the relation given by equation (13). The measured value of α , calculated from the average of two slopes, is given in table I. We have seen in the previous section regarding the heat conduction in doped semiconductors that the photogenerated free-carrier recombination processes also contribute to heat transport in these materials. But in the case of intrinsic semiconductors, similar to dielectrics, only the phonons contribute to the heat transport due to the very low free-carrier density in these materials [66-68].

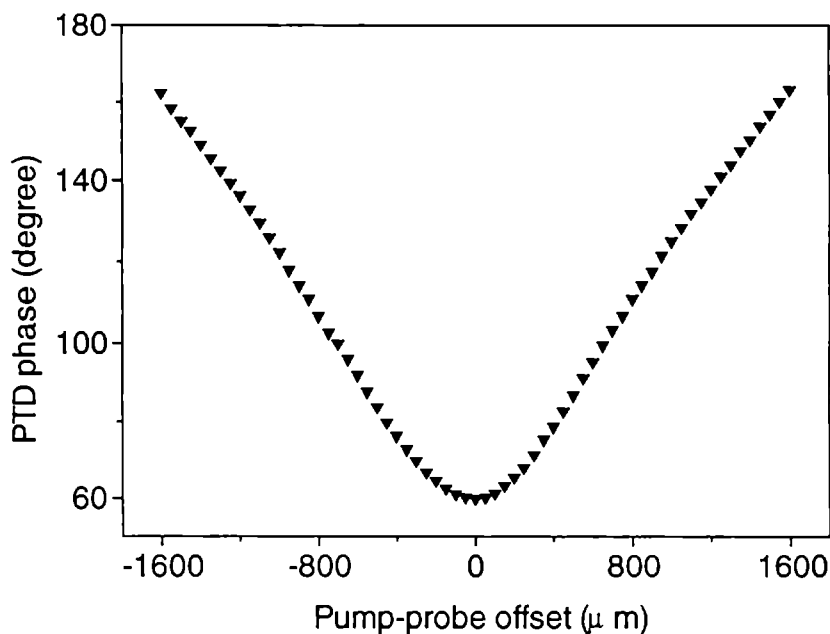


Figure 10: Variation of PTD signal phase with pump-probe offset for *sample 3* (substrate side).

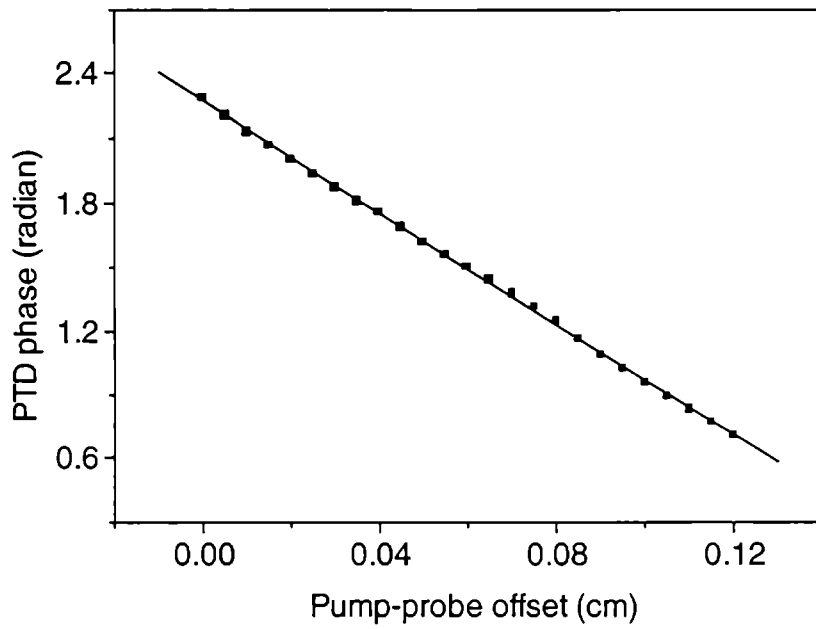


Figure 11(a): Variation of PTD signal phase with pump-probe offset for *sample 3* (substrate side). Here probe is on the left side of the pump.

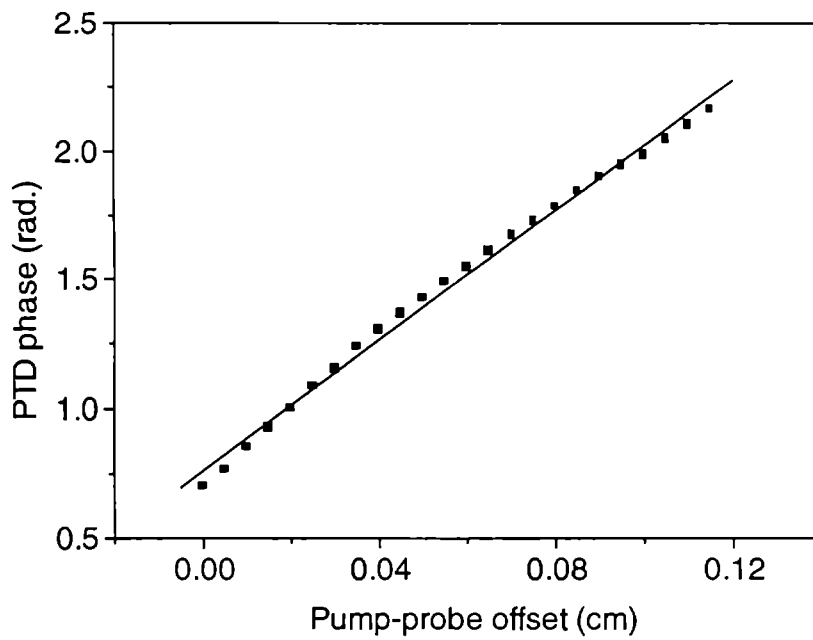


Figure 11(b): Variation of PTD signal phase with pump-probe offset for *sample 3* (substrate side). Here probe is on the right side of the pump.

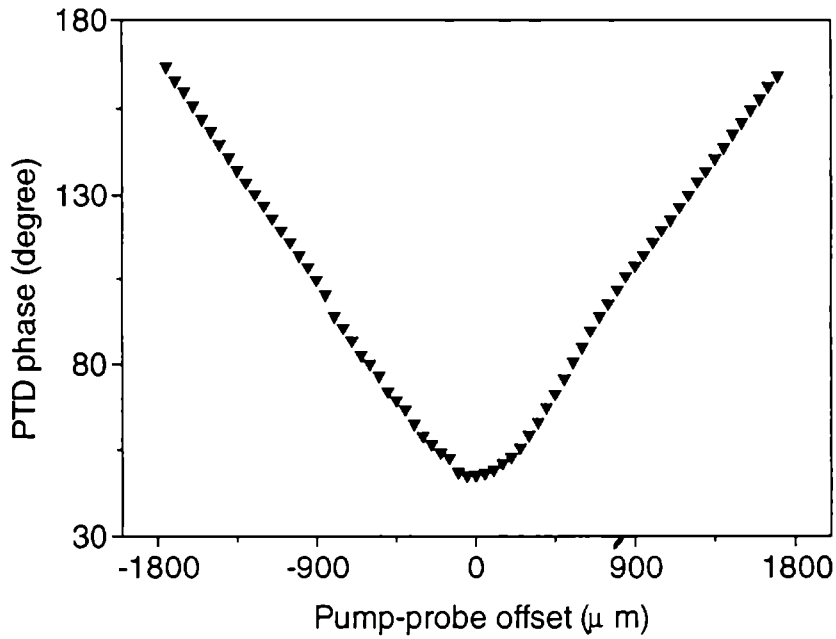


Figure 12: Variation of PTD signal phase with pump-probe offset for *sample 3* (film side).

Figure 12 shows the variation of PTD signal phase with the pump-probe offset for *sample 3* when the thin film side is facing the pump-beam. The n-type epitaxial layers have moderately high carrier concentrations (see figure 9) and the parameter that differentiate one layer from the other is only the temperature at which they are grown, which has some significant role in determining the thin film properties. The pure thermal wave component of the PTD signal arises from the instantaneous intraband electron-phonon interaction. Thermal energy will also be released by nonradiative recombination of the photoexcited carriers which are diffused into the semiconductor. This is the electronic component of heat transport. Fournier *et.al* have made a rigorous theoretical and experimental analysis in this regard and have proved that at very low frequencies, *i.e.* when $\omega\tau \ll 1$, only the pure thermal wave component contributes to the PTD signal and consequently the signal behaviour (both amplitude and phase) is characterised by the thermal diffusivity of the sample [43]. Here, $\omega = 2\pi f$ where f is the pump beam modulation frequency and τ is the minority-carrier lifetime.

On the other hand, when the pump-beam modulation time scale is much shorter than the minority-carrier lifetime, *i.e.* when $\omega\tau \gg 1$, the contribution from pure thermal wave component drops off and the PTD signal is now due to electronic processes. In this regime the signal behaviour is characterised by the electronic diffusivity. Usually, minority-carrier lifetime for n-type GaAs is of the order of microseconds and for p-type GaAs it is as low as nanoseconds

[47,49,94]. Hence, at a modulation frequency of 10.6Hz (=94ms), we are far away from the requirement for the contribution from electronic diffusion and recombination to PTD signal. Intuitively, the PTD signal variation shown in the figure 12 is determined by the pure thermal wave component. Figure 13 (a) and (b) projects the linear portion of the figure 12 and from the slope of these plots the thermal diffusivity of the sample is evaluated using the relation given by equation (13). The measured value of α , when the thin film side is facing the pump beam, is given in table I. Here, the thickness of the thin films are too small compared with the thermal diffusion length and hence the tabulated thermal diffusivity value is expected to be the effective diffusivity of the thin films and that of the substrate.

Figures 14 to 16 shows the variation of PTD signal phase with the pump-probe offset for the other samples (*sample 1, 2 and 4*) with either the thin film side or the substrate side facing the pump-beam. The thermal diffusivity values evaluated in each case are tabulated in table I. Though the observed thermal diffusivity values vary from sample to sample, it is rather difficult to arrive at a general conclusion regarding the heat transport in these multi-layer samples since more than one physical parameter of the thin film samples are different for different epitaxial layers. However, almost identical α values for the substrate side of all the four samples indicates that the thin film epitaxial layers grown on the other surface of the substrates have no influence on the measured PTD signal. The literature values of α of GaAs is in the range $0.2 \text{ cm}^2\text{s}^{-1}$ to $0.36 \text{ cm}^2\text{s}^{-1}$ [47,49,94,112,113] and the experimentally observed values also falls within this range. The wide range of α values reported in the literature is due to the large variation of thermal transport properties of semiconductor materials with the growth condition, defects etc. But, the decrease of α values of the epitaxial layers to a still lesser value points to some interesting but complex heat transport mechanisms in these samples. Though only phonons are contributing to the heat transport in the frequency value of investigation, the increased scattering centers arising from doping of GaAs with either Si or Be and the consequent reduction of phonon mean free path does not seem to be the only reason for the noticeable reduction in the diffusivity values of the epitaxial layers. The thin film layers are thermally very thin and hence the measured α values may be an effective diffusivity of the two epitaxial layers and the substrate layer. Recently, a number of research papers have come out with experimental observation of substantial reduction (up to 50%) in lattice thermal conductivity in semiconductor thin films, when the thin film thickness is of the order of the phonon mean-free-path [113-117].

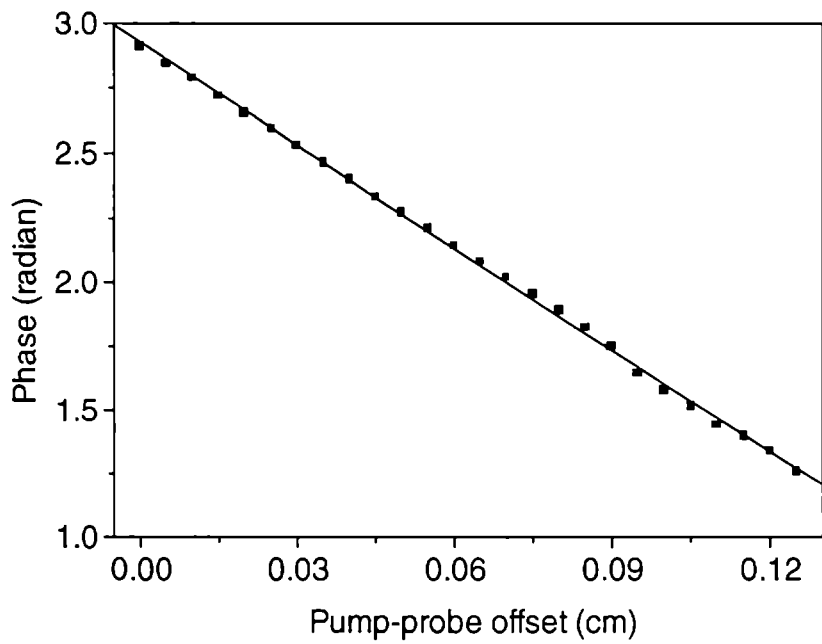


Figure 13(a): Variation of PTD signal phase with pump-probe offset for *sample 3* (film side). Here probe is on the left side of the pump.

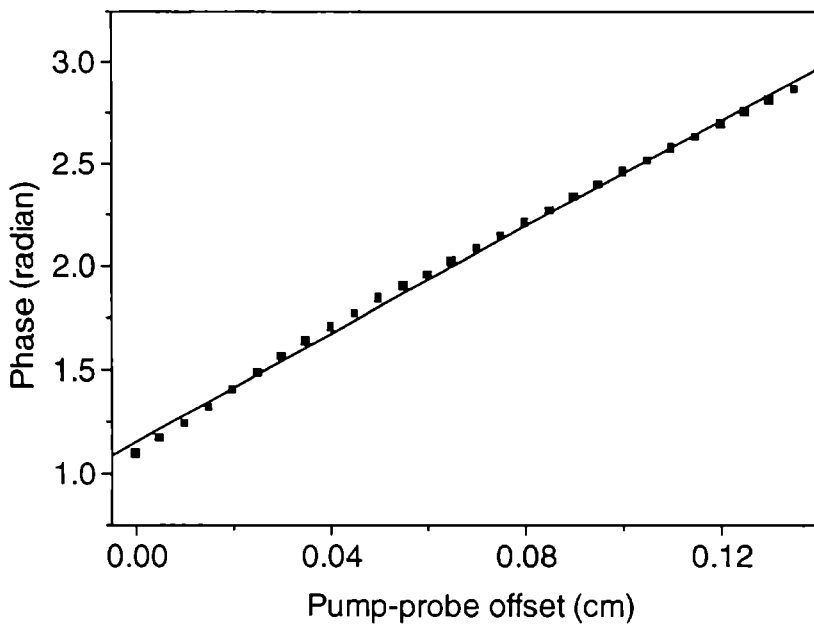
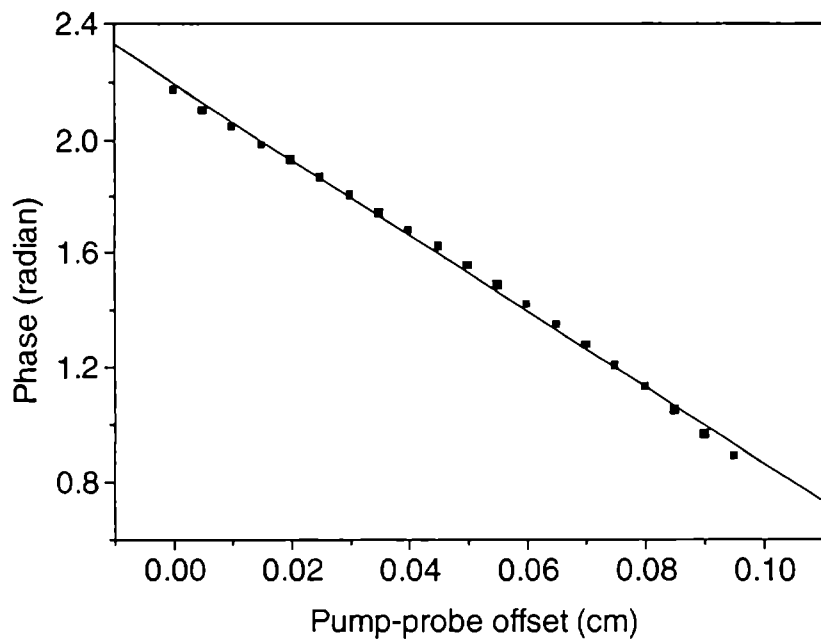
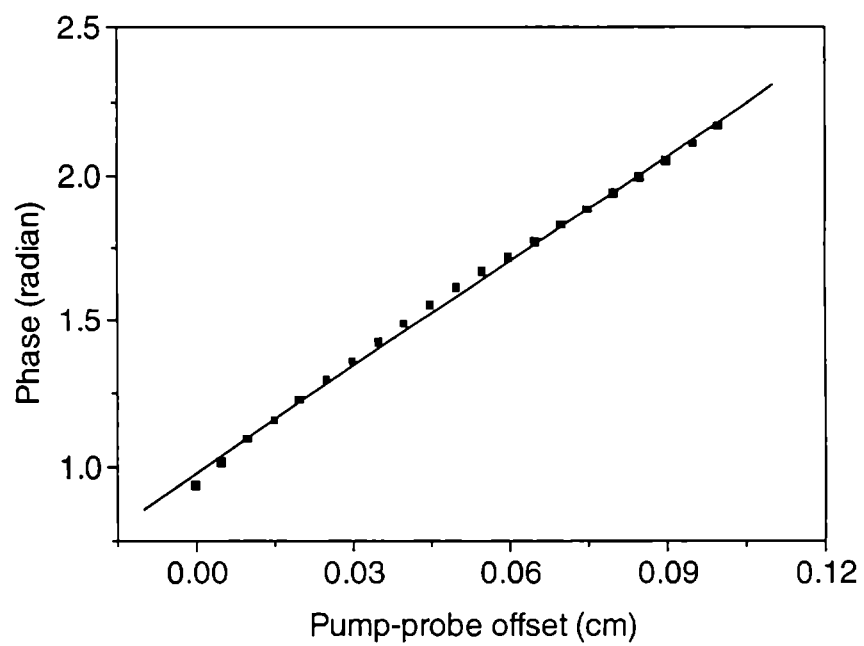


Figure 13(b): Variation of PTD signal phase with pump-probe offset for *sample 3* (film side). Here probe is on the right side of the pump.

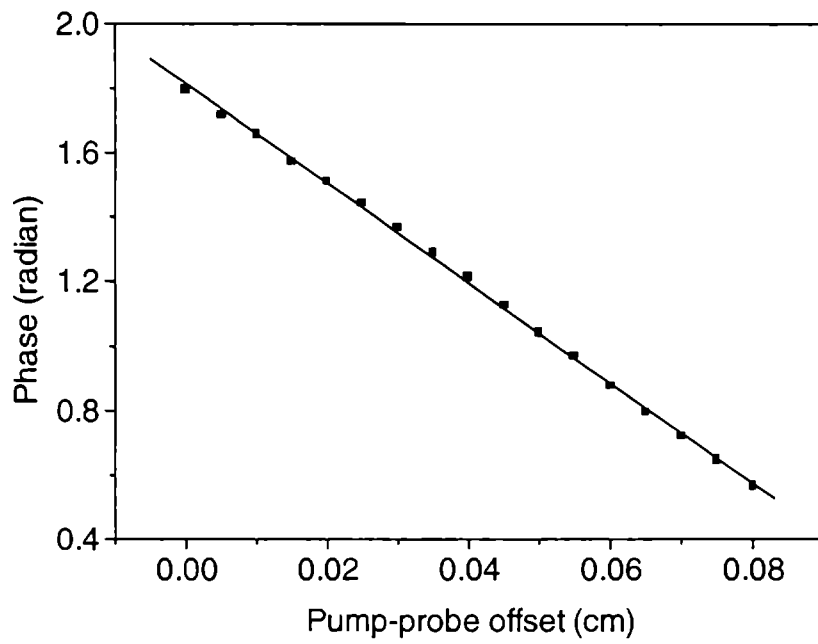


(a)

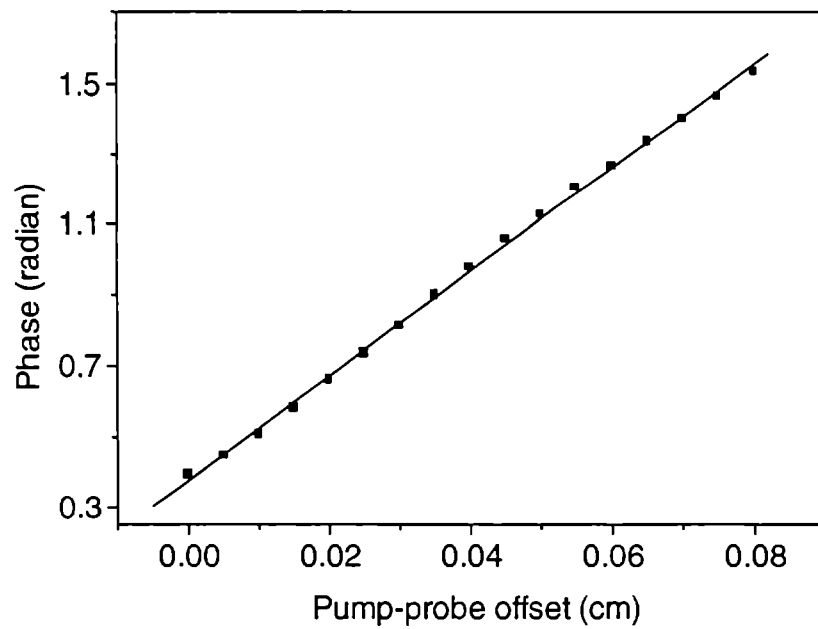


(b)

Figure 14 (a, b): Variation of PTD signal phase with pump-probe offset for *sample 1* (film side). Here, probe is on the left side (a) of the pump and right side (b) of the pump beam.

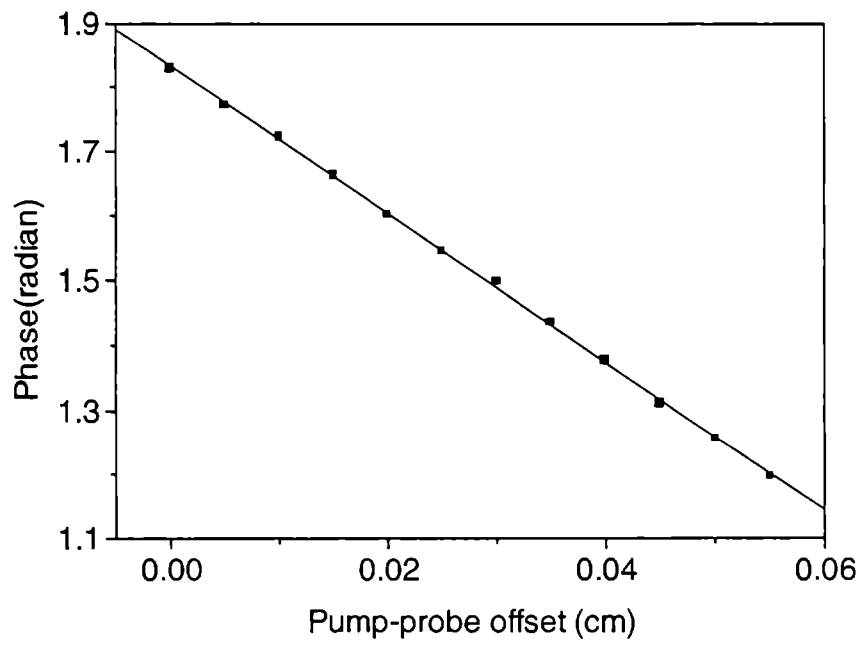


(c)

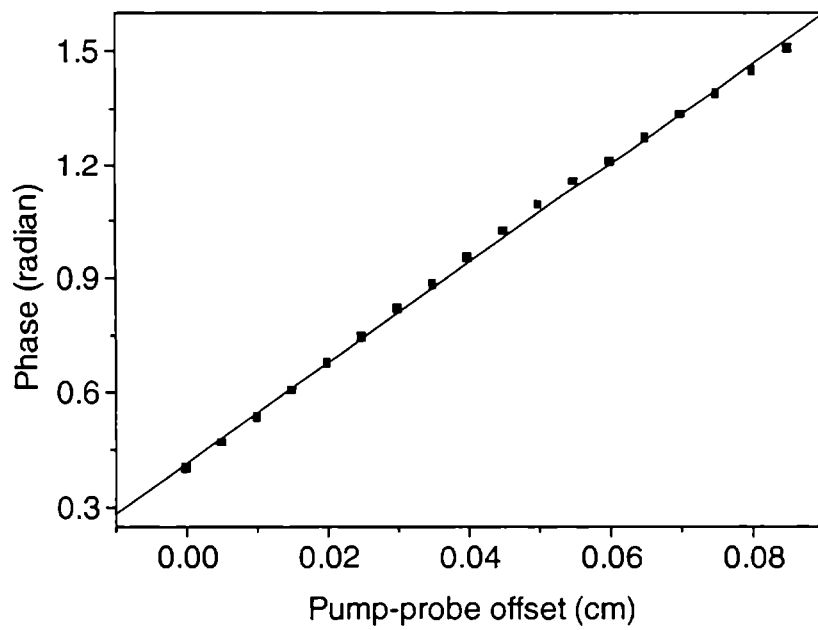


(d)

Figure 14 (c, d): Variation of PTD signal phase with pump-probe offset for *sample 1* (substrate side). Here, probe is on the left side (c) of the pump and right side (d) of the pump beam.



(a)



(b)

Figure 15 (a, b): Variation of PTD signal phase with pump-probe offset for *sample 2* (film side). Here, probe is on the left side (a) of the pump and right side (b) of the pump beam.

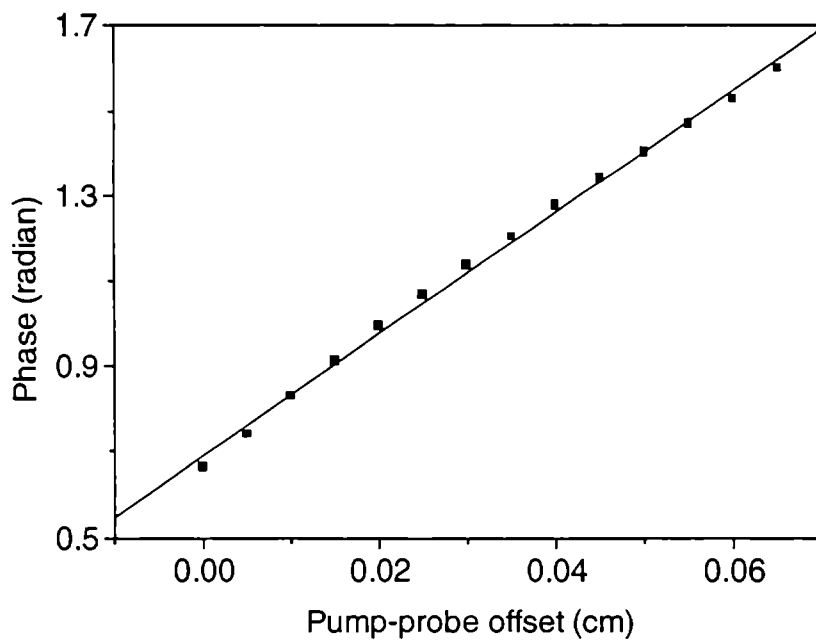
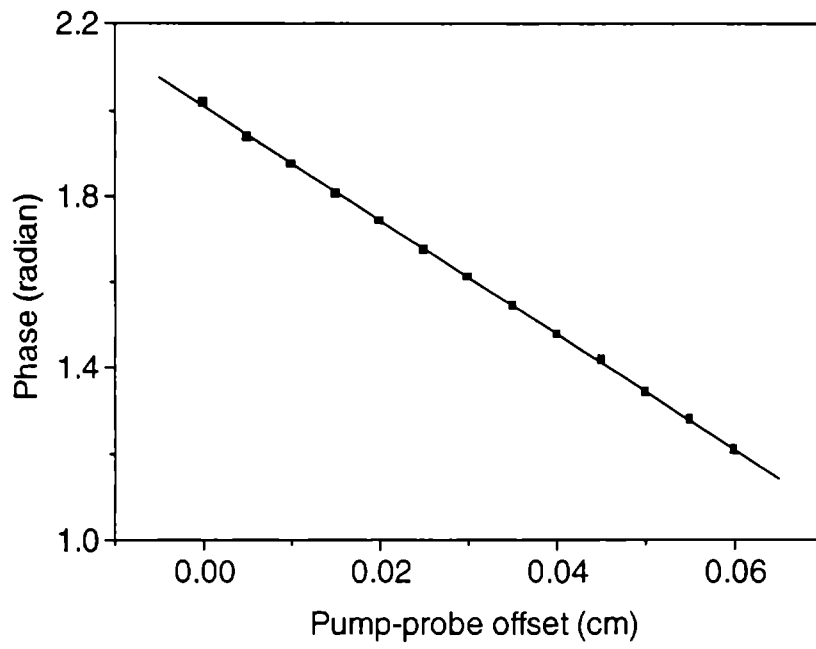
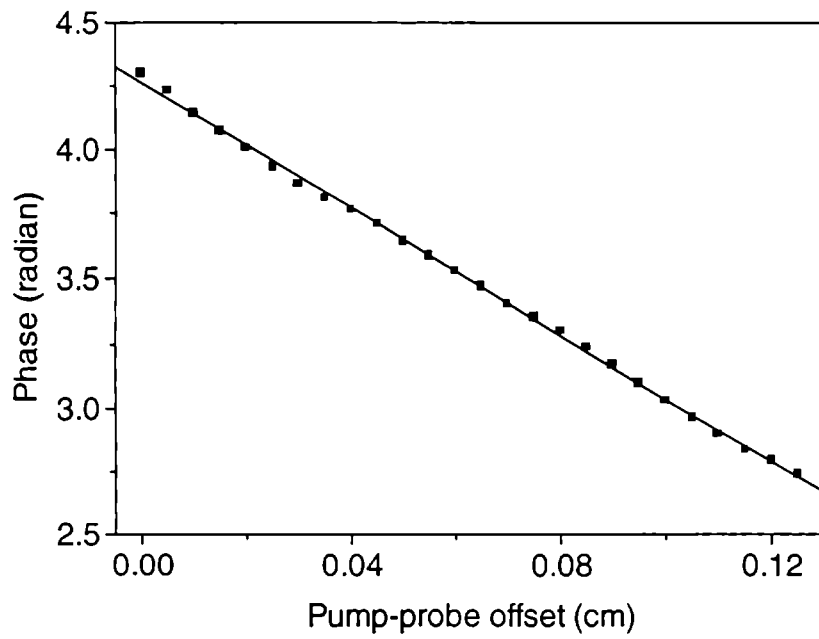
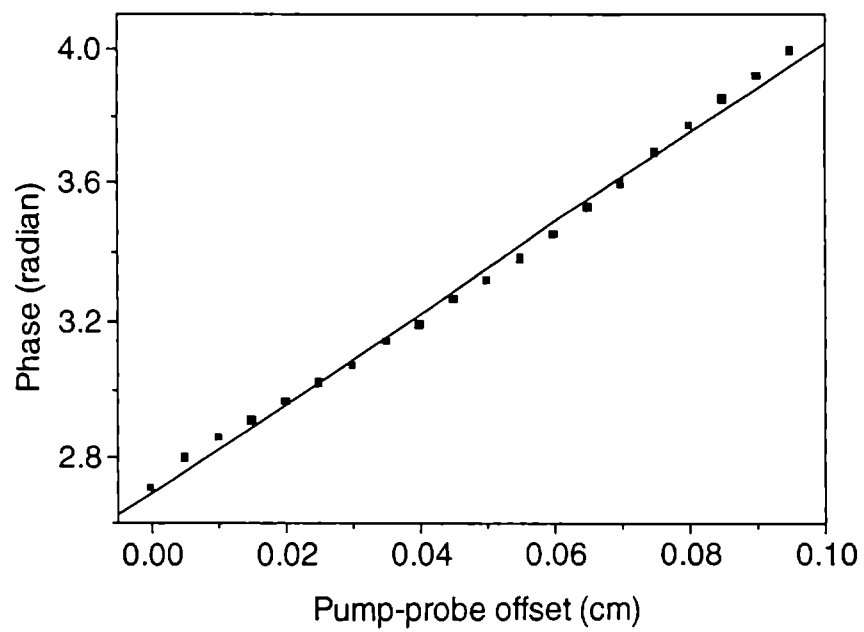


Figure 15 (c, d): Variation of PTD signal phase with pump-probe offset for *sample 2* (substrate side). Here, probe is on the left side (c) of the pump and right side (d) of the pump beam.

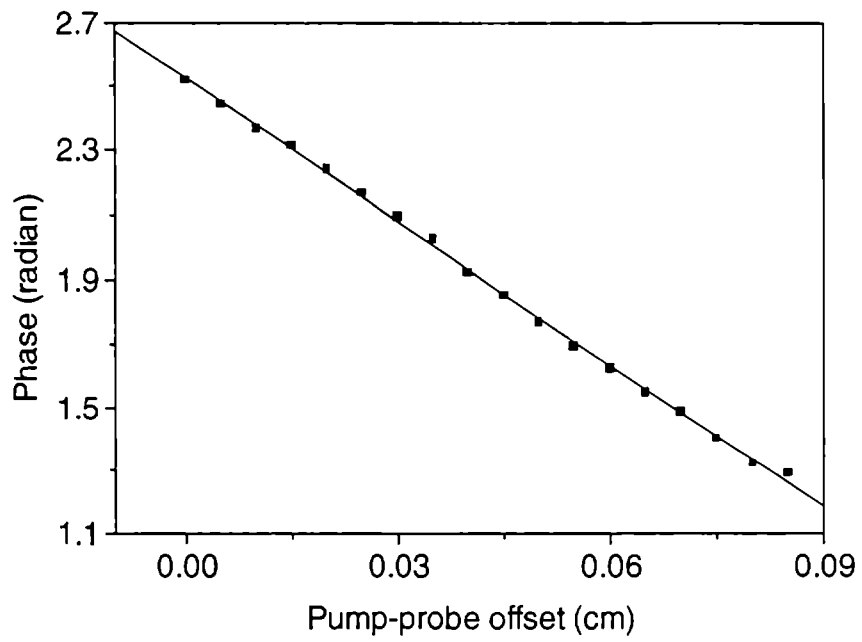


(a)

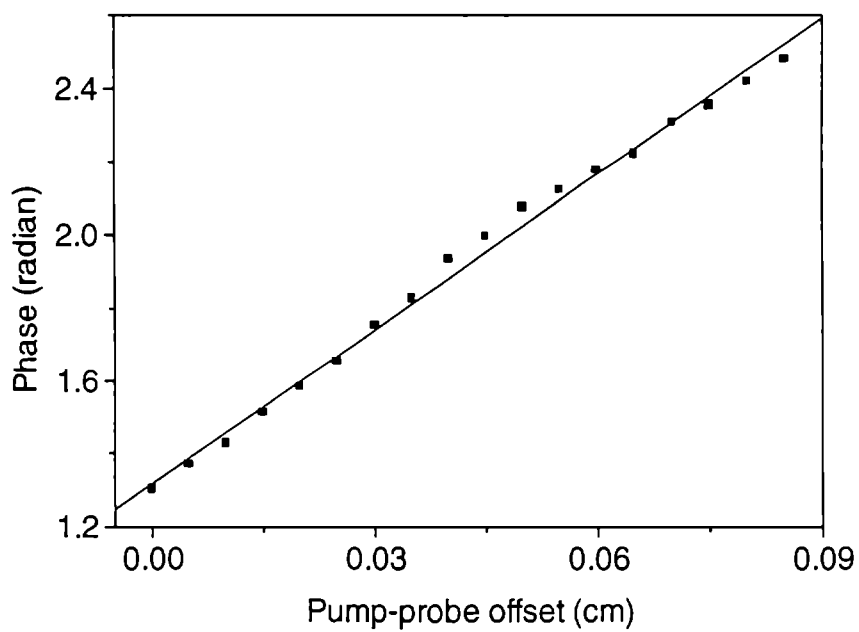


(b)

Figure 16 (a, b): Variation of PTD signal phase with pump-probe offset for *sample 4* (film side). Here, probe is on the left side (a) of the pump and right side (b) of the pump beam.



(c)



(d)

Figure 16 (c, d): Variation of PTD signal phase with pump-probe offset for *sample 4* (substrate side). Here, probe is on the left side (c) of the pump and right side (d) of the pump beam.

Table I: The thermal diffusivity values of GaAs multi-layers evaluated using PTD technique

Sample	Thermal diffusivity α in cm^2s^{-1}	
	Film	Substrate
Sample 1	0.165	0.210
Sample 2	0.187	0.212
Sample 3	0.193	0.212
Sample 4	0.160	0.206

However, no such conclusions are possible with the present data since the exact values of phonon mean-free-path of the samples investigated are not available. Moreover, there exists a large discrepancy between the experimentally observed value of phonon mean-free-path and that evaluated theoretically. For example, in a very recent paper, Ju *et.al* have measured the effective phonon mean-free-path in Si as 300nm while that evaluated using the kinetic theory is only 43nm [114]. However, a kinetic theory expression can be used to evaluate the phonon mean-free-path in the bulk sample Λ_{bulk} as

$$\Lambda_{bulk} = \frac{3k_{bulk}}{Cv} \quad (14)$$

where k_{bulk} is the bulk thermal conductivity, C is the volumetric heat capacity and v is the speed of sound in the material. For bulk GaAs, $k_{bulk} = 0.46\text{W/cm}\cdot^\circ\text{C}$, $C = 0.33\text{J/g}\cdot^\circ\text{C}$, and $v \approx 4.0 \times 10^5\text{cm/s}$, which leads to the estimation of phonon mean-free-path approximately as 100nm [47,49,94,112]. This value is smaller than the surface layer thickness of 200nm or 250nm of the samples. However, the estimated value of phonon mean-free-path need not be strictly true and hence any analysis of the observed thermal diffusivity data without knowing the exact value of Λ_{bulk} is meaningless.

3.7. Conclusions

Two most commonly used and powerful non-destructive and non-contact analytical methods, namely the photoacoustic and photothermal deflection techniques, have been successfully implemented for the thermal characterisation of certain compound semiconductor materials. The thermal diffusivity of n-type InP is evaluated from the phase data of the photoacoustic signal under heat transmission configuration. By employing this approach and using the pure one-dimensional heat flow model of Rosencwaig and Gersho one can easily evaluate the thermal diffusivity of solid disk-like materials having moderately high diffusivity values. The results of the present investigation show that even in the case of semiconductor samples this simple and direct approach can be applied for the thermal diffusivity measurements, provided the investigations are to be done in the frequency region where the pure thermal wave component is the major contributing factor to the signal. The observation of the absence of thermoelastic bending in the case of thick InP wafer is quite reasonable and it is expected that many of the semiconductor materials will behave in this manner as most of them have moderately high thermal diffusivity values.

Dual-beam photothermal deflection technique offers a novel means of measuring the thermal diffusivity of thin films grown on bulk substrates. PTD measurements carried out on GaAs multi-layer samples prove that by employing this approach it is possible to appraise the thermal diffusivity of the substrate alone, without the influence of the thin films grown over its surface. But if the thickness of the thin film(s) is small, such that the thermal diffusion length is much greater than the film thickness, then the evaluated diffusivity value will be only the effective diffusivity of the film(s) and the substrate. In addition to this, very complex thermal wave scattering mechanisms such as the phonon scattering at the interfaces may also have a key role in determining the thermal diffusivity of the thin film(s), especially when the film thickness approaches the phonon mean-free-path.

Compared to the photoacoustic technique, the photothermal deflection method is more complicated and sensitive to ambient conditions such as vibration of the experimental set-up, properties of the coupling fluid etc, which suggests that a very careful experimental arrangement is required for the latter technique. But in the study of materials like thin films coated on bulk substrates the PTD method is more suitable since the irradiation and detection can be easily performed on the same side of the sample.

References

1. Thompson.D.O and Chimenti.D.E (Eds.), *Review of Progress in Quantitative Nondestructive Evaluation*, Vol. 4B, (Plenum Press, New York) (1985)
2. Wang.C and Mandelis.A, *J. Appl. Phys.* **85**, 8366(1999)
3. Christofides.C, Diakonou.F, Seas.A, Christou.C, Nestoros.M and Mandelis.A, *J. Appl. Phys.* **80**, 1715 (1996)
4. Wagner.R.E and Mandelis.A, *Semicond. Sci. Technol.* **11**, 289 (1996)
5. Batista.J.A, Mansanares.A.M, da Silva.E.C, Pimentel.M.B.C, Jannuzzi.N and Fournier.D, *Sensors & Actuators: A. Physical*, **71**, 40 (1998)
6. Wagner.R.E and Mandelis.A, *Semicond. Sci. Technol.* **11**, 300 (1996)
7. Dacal.L.C.O, Mansanares.A.M and da Silva.E.C, *J. Appl. Phys.*, **84** (7), 3491 (1998)
8. Mandelis.A, Othonos.A, Christofides.C and Boussey-Said.J, *J. Appl. Phys.* **80** (9), 5332 (1996)
9. Salnick.A, Mandelis.A and Jean.C, *Appl. Phys. Lett.* **69** (17), 2522 (1996)
10. Batista.J.A, Mansanares.A.M, da Silva.E.C, Fournier.D, *J. Appl. Phys.* **82**(1), 423 (1997)
11. Mandelis.A, Nestoros.M and Christofides.C, *Opt. Eng.* **36** (2), 459 (1997)
12. Salnick.A, Mandelis.A, Ruda.H and Jean.C, *J. Appl. Phys.* **82**, 853 (1997)
13. Mandelis.A, *Solid State Electron.* **42**, 1 (1998)
14. Ikari.T, Salnick.A and Mandelis.A, *J. Appl. Phys.* **85**, 7392 (1999)
15. Sell.J.A, *Photothermal investigations of solids and fluids*, (Academic Press, boston) (1989)
16. Hess.P (Edit.), *Photoacoustic, photothermal and photochemical processes in Gases*, (Springer-Verlag, Berlin) (1989)
17. Rosencwaig.A, *Photoacoustics and photoacoustic spectroscopy*, (John Wiley & Sons, New York) (1980)
18. Pao.Y-H (Edit.), *Optoacoustic spectroscopy and detection*, (Academic press, New York) (1977)
19. Amato.G, Benedetto.G, Boarino.L, Brunetto.N and Spagnolo.R, *Opt. Eng.* **36** (2), 423 (1997)
20. Bertolotti M, Dorogan V, Liakhov G, Voti RL, Paoloni S, Sibilia C, *Rev.Sci.Instru.* **68**, 1521 (1997)
21. Ambacher O, Rieger W, Ansmann P, Angerer H, Moustakas TD, Stutzmann M, *Sol. Stat. Comm.* **97**, 365 (1996)

22. Mandelis.A (Edit.), *Photoacoustic and Thermal Wave Phenomena in Semiconductors*, (North Holland, New York) (1987)
23. Hess.P and Pelzl.J (Eds.), *Photoacoustic and photothermal phenomena*, (Springer-Verlag, Berlin) (1988)
24. Bicanic.D (Edit.), *Proceedings of seventh international topical meeting on photoacoustic and photothermal phenomena*, (Doorwerth, The Netherlands) (1991)
25. Luscher.E, Korpiun.P, Coufal.H and Tilgner.R, *Photoacoustic effect: principles and applications*, (Friedr.Vieweg & Sohn, Braunschweig) 1984.
26. Hess.P (Edit.) *Photoacoustic and photothermal processes at surfaces and thin films*, (Springer-Verlag, Berlin) 1989.
27. Cesar.C.L, Vargas.H, Filho.J.M and Miranda.L.C.M, *Appl.Phys.Lett.* **43**, 555 (1983)
28. Delgadillo.I, Orea.A.C, Vargas.H, Calderon.A, Alvarado-Gil.J.J and Miranda.L.C.M, *Opt.Eng.* **36**, 343 (1997)
29. Sablikov.V.A and Sandomirskii.V.B, *Phys.Status solidi (b)*, **120**, 471 (1983)
30. Dramicanin.M.D, Ristovast.Z.D, Nikolic.P.M, Vasiljevic.D.G and Todorovic.D.M, *Phys.Rev.B*, **51**, 14226 (1995)
31. Siu.E.K.M and Mandelis.A, *Phys. Rev.B* **34**, 7222 (1986)
32. Delgadillo.I, Vargas.M, Cruz-Orea.A, Alvarado-Gil.J.J, Baquero.R, Sánchez-Sinencio.F and Vargas.H, *Appl. Phys. B: Las. Opt.* **64**, 97 (1997)
33. Rodriguez.M.E, Zelaya-Angel.O, Bueno.J.J.P, Jimenez-Sandoval.S and Tirado.L, *J. Cryst. Growth.* **213**, 259 (2000)
34. Nikolic.P.M, Todorovic.D.M, Bojicic.A.I, Radulovic.K.T, Urosevic.D, Elazar.J, Blagojevic.V, Mihajlovic.P and Miletic.M, *J. Phys: Cond. Matt.* **8**, 5673 (1996)
35. Ikari.T, Fukuyama.A, Maeda.K and Futagami.K, *Phys. Rev. B* **46**, 10173 (1992)
36. Pinto Neto.A, Vargas.H, Leite.N.F and Miranda.L.C.M, *Phys. Rev.B* **41**, 9971 (1990)
37. Riech.I, Marin.E, Diaz.P, Alvarado-Gil.J.J, Mendoza-Alvarez.J.G, Vargas.H, Cruz-Orea.A, Vargas.M and Bernal-Alvarado.J, *Phys. Stat. Sol. (a)* **169**, 275 (1998)
38. Marin.E, Riech.I, Diaz.P, Alvarado-Gil.J.J, Mendoza-Alvarez.J.G, Vargas.H, Cruz-Orea.A and Vargas.M, *J. Appl. Phys.* **83**, 2604 (1998)
39. Bernal-Alvarado.J, Vargas.M, Alvarado-Gil.J.J, Delgadillo.I, Cruz-Orea.A, Vargas.H, Velazquez.M, Albor-Aguilera.M.L and Gonzalez-Trujillo.M.A, *J. Appl. Phys.* **83**, 3807 (1998)
40. Shen.Q and Toyoda.T, *Jpn. J. Appl. Phys.* **39**, 511 (2000)
41. Kuwahata.H, Muto.N, Uehara.F and Matsumori.T, *Jpn. J. Appl. Phys.* **38**, 3168 (1999)

42. Shen.Q and Toyoda.T, *Jpn. J. Appl. Phys.* **39**, 3164 (2000)
43. Fournier.D, Boccara.C, Skumanich.A and Amer.N.M, *J.Appl.Phys.* **59**, 787 (1986)
44. Carslaw.H.S and Jaeger.J.C, *Conduction of Heat in solids* (Oxford Press) (1959)
45. Carslaw.H.S, *Introduction to the mathematical theory of the conduction of heat in solids* (McMillan) (1921)
46. Shoucair.F.S, *IEEE transactions on education*, **32** 359 (1989)
47. Levinshtein.M.E, Rumyantsev.S.L and Shur.M (Eds.), *Handbook series on semiconductor parameters*, (World Scientific, London) (1996)
48. Shur.M, *Physics of semiconductor devices*, (Printice Hall) 1990
49. Adachi.S, *Physical properties of III-V semiconductor compounds* (John Wiley & Sons, New York) (1992)
50. Turner.W.J, Reese.W.E and Pettit.G.D, *Phys.Rev.* **136**, 1467 (1964)
51. Blakemore.J.S, *J.Appl.Phys.* **52**, 212 (1982)
52. Sturge.M.D, *Phys.Rev.* **127**, 768 (1962)
53. Daganis.M, Leheney.R.F and Crow.J (Eds.), *Integrated optoelectronics*, (Academic Press, San Diego) (1994)
54. Singh.J, *Semiconductor optoelectronics*, (McGraw-Hill, New York) (1995)
55. Dorren.B.H.P, *Polarisation independent interferometric switches based on III/V quantum wells*, (Ph.D. thesis, Technische Universiteit Eindhoven) (1999)
56. Singh.J, *Physics of semiconductors and their heterostructures*, (McGraw-Hill, New York) (1993)
57. Bhattacharya.P.K, *Semiconductor optoelectronic devices*, (Printice-hall, Englewood Cliffs, NJ) (1994)
58. Wheatley.P, Bradley.P.J, Whitehead.M, Parry.G, Midwinter.J.E, Mistry.P, Pate.M.A and Roberts.J.S, *Elect.Lett*, **92** (1985)
59. Singh.J, Hong.S, Bhattacharya.P.K, Sahai.R, lastufka.C and Sobel.H, *J.Light..Tech.* **6**, 818 (1988)
60. Pamplin.B.R, *Crystal growth*, (Pergamon Press, Oxford) (1975)
61. Rosenberger.F, *Fundamentals of crystal growth*, (Springer, Berlin) (1979)
62. Cho.A.Y, *J.Vacuum.Sci.Technol.* **8**, 531 (1971)
63. Hartman.P, *Crystal growth: an introduction*, (North-Holland, Amsterdam) (1973)
64. Hurlle.D.T.J (Edit.), *Handbook of crystal growth*, (North-Holland, Amsterdam) (1994)
65. Goodman.C.H.L (Edit.), *Crystal growth- theory and techniques*, (Plenum Press, London) (1974)

66. Willardson.A.C and Beer.C (Eds.), *Semiconductors and semimetals*, (Academic Press, New York) (1988)
67. Bhandari.C.M and Rowe.D.M, *Thermal conduction in semiconductors*, (Wiley, New York) (1988)
68. Kireev.P.S, *Semiconductor physics*, (Mir Publishers, Moscow) (1975)
69. Ziman.J.M, *Electrons and phonons*, (Clarendon Press, Oxford) (1960)
70. Kittel.C, *Introduction to solid state physics*, (Wiley, New York) (1996)
71. Kanstad.S.O and Nordal.P.E, *Opt.Comm.* **26**, 367 (1978)
72. Marquezini.M.V, Cella.N, Mansanares.A.M, Vargas.H and Miranda.L.C.M, *Meas.Sci.Technol.* **2**, 396 (1991)
73. Dioszeghy.T, Miklos.A, Kelemen.A and Lorincz.A, *J.Appl.Phys.* **58**, 2105 (1985)
74. Ganguly.P and Somasundaram.T, *Proceedings of the indian academy of sciences-chemical sciences*,**98**, 305 (1987)
75. Leite.N.F and Miranda.L.C.M, *Rev.Sci.Instru.* **63**,4398 (1992)
76. Chirtoc.M, Bicanic.D, Lubbers.M, Arnscheidt.B and Pelzl.J, *J.Mol.Struct.* **348**, 469 (1995)
77. DaCosta.A.C.R and Siqueira.A.F, *J.Appl.Phys.* **80**, 5579 (1996)
78. CruzOrca.A, Delgadillo.I, AlvaradoGil.J.J, SanchezSinencio.F and Vargas.H, *Prog.Natural Sci.* **6**, S487 (1996)
79. Garcia-Segundo.C, Villagran-Muniz.M and Muhl.S, *J.Phys.D:Appl.Phys.* **31**, 165 (1998)
80. Valcarcel.J.P and Alvarado-Gil.J.J, *Revista Mexicana De Fisica*, **44**, 43 (1998)
81. Barja.P.R and Mansanares.A.M, *Instru. Sci.Technol.* **26**, 209 (1998)
82. Delgado-Vasallo.O, Valdes.A.C, Marin.E, Lima.J.A.P, da Silva.M.G, Sthel.M, Vargas.H and Cardoso.S.L, *Meas.Sci.Technol.* **11**, 412 (2000)
83. Rosencwaig.A and Gersho.A, *J.Appl.Phys.* **47**, 64 (1976).
84. Perondi.L.F and Miranda.L.C.M, *J.Appl.Phys.* **62**, 2955 (1987).
85. Mansanares.A.M., Vargas.H, Galembeck.F, Buijs.J and Bicanic.D, *J.Appl.Phys.* **70**, 7046 (1991).
86. Charpentier.P, Lepoutre.F and Bertrand.L, *J.Appl.Phys.* **53**, 608 (1982)
87. Leite.N.F, Cella.N, H.Vargas and Miranda.L.C.M, *J.Appl.Phys.* **61**, 3025 (1987)
88. Marquezini.M.V, Cella.N, Mansanares.A.M, Vargas.H and Miranda.L.C.M, *Engineering Optics*, **2**, 396 (1991)
89. Todorovic.D.M and Nikolic.P.M, *Opt.Eng.* **36**, 432 (1997)
90. Barin.I, Knacke.O and Kubaschewski.O, *Thermochemical properties of inorganic substances*, (Springer, Berlin) (1977)

91. Kudman.I and Steigmeier.E.F, *Phys.Rev.A* **133**, 1665 (1964)
92. Maycock.P.D, *Solid State Electron.* **10**, 161 (1967)
93. Adachi.S, *J.Appl.Phys.* **54**, 1844 (1983)
94. Dargys.A and Kundroats.J, *Handbook on physical properties of Ge, Si, GaAs and InP*, (Vilius Science and Encyclopedia Publishers) (1994)
95. Bertolotti.M, Liakhov.G.L, Voti.R.L, Paolini.S and Sibia.C, *J.Appl.Phys.* **83**, 966 (1998)
96. Boccara.A.C, Fournier.D and Badoz.J, *Appl.Phys.Lett.* **36**, 130 (1979)
97. Jackson.W.B, Amer.N.M, Boccara.A.C and Fournier.D, *Appl.Opt.* **20**, 1333 (1981).
98. Aamodt.L.C and Murphy.J.C, *J.Appl.Phys.* **52**, 4903 (1981).
99. Grice.K.R, Inglehart.L.J, Favro.L.O, Kuo.P.K and Thomas.R.L, *J.Appl.Phys.* **54**, 6245 (1983).
100. Charbonnier.F and Fournier.D, *Rev.Sci.Instrum.* **57**, 1126 (1986).
101. Salazar.A, Lavega.A.S and Fernandez.J, *J.Appl.Phys.* **65**, 4150 (1989).
102. Cheng.J.C, Li.F.H, Guo.L and Zhang.S.Y, *Appl.Phys.A.* **61**, 441 (1995).
103. Salazar.A, Lavega.A.S and Fernandez.J, *J.Appl.Phys.* **74**, 1539 (1993).
104. Murphy.J.C and L.C.Aamodt, *J.Appl.Phys.* **51**, 4580 (1980)
105. Kuo.P.K, Lin.M.J, Reyes.C.B, Favro.L.D, Thomas.R.L, Kim.D.S, Zhang.S, Inglehart.L.J, Fournier.D, Boccara.A.C and Yacoubi.N, *Can.J.Phys.* **64**, 1165 (1986)
106. M.Bertolotti, Voti.R.L, Liakhov.G and Sibia.C, *Rev.Sci.Instrum.* **64**, 1576 (1993).
107. Salazar.A and Lavega.A.S. *Rev.Sci.Instrum.* **65**, 2896 (1994).
108. Salazar.A, Lavega.A.S and Fernandez.J, *J.Appl.Phys.* **69**, 1216 (1991)
109. Salazar.A, Lavega.A.S and Fernandez.J, *J.Appl.Phys.* **74**, 1539 (1993)
110. Winefordner.J.D (Edit.), *Photothermal spectroscopy method for chemical analysis*, (Wiley, New York) (1996)
111. *CRC Handbook of Chemistry and Physics*, (CRC Press, Boca Raton) (1999)
112. Soltanolkotabi.M, Bennis.G.L and Gupta.R, *J.Appl.Phys.* **85**, 794 (1999)
113. Chen.G, Tien.C.L, Wu.X and Smith.J.S, *J.Heat.Transfer*, **116**, 325 (1994)
114. Ju.Y.S and Goodson.K.E, *Appl.Phys.Lett.* **74**, 3005 (1999)
115. Chen.G, *J.Heat.Transfer*, **121**, 945 (1999)
116. Zeng.T and Chen.G, *J.Heat.Transfer*, **123**, 1 (2001)
117. Asheghi.M, Leung.Y.K, Wong.S.S and Goodson.K.E, *Appl.Phys.Lett.* **71**, 1798 (1997)

Chapter 4

Photoacoustic evaluation of thermal effusivity of transparent liquids and liquid crystals

Open photoacoustic cell is a renewed form of conventional photoacoustic configuration and it possesses a number of advantages over its predecessors. In this chapter the use of an open photoacoustic cell in the study of thermal effusivity of non-absorbing liquids and liquid crystalline samples are discussed. A simple and sensitive minimum-volume open photoacoustic cell is designed and fabricated for room temperature measurements. Investigations at elevated temperatures are performed using a conventional resonant cell by modifying it into the open cell configuration.

4.1. An introduction to liquid crystals

The molecules in a solid exhibit both positional and orientational order, in other words they are constrained to orient in certain directions and to occupy certain specified positions with respect to each other. In liquids the molecules do not have any positional or orientational order, *i.e.* the molecules are aligned randomly and it occupies random positions. The liquid crystalline phase exists in between the solid and the liquid phase. The molecules in a liquid crystal (LC) do not exhibit positional order, but they do possess a certain degree of orientational order. Consequently, LCs are anisotropic materials, and the physical properties of the system vary with the average alignment of the molecules [1-7]. If the alignment is large, the material is very much anisotropic. Similarly, if the alignment is small, the material is almost isotropic. Although the LC phase is a hybrid state between the liquid and solid phases, the LC is much more like a liquid than a crystal. When a solid melts to a liquid crystal, it loses most of its original order, leaving only a small amount to be lost when the substance changes to a conventional liquid. Evidence of this is found in the calculations of latent heat of melting from solid to LC and from LC to liquid [1-5]. A typical material having a LC phase will exhibit a heat of melting from solid to LC, which is 10 times its heat of melting from LC to liquid.

By and large, the term liquid crystal covers a wide area of chemical structures, physical properties and technical applications. A very large number of chemical compounds are known to exhibit one or several liquid crystalline phases. But not all substances can form a liquid crystal phase. Despite significant differences in chemical composition, these molecules have some common features in chemical and physical properties. They have rod-like or disc-like molecular structure, rigidity of the long axis and strong dipoles and/or easily polarisable substituents. Typical rod-shaped organic moieties forming LC phase are about 25 angstrom in length and 5 angstrom thick. Some typical chemical structures that can form a LC phase are: cholesterol ester, phenyl benzoates, surfactants, paraffines, glyco lipids, cellulose derivatives etc [1-7,9].

Liquid crystals are broadly classified into two categories: *thermotropic* LCs, and *lyotropic* LCs. These two types of LCs are distinguished by the mechanisms that drive their self-organisation, but they are also identical in many ways. Majority of LCs are thermotropic, in which the transitions to the liquid crystalline state are induced thermally [1-8]. Thermotropic LCs can be further classified into two types: *enantiotropic* and *monotropic*. The former type can be changed into the liquid crystal state by lowering the temperature of a liquid or by raising the temperature of a solid. However, the *monotropic* LCs can only be changed into the liquid crystal state by either an increase in the temperature of a solid or a decrease in the temperature of a

liquid, but not both. In general, thermotropic mesophases occur because of anisotropic dispersion forces between the molecules and because of packing interactions. Thermotropic LCs are usually made of *discotics* or *rod-shaped* molecules. Discotics are flat disc-like molecules consisting of a core of adjacent aromatic rings. This allows for two-dimensional columnar ordering. Rod-shaped molecules have an elongated and anisotropic geometry which allows for preferential alignment along any spatial direction.

In contrast to thermotropic mesophases, lyotropic LC transitions occur with the influence of solvents, not by a change in temperature. Lyotropic mesophases occur as a result of solvent-induced aggregation of the constituent mesogens into micellar structures [1-7]. Lyotropic mesogens are typically amphiphilic, meaning that they are composed of both lyophilic (solvent-attracting) and lyophobic (solvent-repelling) parts. This causes them to form into micellar structures in the presence of a solvent, since the lyophobic ends will stay together as the lyophilic ends extend outwards towards the solution. As the concentration of the solution is increased and the solution is cooled, the micelles increase in size and eventually coalesce. This separates the newly formed liquid crystalline state from the solvent.

Though the LC phases show long range orientational order, all the molecules will not align in the same direction all the time. However, they tend to align more in one direction over time than other directions. This direction is referred to as the *director* of the liquid crystal. The amount of order is measured by a quantity called the *order parameter* of LC [1,10]. This order parameter is highly dependent on the temperature of the sample. The order parameter "s" is defined as

$$s = \frac{1}{2} \langle 3 \cos^2 \theta - 1 \rangle \quad (1)$$

where θ is the angle which the long molecular axis makes with the director and the angular brackets denote a statistical average. For perfectly parallel alignment $s = 1$, while for random orientation $s = 0$. Typical values for the order parameter of a liquid crystal range between 0.3 and 0.9, which varies with temperature due to kinetic molecular motion.

4.1.1. Liquid crystalline phases

Liquid crystalline phases are named according to their degree of molecular ordering [1-4]. For smectic phases there are various possible ways in which the constituent molecules can order and this enables the generation of six *quasi-smectic* crystal mesophases and five true smectic liquid crystal phases. The *quasi-smectic* crystal phases are given the letters B, J, G and

E, K, H which are rather arbitrary but relate to the degree of ordering of the constituent molecules. True smectic liquid crystals are given the symbol S and a subscript which indicates the phase type (S_A , S_C and S_B , S_I , S_F).

Smectic liquid crystals have a soapy texture and are usually found at lower temperatures than the nematic. In smectic phases the molecules are arranged in layers which are not well defined and the different types of smectic phases arise because of the different possibilities of molecular ordering within the phase structure. The smectics are thus positionally ordered along one direction. Many compounds are observed to form more than one type of smectic phase. In the smectic-A mesophase, the director is perpendicular to the smectic plane, and there is no particular positional order in the layer. Similarly, the smectic-B mesophase orients with the director perpendicular to the smectic plane, but the molecules are arranged into a network of hexagons within the layer. In the smectic-C mesophase, molecules are arranged as in the smectic-A mesophase, but the director is at a constant tilt measured normally to the smectic plane. There are also tilted phases which have hexatic in-plane ordering, like the Smectic I and Smectic F, as well as various crystalline smectics. In simple terms, the smectic phase arises if the lateral intermolecular forces of attraction are stronger than the terminal forces. Hence, on heating, the terminal forces breakdown first, in-plane translational order is lost and this results in a lamellar arrangement of molecules in which the layers are not well defined.

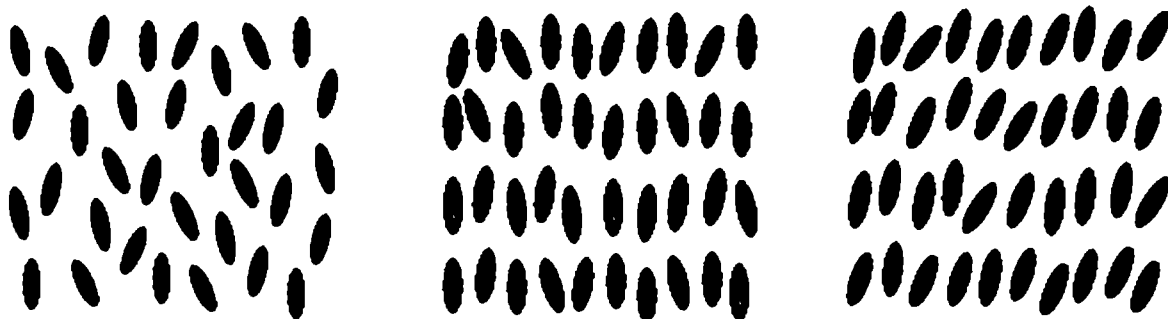


Figure 1: Schematic representation of Nematic (left), Smectic-A (middle) and Smectic-C (right) phase of a liquid crystal.

The nematic phase is given the symbol N and there is only one nematic phase. The *nematic* liquid crystal phase is characterised by molecules that have no positional order but tend to point in the same direction (along the director). Consequently, nematic liquid crystals are the least ordered of the liquid crystals. They tend to lie nearly parallel to one another, forming a 'threadlike' pattern. The nematic phase does not have a layered structure and the only degree of

ordering is the statistically parallel arrangement of the molecules in the direction of the director. Accordingly, the nematic phase is very fluid and much like a conventional liquid. When placed next to the wall of the container they will lie parallel to the wall (or perpendicular, depending on the exact properties of the liquid crystal).

The *cholesteric* or chiral nematic liquid crystal phase is typically composed of nematic mesogenic molecules containing a chiral center which produces intermolecular forces that favour alignment between molecules at a slight angle to one another. That is cholesteric liquid crystal exhibits a twisted structure, the director rotates about an axis as we move through the material.

Columnar liquid crystals are different from the previous types because they are shaped like disks instead of long rods. This mesophase is characterised by stacked columns of molecules. The columns are packed together to form a two-dimensional crystalline array.

Figure 2: Columnar liquid crystal

4.1.2. Liquid crystalline polymers

Liquid crystalline polymers (LCPs) are a class of materials that combine the properties of polymers with those of liquid crystals. These hybrids show the same mesophases characteristic of ordinary liquid crystals, yet retain many of the useful and versatile properties of polymers [11-21]. Normally flexible polymers will display liquid crystal characteristics on incorporating rod-like or disk-like elements called mesogens into their chains. The placement of the mesogens plays a large role in determining the type of LCP that is formed. *Main-chain* polymer liquid crystals are formed when the mesogens are themselves part of the main chain of a polymer. Conversely, *side-chain* polymer liquid crystals are formed when the mesogens are connected as side chains to the polymer by a flexible bridge called the spacer.

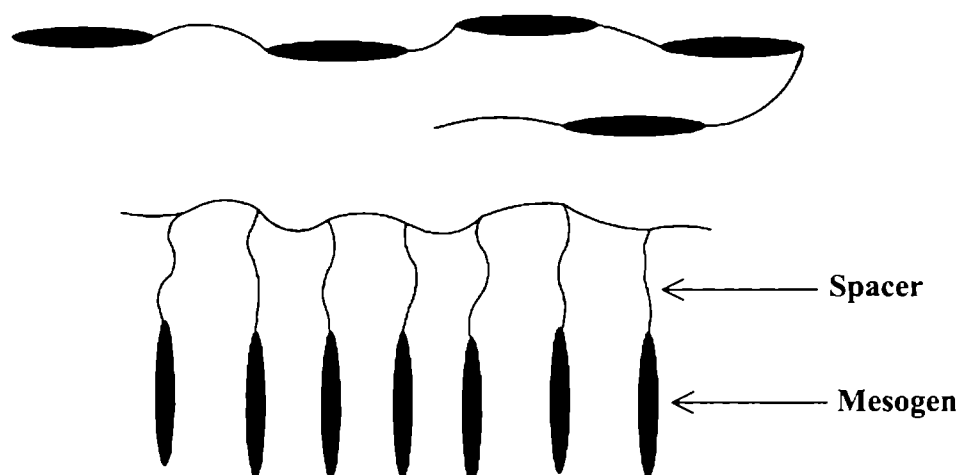


Figure 3: Main-chain (top) and side-chain (bottom) liquid crystal polymer structure. Here, the bead like structure corresponds to the mesogen.

4.1.3. Liquid crystal mixtures

Although all the liquid crystalline compounds have, in general, the familiar long, lath-like structure, in many respects their structural composition is completely different. In the design of liquid crystal compounds the most important aspect is that they must exhibit the correct type of liquid crystalline phase over the desirable temperature, usually room temperature. Additionally liquid crystals must have a suitable combination of structural features to enable the generation of a rather subtle blend of physical properties. Clearly, to obtain everything from one material is not possible and so liquid crystals for commercial applications are all mixtures of appropriate materials that provide the best compromise of different properties. However, a complex balance has to be struck to achieve optimum results [22-29]. Nematic mixtures are of great interest in many liquid crystal applications and they are important in many ways. There are many nematic mixtures with thermodynamic stability. The best liquid crystal materials for displays are multi-component nematic mixtures with a wide temperature range. The liquid crystal mixtures are generally used to

- (i) widen the temperature range of phases.
- (ii) investigate interaction between different phases
- (iii) investigate pre-transitional behaviour
- (iv) identify unknown substances by mixing with substances with well known phase behaviour.

4.1.4. Induced alignment in liquid crystals

We have seen that the molecules in liquid crystalline phase possess certain kind of alignment in some preferred direction. But a perfect alignment of these molecules in any desired direction can be achieved by some externally controlled methods. The best method is to use electric or magnetic fields in the desired direction [1-4,7,30-33]. The interaction of external fields with the dipole moment of the medium will result in a change in the orientational order or macroscopic reorientation of the director. Consequently, these external fields may alter the optical and thermal properties of the sample. Due to the anisotropy of the dielectric constant and diamagnetic susceptibility, the free energy of the liquid crystal in an external field has a minimum value for a completely defined orientation of the director relative to the field. An easiest way to achieve orientation in LC thin films or surface alignment in bulk samples is to bring the sample in contact with a previously treated solid surface [1-4,34-36]. Usually polymer films coated on glass plates rubbed in a particular direction are used for this purpose.

4.2. Thermal effusivity

The thermal effusivity, similar to thermal diffusivity, is a unique thermal property of a material [37]. The major difference between the two is that diffusivity is a bulk property of the sample whereas the effusivity is a surface property. The thermal effusivity is defined by $e_s = \sqrt{k\rho C}$ with dimension $W s^{1/2} cm^{-2} K^{-1}$, where k is the thermal conductivity, ρ is the density and C is the specific heat capacity. Though the thermal effusivity is an abstract thermal quantity and is a relevant thermophysical parameter for surface heating and cooling as well as in quenching processes, it is one of the least explored quantities in physics. Actually, the thermal effusivity is a measure of the sample's thermal impedance or it is a measure of the sample's ability to exchange heat with the environment. The thermal effusivity of liquid crystals has great importance when they are used as temperature sensors or in temperature sensitive devices/applications. For example, one of the most recently introduced and important applications of liquid crystalline polymers is in the field of optical data storage [38-41]. The thermo-optic recording is achieved by incorporating a dye into the sample, which on irradiation with laser beam absorbs the light energy and re-radiates it as heat. Consequently the sample is locally heated into the isotropic phase and a change in the optical density takes place on cooling. Usually very thin films (5-10 μm) are used for the optical data storage. Here, the speed with which the laser treated area cools back into the glassy or liquid crystalline phase is mainly determined by the thermal effusivity of the thin film.

4.3. Theoretical outline

Details of the open photoacoustic cell configuration and a general theoretical treatment regarding the same are given in *chapter 2*. Schematic diagram of an open cell photoacoustic configuration used for the present investigation is shown in figure 4. Consider a thin, solid, absorbing layer in contact with a non-absorbing liquid. If this system is exposed to a modulated optical radiation, the absorbing layer absorbs the light and periodic heat is generated at the surface of this layer in contact with the liquid sample, *i.e.* at $x = -l_0$. The thermal wave thus generated gets diffused through the thermally thin absorbing layer to the gas column behind it. The thermal diffusion equations for the configuration shown in figure 4 are [42],

$$\frac{\partial^2 T_s}{\partial x^2} = \frac{1}{\alpha_s} \frac{\partial T_s}{\partial t} \quad (2a)$$

$$\frac{\partial^2 T_0}{\partial x^2} = \frac{1}{\alpha_0} \frac{\partial T_0}{\partial t} - \frac{\beta I_0}{2k_0} e^{\beta x} (1 + e^{j\omega t}) \quad (2b)$$

and
$$\frac{\partial^2 T_g}{\partial x^2} = \frac{1}{\alpha_g} \frac{\partial T_g}{\partial t} \quad (2c)$$

where $\alpha_i = \frac{k_i}{\rho_i C_i}$ is the thermal diffusivity of the medium i . Here the suffix i denotes different media, $i = s$ refers to the liquid sample, $i = 0$ refers to the absorbing layer and $i = g$ refers to the air in the microphone chamber. And β is the optical absorption coefficient of the thin layer. Assume that the entire light is absorbed at $x = -l_0$.

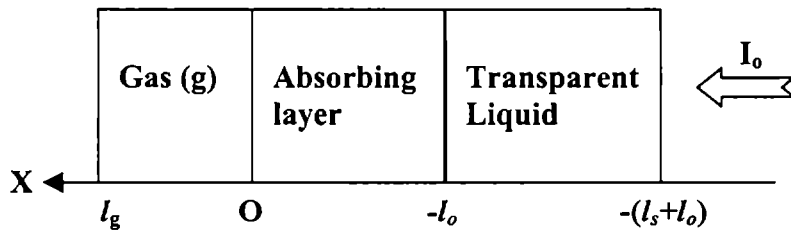


Figure 4: Schematic diagram of open photoacoustic cell configuration.

Then, solving equations (2) together with the boundary conditions of temperature and heat flux continuity, we can arrive at the expression for the acoustic pressure in the microphone chamber as,

$$\delta Q_1 = \frac{\mathcal{P}_0 I_0 (\alpha_g \alpha_s)^{1/2}}{2\pi T_0 l_g k_s} \frac{e^{j(\omega t - \pi/2)}}{f} \quad (3)$$

Equation (3) implies that the acoustic signal now varies as f^{-1} and is proportional to the ratio $\sqrt{\alpha_s}/k_s = e_s^{-1}$, the inverse of the thermal effusivity of the transparent liquid.

On the other hand, if there is no liquid sample in contact with the absorbing layer, then the pressure fluctuation δQ_2 inside the cavity is given by

$$\delta Q_2 = \frac{\gamma P_0 I_0 \alpha_g^{1/2} \alpha_0}{(2\pi)^{3/2} T_0 l_g l_0 k_0} \frac{e^{j(\omega t - 3\pi/4)}}{f^{3/2}} \quad (4)$$

Thus, according to equation (4), the signal varies as $f^{-3/2}$ and depends on the ratio α_0/k_0 . Using this as a reference signal and from the ratio of equations (3) and (4), one can easily eliminate all the constants and other geometrical parameters of the cell. Then the thermal effusivity of the liquid sample can be evaluated by measuring the signal amplitudes as a function of modulation frequency from the absorbing layer with and without liquid sample, provided the thickness, density and specific heat capacity of the thin layer are known.

4.4. Experimental details

Investigations are carried out with two different open photoacoustic cells. For room-temperature studies, a simple and minimum-volume OPC is designed and fabricated and its details are given in the next section. Measurements at elevated temperatures are carried out using a temperature variable resonant photoacoustic cell. This cell is converted into an open cell by simply removing the glass window. The former cell is used for investigating the room-temperature nematic liquid crystal mixtures. Studies on liquid crystalline polymers and cyanobiphenyl liquid crystals (7OCB and 8OCB) are carried out using the latter cell. The liquid crystal sample holder used for the investigations is made of a nylon ring of thickness 3mm and inner diameter 7mm. Bottom of the ring is closed with a 60 μ m thick copper foil. The liquid sample (liquid crystal) is filled inside the ring and the entire sample holder is placed on the top of the sample chamber of the cell. Cross-sectional view of the sample-holder resonant-cell assembly is shown in figure 5. Different fixed temperatures are used for the present measurements. For this purpose a sensitive temperature controller (Aplab 9602) is used. The heater coil (60W) wound over the sample compartment is connected to the dc power supply through the temperature controller. The temperature controller measures the temperature of the sample using a chromel-alumel thermocouple inserted into the body of the sample chamber through a 1mm bore which ends up very close to the sample. The output voltage from the thermocouple drives the electronic part of the temperature controller and hence it always forced

to maintain the sample temperature (by putting the heater on-off) to a manually set value on the controller. Since the sample chamber has very small volume, the fluctuation in the measured value of the sample temperature is only about ± 0.13 °C. This, in fact, is found to be a reasonably good temperature stability that gives an almost stable photoacoustic signal.

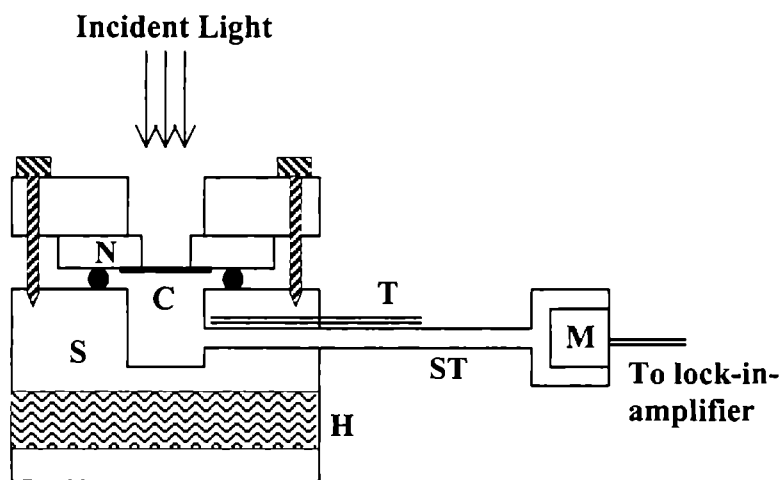


Figure 5: Cross-sectional view of the open photoacoustic cell - sample holder assembly. N the nylon ring, C the copper foil, T the thermocouple, S the stainless steel body, H the heater coil, ST the stainless steel tube and M the microphone.

4.4.1 Design and fabrication of an open photoacoustic cell

A minimum-volume open photoacoustic cell is designed and fabricated for room-temperature studies on the nematic liquid crystal mixtures. Cross-sectional view of the cell is depicted in figure 6. The bottom half of the cell is fabricated by drilling a cavity of diameter 1cm and depth 5mm at the center of a circular acrylic (perspex) block of thickness 1cm and diameter 10.5cm. An electret microphone (Knowles BT 1834) is fixed at the bottom of this chamber and electrical connections to the microphone are taken through the bottom of the chamber. In order to eliminate electromagnetic interference, high quality shielded wires are used for taking the output from the microphone as well as the battery connection to it. Also, both the connections are taken directly from the microphone by avoiding intermediate junctions which may result in the generation of noises. A rubber O-ring (having diameter slightly greater than that of the cavity) fixed in a groove at the surface of the chamber ensures airtight arrangement. Another acrylic sheet having the same dimensions and with a 1cm (diameter) hole at its center, serves as the top of the cell. Both the acrylic blocks are tightly fixed on two brass frames. The entire structure is fixed on a flat horizontal platform made of stainless steel. The performance of

this minimum-volume open photoacoustic cell is found to be excellent with a very high signal to noise ratio.

The sample holder used together with this cell is the same as that used with the resonant cell. Here, the bottom of the ring is closed with a copper foil of thickness $75\mu\text{m}$ instead of $60\mu\text{m}$. The liquid (liquid crystal) is filled upto half of the sample holder it is placed directly on the microphone chamber, leaving a small volume of air in the chamber.

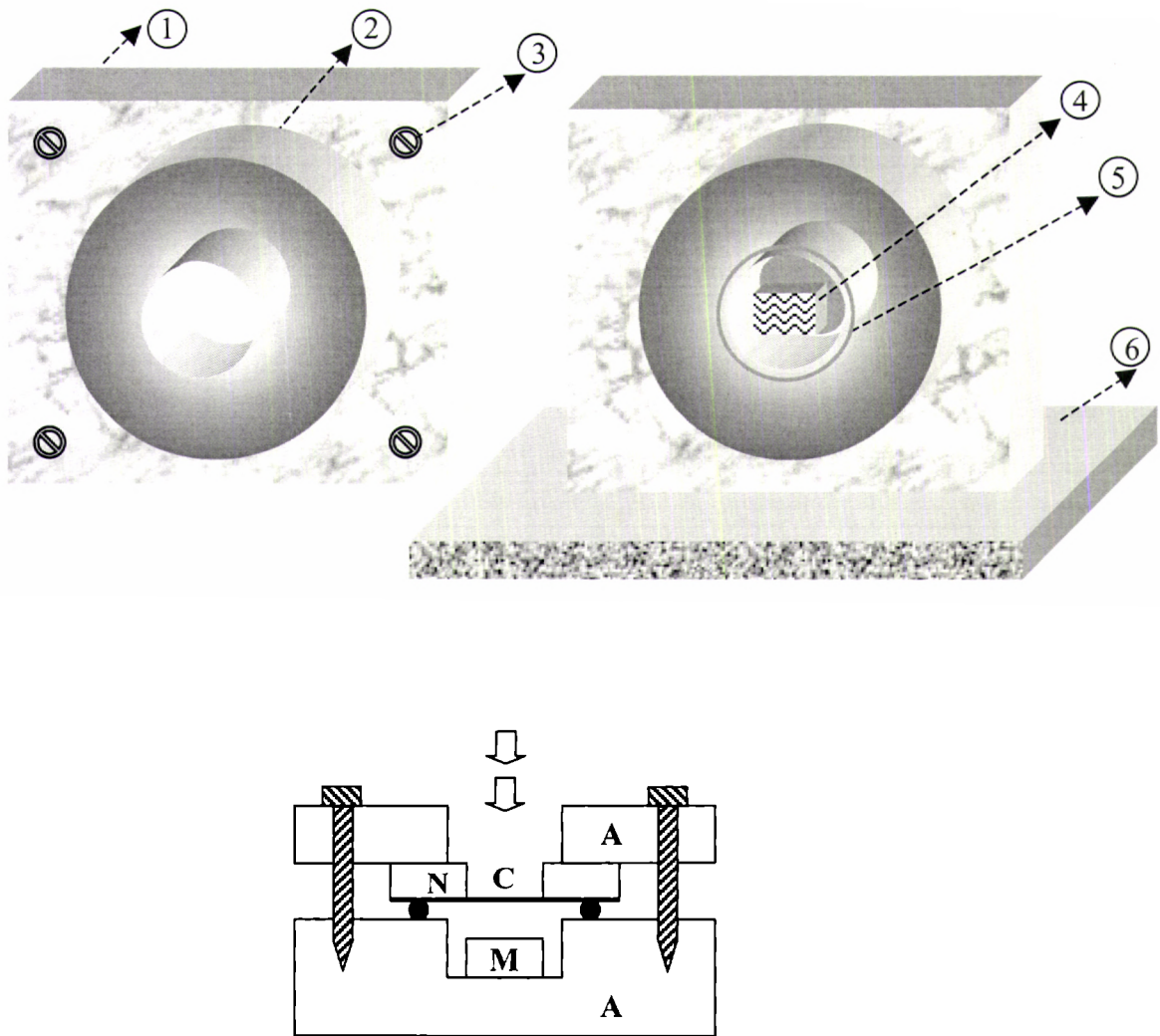


Figure 6: Cross-sectional view of the open photoacoustic cell for room temperature measurements. (**Top**); 1 the brass frame, 2 the acrylic sheet, 3 the screws, 4 the microphone, 5 O-ring and 6 the platform. (**Bottom**); N the nylon ring, C the copper foil, A the acrylic sheet, and M the microphone.

4.4.2 Experimental procedure

In addition to the open photoacoustic cell, other components used in the present experimental set-up are an argon ion laser (Liconix 5000), a mechanical light beam chopper (Ithaco HMS 230), and a lock-in-amplifier (Stanford Research Systems SR 510). In the case of measurements carried out using the temperature variable cell, a temperature controller (Aplab 9602) and a dc power supply are used along with the cell. A block diagram of the experimental set-up is shown in figure 7. The same set-up, excluding the temperature sensing and controlling unit, is used for the room-temperature measurements using the minimum volume open cell. Laser emission at 488nm is used in all the measurements. When the large-volume resonant cell is used for the investigations, laser power of 200mW is used to ensure a high signal-to-noise ratio. But for the investigations using the minimum-volume open cell, laser power of 100mW is found to be sufficient to give high, stable signal. All the measurements are carried out in the absence of any external electric or magnetic fields. The photoacoustic signal detected using the microphone is processed using the lock-in-amplifier.

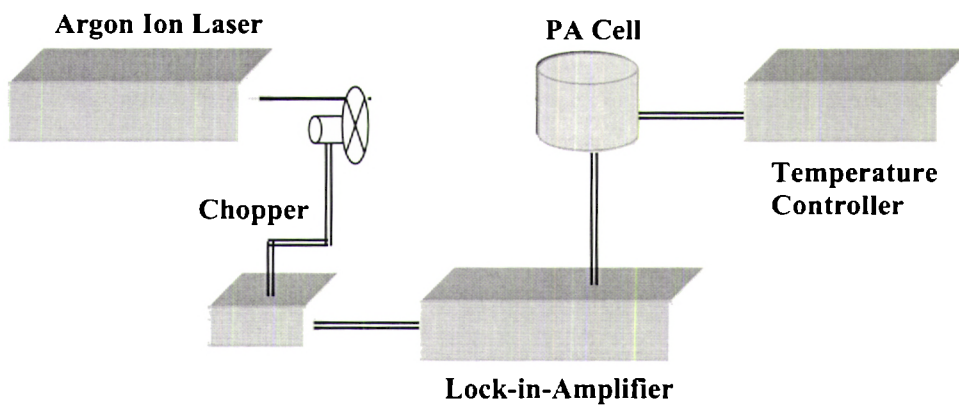


Figure 7: Block diagram of the experimental set-up

The experimental procedure adopted for thermal effusivity measurements is as follows. Initially, the signal amplitude is recorded as a function of modulation frequency of the incident laser beam when the sample holder is empty. This signal produced by thermally thin copper foil with air in the sample holder is taken as the reference signal. Then, without disturbing the experimental set-up, the sample holder is filled with the non-absorbing liquid (liquid crystal) and again the signal amplitude is recorded at the same laser power and over the same frequency range as used earlier. The thermal effusivity of the liquid sample is then calculated from the

ratio of the two signal amplitudes and from the known values of specific heat capacity, density and thickness of the copper foil.

In the case of transparent liquid samples such as water and glycerol, filling the sample holder with these liquids has not resulted in a reduction in the incident intensity on the copper foil. However, though all the liquid crystals used are optically non-absorbers at 488nm, scattering loss in different phases reduces the incident light intensity on the copper foil. Hence, the fractional change in transmitted intensity is to be measured for the evaluation of thermal effusivity. The same experimental set-up, with another sample holder, is used to measure the percentage transmittance at 488nm. For this purpose copper foil at the bottom of the sample holder is replaced with a glass plate (1.5mm thick) and its outer surface is coated with a thick carbon black film. For an empty sample holder, linear dependence of the photoacoustic signal amplitude on incident light intensity is observed, which is in accordance with the Rosencwaig-Gersho theory. Then the sample holder is filled with the liquid crystal and the photoacoustic signal at a fixed light intensity is recorded and from this value the percentage transmittance in each of the mesophases of the different samples are accurately estimated.

4.5. Results and discussion

4.5.1. Thermal effusivity of water and glycerol

Initially, the present experimental approach is verified using water and glycerol as the non-absorbing liquids. These liquids are well transparent in the visible region and their thermal properties are well known. Both the minimum-volume cell and the resonant cell are employed for the measurements. In either case the acoustic signal produced by the empty sample holder and that obtained after filling it with these liquids are measured as a function of the modulation frequency. Typical variation of the signal amplitude for glycerol-copper system and water-copper system measured using the two cells are shown in figures 8 and 9.

It is worthwhile to note here that, in either case, amplitude of the signal produced by the empty sample holder (copper foil alone) is greater than that from copper-liquid (water or glycerol) composite sample. This indicates that the liquid acts as a heat sink, or part of the thermal energy generated at the liquid-copper interface is absorbed by the liquid due to its finite thermal conductivity. A comparison of figures 8 and 9 also confirms this. The thermal conductivity values of water, glycerol and air are $0.591 \text{ Wm}^{-1}\text{K}^{-1}$, $0.270 \text{ Wm}^{-1}\text{K}^{-1}$ and $0.0241 \text{ Wm}^{-1}\text{K}^{-1}$, respectively [43]. Consequently, water, being a liquid with higher thermal conductivity than glycerol, produces a lesser signal compared to the latter.

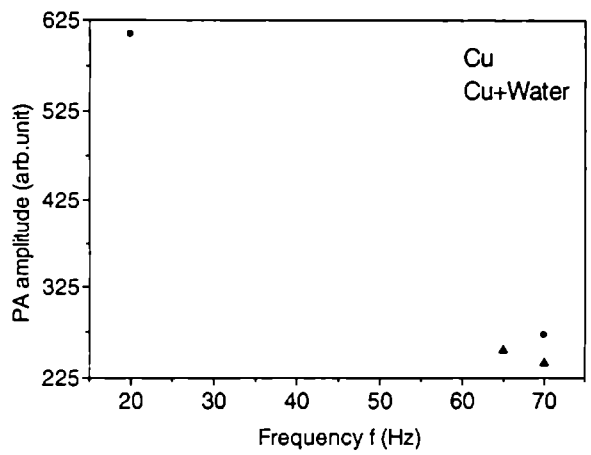
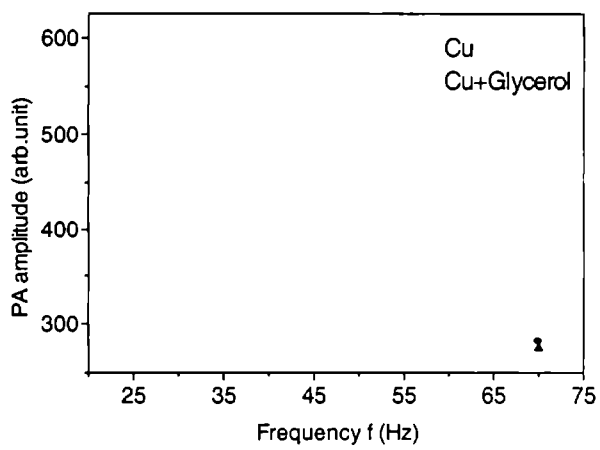


Figure 8: PA signal variation with modulation frequency for glycerol and water, measured using the non-resonant open photoacoustic cell

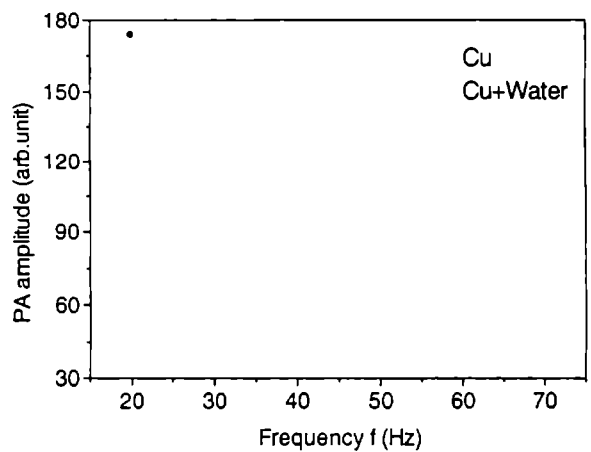
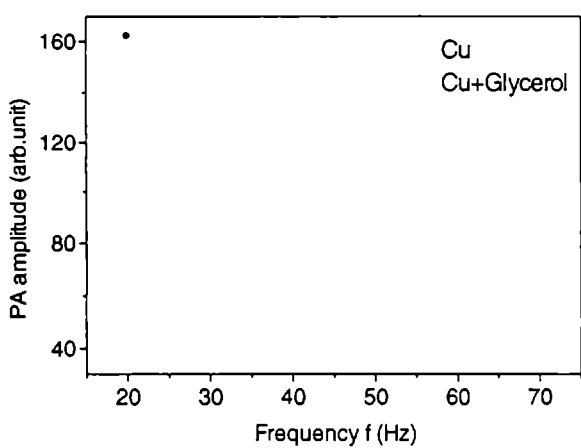


Figure 9: PA signal variation with modulation frequency for glycerol and water, measured using the resonant open photoacoustic cell

Figures 10 and 11 show the $\log(f^{1/2})$ versus $\log(R)$ plot for water and glycerol. Here f is the chopping frequency and $R = (PA_f / PA_e)$ where PA_f is the signal produced by the liquid filled sample holder and PA_e is that from the empty sample holder. The thermal effusivities are evaluated from the y-intercept of the straight line fit to the experimental data. The calculated values of thermal effusivities of water and glycerol are given in Table I. The measured values are found to agree well with the literature values. The density and specific heat capacity of the copper foil are $\rho_0 = 8.96 \text{ g cm}^{-3}$ and $C_0 = 0.385 \text{ J g}^{-1} \text{ K}^{-1}$ respectively [43]. Copper foils of two different thickness are used for the measurements using the minimum-volume cell and resonant cell and are $l_0 = 75\mu\text{m}$ and $l_0 = 60\mu\text{m}$ respectively.

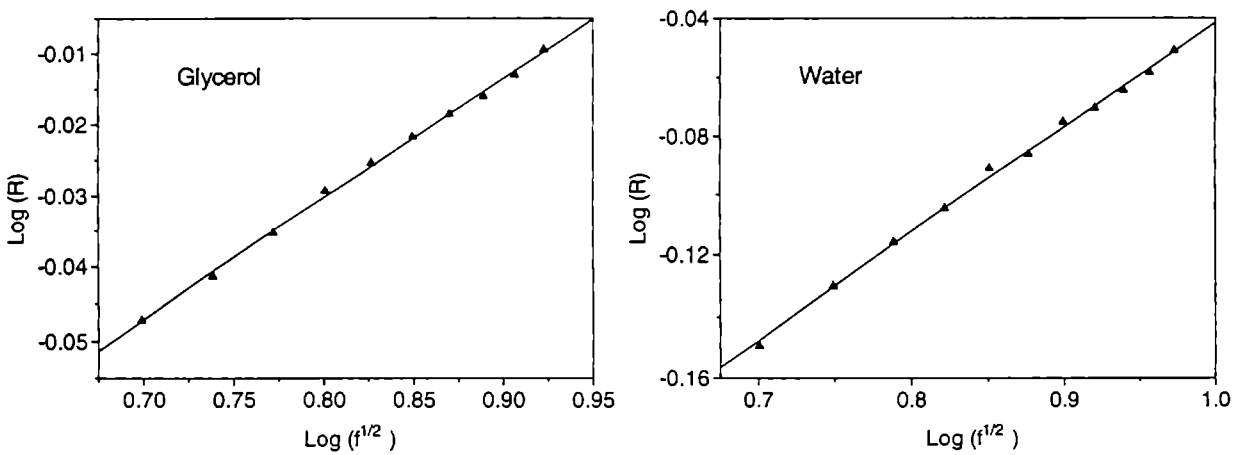


Figure 10: Normalised signal amplitudes with respect to the modulation frequency for glycerol and water, measured using the non-resonant photoacoustic cell

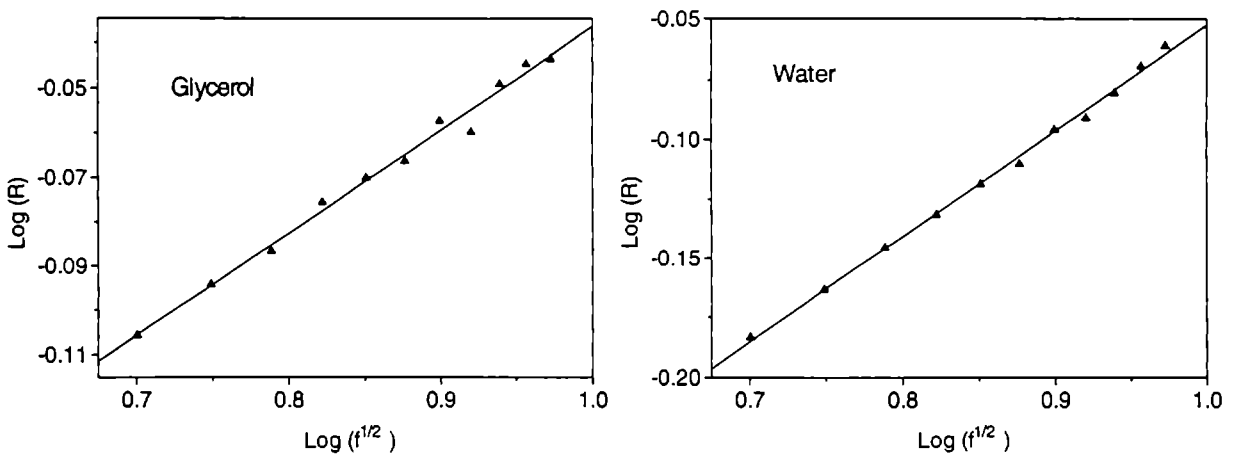


Figure 11: Normalised signal amplitudes with respect to the modulation frequency for glycerol and water, measured using the resonant photoacoustic cell

Table I: Thermal effusivity of water and glycerol measured using open photoacoustic cell

Liquid sample	Thermal effusivity in $W s^{1/2} cm^{-2} K^{-1}$ measured using		
	Minimum-volume cell	Resonant cell	Literature value*
Water	0.155 (± 0.002)	0.154 (± 0.002)	0.158
Glycerol	0.094 (± 0.001)	0.093 (± 0.001)	0.093

*CRC Handbook of Physics and Chemistry

4.5.2. Thermal effusivity of liquid crystalline polymers

Thermotropic, side-chain, liquid crystalline polymers LCP1, LCP93 and LCP95 are obtained from Merck Inc. UK and are used without further purification. The molecular structure of these materials are given in figure 12. LCP1 and LCP95 are homopolymers whereas LCP93 is a copolymer. Since the first two compounds are made of flexible poly siloxane backbone the glass transition temperature of these materials are very low. But the stiffer poly acrylate backbone of LCP95 results in a very high glass transition temperature in this material. Some of the important thermal and structural parameters of these materials provided by the manufacturer are given in Table II. Here, investigations are carried out only in the isotropic phase as the smectic phases of all these compounds are highly scattering which ultimately results in complete loss of transparency in these phases.

Table II: Some of the important thermal and structural parameters of comb-shaped liquid crystalline polymers LCP1, LCP93 and LCP95.

Liquid crystalline polymer	Chain length N	Transition temperatures in $^{\circ}C$		
		T_g	S_C-I	S_A-I
LCP1	35	-10.9	70.7	
LCP93	20	-9.3		76
LCP95	12.5	49.5		85.4

* T_g : Glass transition temperature, S_C-I ; Smectic-C-Isotropic, S_A-I ; smectic-A-Isotropic.

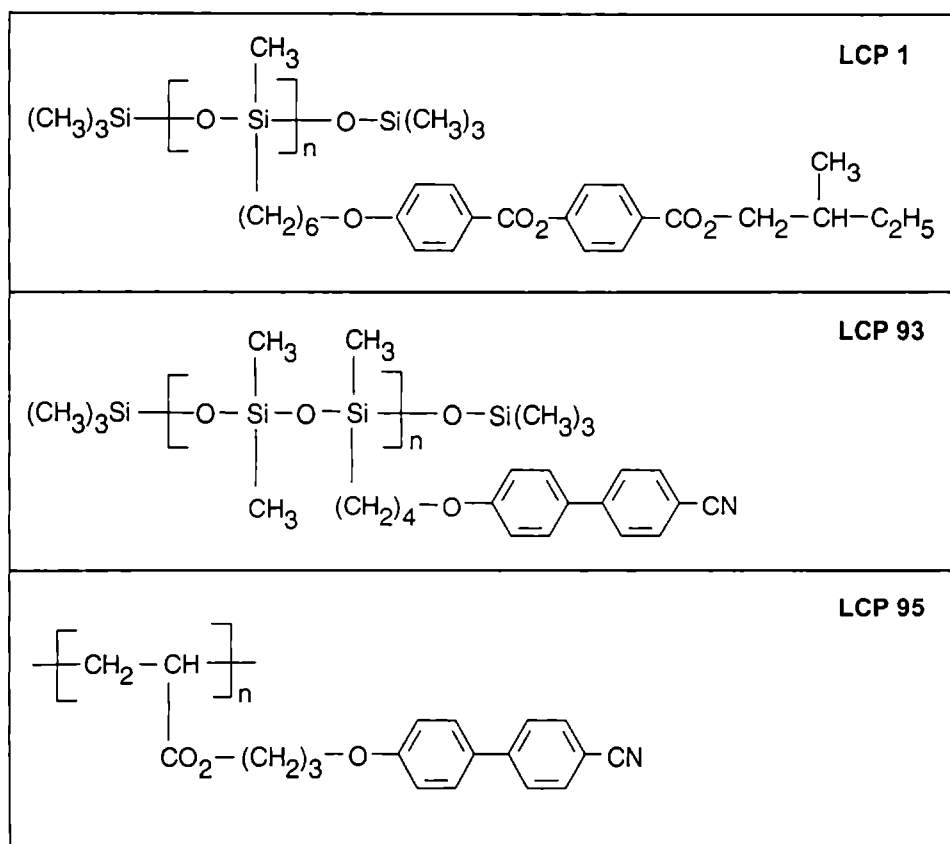


Figure 12: Molecular structure of the liquid crystalline polymers LCP1, LCP93 and LCP95

In order to arrive at the expression (3) we have assumed that the liquid in contact with the copper foil is perfectly transparent at the excitation wavelength. Though all the above liquid crystalline polymers in the isotropic phase are optically non-absorbers in the visible region, the highly viscous nature of the samples in this phase reduces the optical transmission at 488nm by a substantial amount. The percentage transmittance of LCP1, LCP93 and LCP95 at 90 °C are measured as 70%, 77% and 54% respectively.

Figure 13 (a-f) shows the variation of signal amplitudes with modulation frequency (f) and the $\log f^{1/2}$ versus $\log R$ plots of the liquid crystal polymers LCP1, LCP93 and LCP95. Again, f and R have the same meaning as described earlier. The thermal effusivities are evaluated from the y-intercept of the straight line fit to the experimental data. The estimated values in the isotropic phase at 90 °C are summarised in Table III. It is a clearly established fact that the thermal properties such as the thermal conductivity or specific heat capacity in a particular thermodynamic state of a liquid crystal remains constant irrespective of the temperature value. At 90 °C all the materials investigated above are perfectly in the isotropic phase and hence the values reported in Table III are unique.

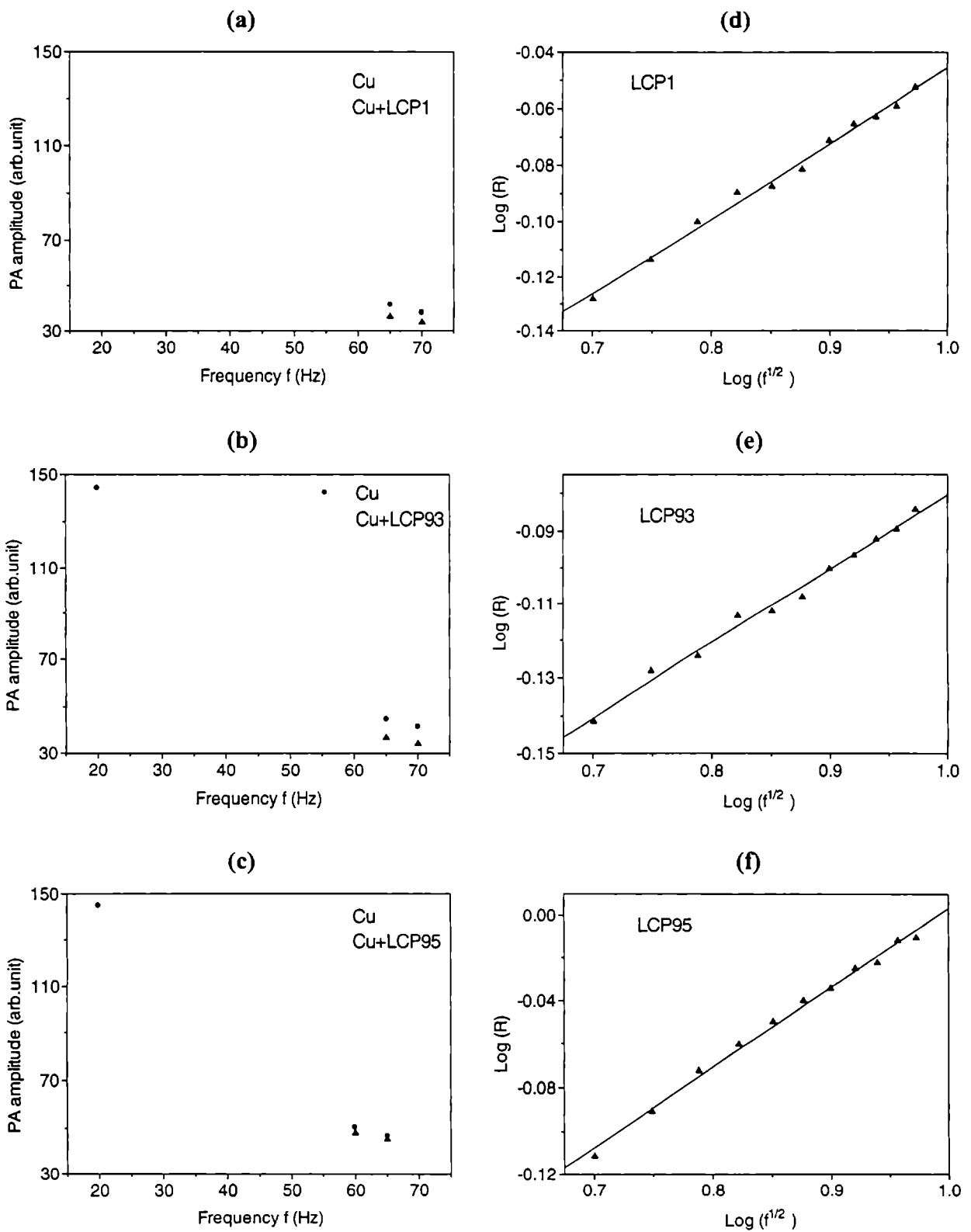


Figure 13: Photoacoustic signal variation with modulation frequency for different liquid crystalline polymers (a-c). Plots (d-f) show the normalised signal amplitude variations with the square root of modulation frequency.

Table III: Thermal effusivity values in the isotropic phase of liquid crystalline polymers

Liquid crystal	Thermal effusivity in $W s^{1/2} cm^{-2} K^{-1}$
LCP1	0.074
LCP93	0.073
LCP95	0.069

A closer look into Table III reveals that the thermal effusivity of LCP95 is much less than that of LCP1 and LCP93. The chain length of LCP1 is approximately 35 units while that of LCP93 and LCP95 are approximately 20 units and 12.5 units [44]. Hence, the present observation suggests that an increase in chain length could result in an increased value of thermal effusivity which is in accordance with the earlier observation of Rondelez *et.al.* that the thermal conductivity of liquid crystals is directly related to its chain length [45]. Even though the effective length of the main chain in LCP93 is slightly greater than that of LCP1, the latter possesses a slightly increased thermal effusivity than the former. This indicates that in a comb-shaped liquid crystalline polymer the thermal transport is not only determined by the main chain but the side chains also have some substantial influence, as the side chain including the spacer of LCP1 is much longer than that of LCP93. Similarly, the notable decrease in the thermal effusivity value of LCP95 may be due to the decreased chain length of this compound. But the fact that this compound is made of a different polymer backbone should also be taken into account while comparing with LCP1 or LCP93. Hence, the generalisation of thermal properties of comb-shaped liquid crystalline polymers by analysing the data from only a couple of compounds is rather difficult because the features of the structure of these materials together with the mutual effect of the individual structural elements of the macromolecules significantly complicate the identification of common behaviour in their properties.

4.5.3. Thermal effusivity of 7OCB and 8OCB

Liquid crystals 8OCB and 7OCB are obtained from Merck Inc, U K and are used without further re-crystallisation. The literature values of phase transition temperatures of 8OCB are 54 °C, 67.5 °C and 80.5 °C corresponding to the crystalline to smectic-A, smectic-A to nematic and nematic to isotropic transitions respectively and that of 7OCB are 55 °C, 73.5 °C for the crystalline to nematic and nematic to isotropic transitions respectively [46-53]. The thermal effusivities in all these phases except in the crystalline phase are measured using the

present method. Measurements are carried out at 60 °C, 72 °C and 90 °C respectively for the 8OCB samples in the smectic-A, nematic and isotropic phases. While, in the case of 7OCB samples, the investigations are performed at 60 °C and 90 °C corresponding to the nematic and isotropic phases respectively. The fixed temperatures for the measurements in each phase are selected so to ensure that the samples are in thermal equilibrium in the respective phases. For the same sample thickness as used for the thermal effusivity measurements (1.5mm), the optical transmittance (at 488nm) of 8OCB at 60 °C, 72 °C and 90 °C are 67%, 71% and 97.4% respectively. The optical transmittance of 7OCB at 488nm is measured as 65% and 95.8% at 60 °C and 90 °C respectively. Variation of the signal amplitude with modulation frequency and the logarithmic plot connecting the square root of the modulation frequency and the ratio of signal amplitude to the reference signal in each phase of 8OCB are shown in figure 14 (a-f). The thermal effusivities are evaluated from the y-intercept of the straight line fit to the experimental data and the estimated values are summarised in Table IV. From the tabulated values of thermal effusivities it can be seen that the smectic-A phase has the minimum thermal effusivity followed by a slight increase in the nematic phase. The isotropic phase at 90 °C shows the maximum thermal effusivity. The literature values of specific heat capacity of 8OCB shows a slight increase in the isotropic phase [48]. This may be one of the reasons for the increase in effusivity in the isotropic phase. The variation in the density between the different mesophases is reported to be very small compared to the percentage change in the thermal effusivity value.

Table IV: Thermal effusivity in the various mesophases of 7OCB and 8OCB

Liquid crystal	Thermal effusivity in $W s^{1/2} cm^{-2} K^{-1}$		
	Smectic-A	Nematic	Isotropic
7OCB	No smectic phase	0.051 ± 0.003	0.068 ± 0.003
8OCB	0.056 ± 0.003	0.057 ± 0.003	0.071 ± 0.003

In terms of the liquid crystal molecular orientation, the nematic phase has the translational symmetry of a fluid, but a broken rotational symmetry characterised by long-range orientational order produced by the alignment of their long molecular axes along the director. In the nematic phase, however, the centers of mass of the molecules are still randomly distributed. Therefore, in the absence of any external magnetic or electric fields to align the molecules in a preferred direction, any measured value of thermal conductivity will be its average value given by

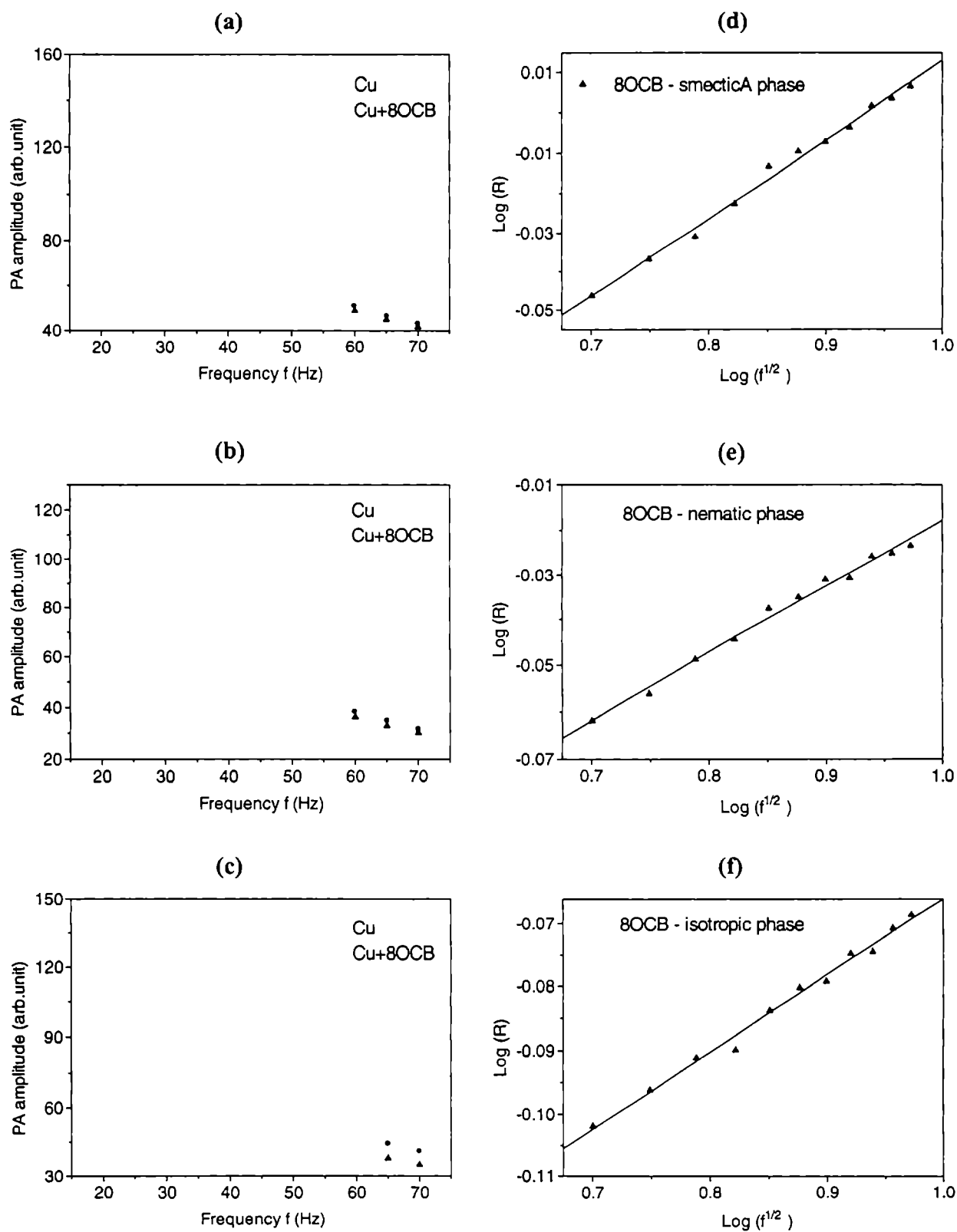


Figure 14: Photoacoustic signal variation with modulation frequency in different phases of 80CB (a-c). Normalised signal amplitude versus the square root of modulation frequency are given in (d-f).

$$\langle k \rangle = \frac{1}{3}(k_x + 2k_y) \quad (5)$$

where k_x and k_y are the thermal conductivities parallel and perpendicular, respectively, to the director in oriented samples [2]. We can rewrite the above expression in terms of the thermal effusivity e_s as

$$\langle e_s \rangle = \frac{1}{3} \left[(e_s)_x + (2e_s)_y \right] \quad (6)$$

Similar observations are made in the case of 7OCB. The experimental plot connecting the signal amplitude and modulation frequency and the square root of the frequency versus ratio of signal amplitudes in the logarithmic scale are shown in figure 15. The thermal effusivity values in the nematic and isotropic phases are summarised in Table IV. In this case also the thermal effusivity in the nematic phase is lower than that in the isotropic phase. This observation is quite reasonable since 7OCB and 8OCB are identical materials. Here also, in the nematic phase, the measured value of thermal effusivity will be its average value given by the expression (6).

A comparison of the present data with any of the reported thermal parameters of 8OCB or 7OCB is rather difficult because all the required parameters at the respective temperatures are not clearly available in the literature. Also, the data such as the specific heat capacity values varies significantly from sample to sample depending on small changes in their purity [54]. In the present case, a major reason for the decrease in the thermal effusivity value in the nematic phase may be due to the fact that the photoacoustic signal amplitude is mainly determined by a very thin surface layer called the first thermal diffusion length within the sample. The thermal diffusion length is defined as $\mu = (2\alpha/\omega)^{1/2}$ where $\alpha = (k/\rho C)$ is the thermal diffusivity, k is the thermal conductivity, ρ is the density, C is the specific heat capacity and ω is the modulation frequency of the incident optical radiation. The thermal diffusion length in liquid crystals will be only a few tens of microns in the frequency range used in the above measurements. In many situations surface layers of liquid crystals are reported to show a totally different behaviour compared to their bulk properties. Consequently, from the above observations it is quite reasonable to assume that the surface effects in the nematic and smectic-A phases plays a dominant role in determining the thermal effusivity in these phases. Moreover, the closeness in the thermal effusivity values of 8OCB in the smectic-A and nematic phases is also a reasonable observation as the thermal conductivity and specific heat capacity in these two phases are reported to be almost constant [1-5,48,49].

A comparison of the two materials shows that the thermal effusivities in the nematic and isotropic phases of 7OCB are slightly less than that of 8OCB in the corresponding phases. This can be explained using the simple arguments introduced by Rondelez *et.al.*, that the thermal conductivity is strongly affected by the structure of the liquid crystal molecule [45]. By treating liquid crystalline molecules as rigid rods, they have proved that the intramolecular thermal conductivity is exceedingly high with respect to the intermolecular one. Consequently, 7OCB a shorter homolog of 8OCB, possesses a lower thermal conductivity and hence a lower thermal effusivity than 8OCB.

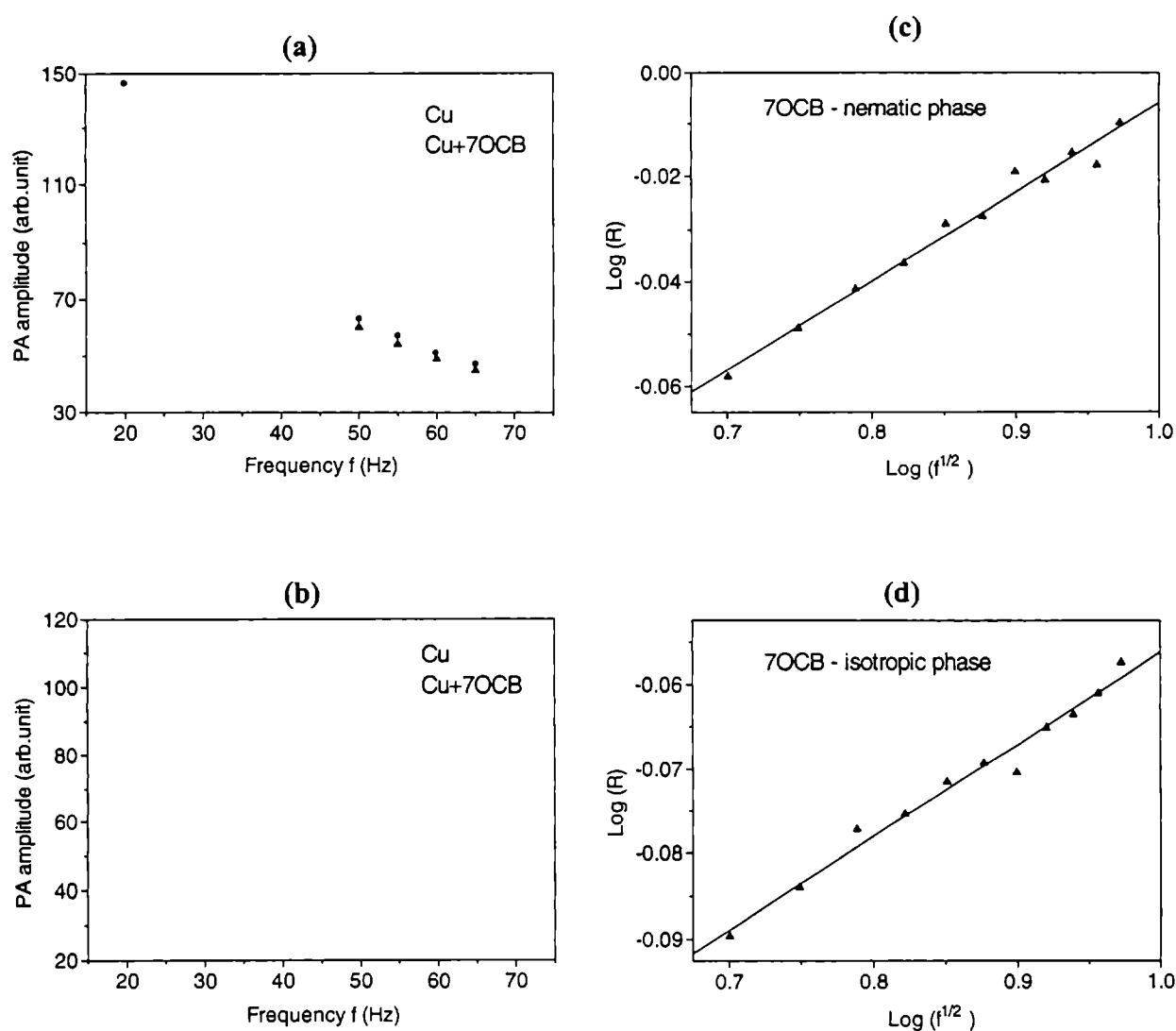


Figure 15: Photoacoustic signal variation with modulation frequency in different phases of 7OCB (a-b). Normalised signal amplitude versus the square root of modulation frequency are given in (c-d).

4.5.4. Thermal effusivity of nematic liquid crystal mixtures

The nematic liquid crystal mixtures BL001, BL002, BL032 and BL035 are obtained from Merck Inc. UK and are used without further purification. All these compounds are multi-component liquid crystal mixtures, which exist in the nematic phase at room temperature. Each mixture contains four to nine components and are primarily based on cyanobiphenyl group. The nematic to isotropic transition temperatures of BL001, BL002, BL032 and BL035 are at +61 °C, +72 °C, +87 °C and +96 °C respectively, and the nematic to smectic transition temperatures of all the compounds are below -20 °C [44]. The thermal effusivities in the nematic phase of these mixtures are measured at 27 °C. For this purpose, initially, the optical transmittance of these samples at 488nm is estimated at 27 °C and are found to be 67%, 66%, 64% and 65% respectively, for BL001, BL002, BL032 and BL035.

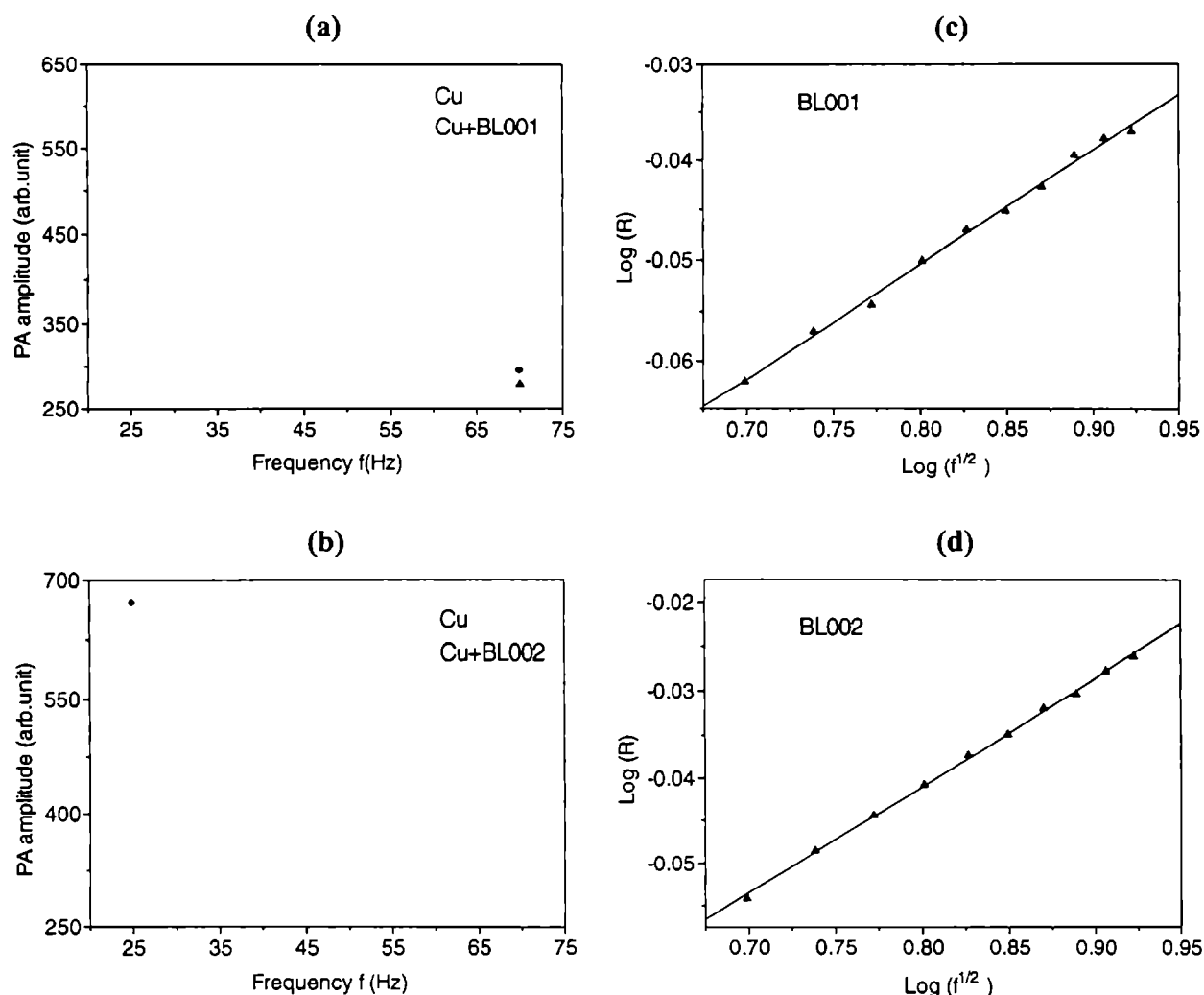


Figure 16: Photoacoustic signal variation with modulation frequency in the nematic phase of BL001 and BL002 (a-b). Normalised signal amplitudes versus square root of modulation frequency are given in (c-d).

Figures 16 and 17 show the frequency versus PA amplitude and $\log f^{1/2}$ versus $\log R$ plots of the liquid crystals BL001, BL002, BL032 and BL035. Again f is the chopping frequency and $R = (PA_f / PA_e)$ where PA_f is the signal produced by the liquid crystal filled sample holder and PA_e is that from the empty sample holder. The straight lines represent best linear fit to the experimental data. The thermal effusivities are evaluated from the y-intercept of the straight line fit to the experimental data and the estimated values are summarised in Table V. Here also the tabulated values in the table are only the average thermal effusivity given by expression (6). As the specific heat capacity or thermal conductivity data of these liquid crystals are not available in the literature a comparative study of the present data is rather difficult. But the measured values of the thermal effusivity fall in the range of several other liquid crystals in the nematic phase [1-5].

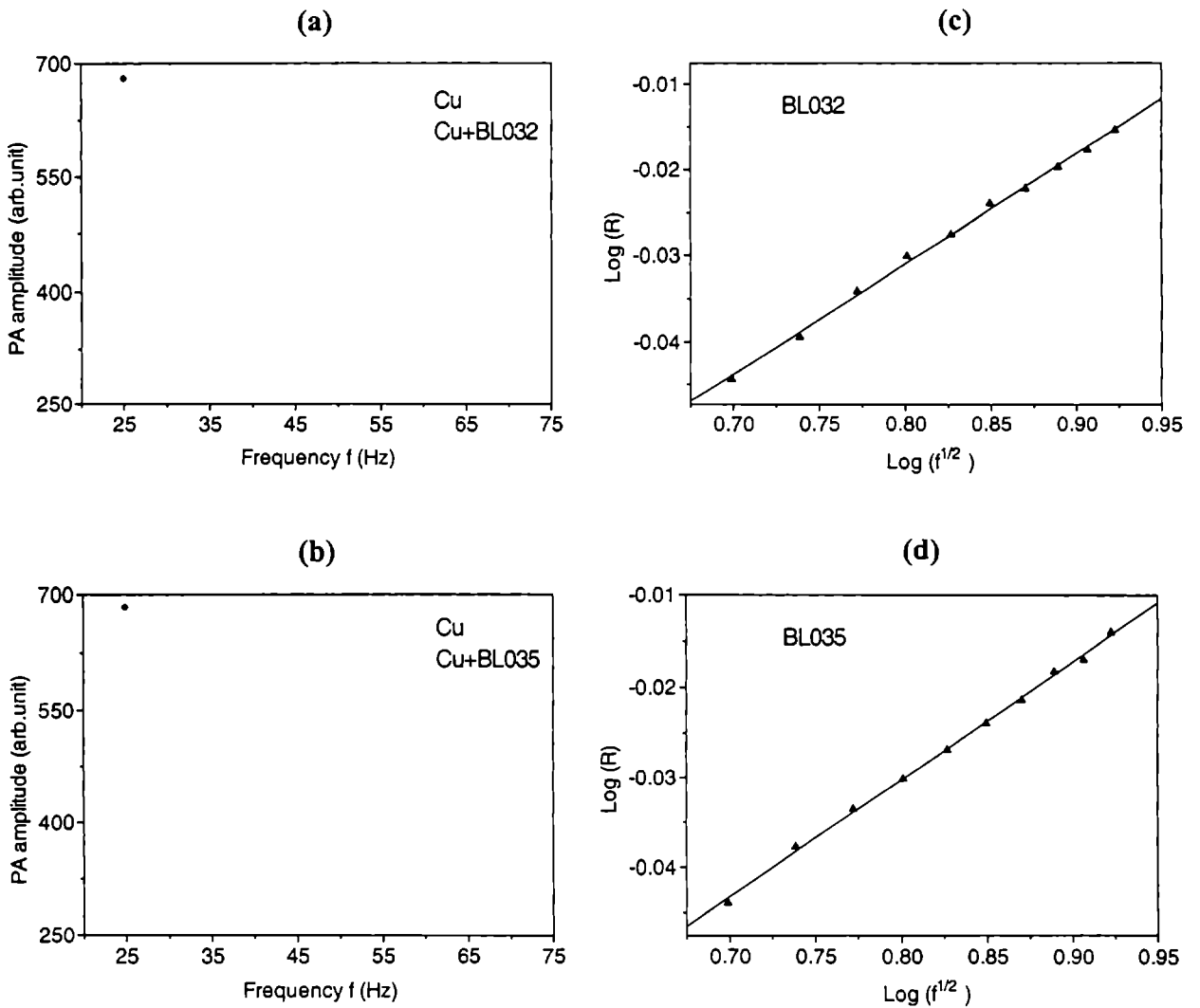


Figure 17: Photoacoustic signal variation with modulation frequency in the nematic phase of BL032 and BL035 (a-b). Normalised signal amplitude versus the square root of modulation frequency are given in (c-d).

Table V: Thermal effusivity of nematic liquid crystal mixtures

Liquid Crystal	Thermal effusivity in $\text{W s}^{1/2} \text{ cm}^{-2} \text{ K}^{-1}$
BL001	0.063 (± 0.002)
BL002	0.062 (± 0.002)
BL032	0.057 (± 0.002)
BL035	0.056 (± 0.002)

An important observation to be pointed out here is that the thermal effusivity of BL001 and BL002 are almost the same but differ from those of BL032 and BL035. This obviously suggests a different molecular composition for the first two liquid crystal mixtures compared to the other two mixtures. However, being a patented commercial product of Merck, the structural or compositional details of any of these mixtures are not known for an elaborate analysis of the results.

4.6. Conclusions

In conclusion, the usefulness of open photoacoustic cell configuration for the thermal characterisation of non-absorbing liquids and liquid crystals is demonstrated. Besides the interest in its value, the importance of thermal effusivity as a physical quantity is due to the fact that it is a unique thermal parameter for each material. Knowledge of its absolute value leads us to the evaluation of thermal conductivity or specific heat capacity, if any one of these is known, density being an easily measurable quantity. Investigations are carried out in a variety of low molecular-weight liquid crystals and high molecular-weight liquid crystalline polymers. Measurements carried out in various mesophases of 8OCB and 7OCB are found to be very interesting. The influence of surface effects in these liquid crystals on its thermal effusivity values is highlighted. The effect of molecular structure is also clearly visible in the thermal effusivity values of different members of a particular family of liquid crystals. The comb-shaped liquid crystalline polymers are studied only in the isotropic phase, as their liquid crystalline phases are not transparent. But the observed values of thermal effusivity in the isotropic phase are, to some extent, sufficient for a careful analysis of the data with respect to the molecular structure and related parameters. Multi-component liquid crystalline mixtures are another class of materials that are investigated.

The present method overcomes the basic requirement of conventional photoacoustic method that the sample under investigation should absorb the excitation radiation. In the present experimental approach the sample to be investigated should be optically transparent at the excitation wavelength, which is satisfied by almost all liquid crystals and a large variety of liquids in the visible region of the optical spectrum. Consequently, a number of powerful lasers emitting in this regime can be effectively used for the above type of measurements. The new photoacoustic approach is very simple and less time consuming and its high accuracy may render it as a valuable tool for the thermal characterisation of liquid crystals. A combination of the present method with the earlier reported conventional photoacoustic configurations can be used for a complete thermal characterisation of liquid crystals and non-absorbing liquids.

References

1. Chandrasekhar.S, *Liquid crystals*, (Cambridge University Press, Cambridge) (1992)
2. De Gennes.P.G, *The physics of liquid crystals*, (Oxford University Press, New York) (1974)
3. Gray.G (Edit.), *Physical properties of liquid crystalline materials*, (Gordon and Breach) (1980)
4. Collings.P.J and Patel.J.S (Eds.), *Handbook of Liquid Crystal Research*, (Oxford University Press) (1997)
5. Martellucci.S and Chester.A.N (Eds.), *Phase transitions in liquid crystals*, (Plenum Press, New York) (1992)
6. Saeva.F.D (Edit.), *Liquid crystals, the fourth state of matter*, (Marcel Dekker, New York) (1979)
7. Vertogen.G, De Jeu.W.H, *Thermotropic liquid crystals: fundamentals*, (Springer-Verlag, Berlin) (1993)
8. Elston.S and Sambles.R, *The optics of thermotropic liquid crystals*, (Taylor and Francis, London) (1998)
9. Reinitzer.F; *Monatsh.Chem.* **9**, 421, (1888)
10. Maier.W and Saupe.A, *Z.Naturforsch*, **A14**, 882 (1959)
11. Plate.N.A (Edit.), *Liquid crystal polymers*, (Plenum Press, New York) (1993)
12. Blumstein.A (Edit.), *Liquid crystalline order in polymers*, (Academic Press, New York) (1978)
13. Plate.N.A and Shibaev.V.P, *Comb shaped polymers and liquid crystals*, (Plenum Press, New York) (1987)
14. Ciferri.A, Krigbaum.W.R and Meyer.R.B (Eds.), *Polymer liquid crystals*, (Academic Press, New York) (1982)
15. McArdle.C.B (Edit.), *Side chain liquid crystal polymers*, (Blackie, Glasgow) (1989)
16. Shibaev.V.P, Plate.N and Freidzon.Y, *Polym.Sci.Chem.* **17**, 1655 (1979)
17. Finkelmann.H, Ringsdorf.H and Wendorff.J.H, *Macromol.Chem.* **179**, 273 (1978)
18. Gray.G.W, Lacey.D, Nestor.G and White.M, *Makromol.Chem. Rapid.Comm.* **7**, 71 (1986)
19. Reck.B and Ringsdroff.H, *Makromol.Chem. Rapid.Comm.* **6**, 291 (1985)
20. Ju.M.Y, Chen.M.Y and Chang.F.C, *Makromol.Chem.Phys.* **201**, 2298 (2000)
21. Kventsel.G.F and T.J. Sluckin. *Phys. Rev.A.* **36**, 4386 (1987)

22. Chiu.H.W and Kyu.T, *J. Chem. Phys.* **103**, 7471 (1995)
23. CollingsP.J, *Amer. J. Phys.* **63**,1044 (1995)
24. Musgrave.B, Lehmann.P and Coles.H.J, *Liq.Cryst.* **26**, 1235 (1999)
25. Hakemi.H, Jagodzinski.E.F and DuPre.D.B, *Mol.Cryst.Liq.Cryst.* **91**, 129 (1983)
26. Raszewski.Z, Rutkowska.J, Kedzierski.J, Zmija.J and Dabrowski.R, *Mol.Cryst.Liq.Cryst.* **207**, 59 (1991)
27. Dabrowski.R, *Mol.Cryst.Liq.Cryst.* **191**, 17 (1990)
28. Lackner.A.M, Margerum.J.D and Ast.C, *Mol.Cryst.Liq.Cryst.* **141**, 289 (1986)
29. Greeff.C.W, *Mol.Cryst.Liq.Cryst.Sci.Technol.Sect.A.* **238**, 179 (1994)
30. McNamee.S.G, Ober.C.K, Bunning.T.J, McHugh.C.M and Adams.W.W, *Liq. Cryst.* **17**, 179 (1994)
31. Barbero.G, Bourdon.A, Bee.A and Figueiredo Neto.A.M, *Phys. Lett.A*, **259**, 314 (1999)
32. Andrienko.D, Kurioz.Y, Reznikov.Y, Rosenblatt.C, Petschek.R.G, Lavrentovich.O.D and Subacius.D, *J. Appl. Phys.* **83**, 50 (1998)
33. Kang.D, Mahajan.M.P, Petschek.R.G, Rosenblatt.C, He.C, Liu.P, and Griffin.A.C, *Phys. Rev.E*, **58**, 2041 (1998)
34. Mahajan.M.P and Rosenblatt.C, *Appl. Phys. Lett.* **75**, 3623 (1999)
35. Kim.J.H and Rosenblatt.C, *J. Appl. Phys.* **84**, 6027 (1998)
36. Mahajan.M.P and Rosenblatt.C, *J. Appl. Phys.* **83**, 7649 (1998)
37. Auciello.O and Flamm.D.L (Eds.), *Plasma diagnostics-Surface analysis and interactions, Vol 2*, (Academic Press, New York) (1988)
38. Trifunac.A.D and Krongauz.V.V (Eds.), *Processes in photorefractive polymers*, (Chapman and Hall, London) (1994)
39. Bowry.C, Bonnett.P, *Opt.Computing.Processing.* **1**, 13 (1991)
40. Mcardle.C.B, Clark.M.G, Haws.C.M, Wiltshire.M.C.K, Parker.A, Nestor.G, Gray.G.W, Lacey.D and Toyne.K.J, *Liq.Cryst.* **2**, 573 (1987)
41. Bowry.C., Bonnet.P, Clark.M.G, Mohlmann.G, Wreesman.C, Erdhuisen.P, Jenneskens.L.W, Gray.G.W, McRoberts.A.M, denman.R, Lacey.D, Scrowston.R.M, Griffiths.J and Tailor.S, *Proceedings of eurodisplay '90*, 158 (1990)
42. Rosencwaig.A and Gersho.A, *J.Appl.Phys*, **47**, 64 (1976)
43. *CRC Handbook of physics and chemistry* (CRC Press, Boca Raton) (1999)
44. *Liquid Crystal Data Sheet*, (Merck. Inc., England) (1995)
45. Rondelez.F, Urbach.W and Hervet.H, *Phys.Rev.Lett.* **41**, 1058 (1978)
46. Cladis.P.E, Bogardus.R.K and Aadsen.D, *Phys.Rev.A*, **18**, 2922 (1978)

47. Viner.J.M and Huang.C.C, *Solid.Stat.Comm.* **39**, 789 (1981)
48. Kasting.G.B, Lushington.K.J and Garland.C.W, *Phys.Rev.B.* **22**, 321 (1980)
49. Garland.C.W, Kasting.G.B and Lushington.K.J, *Phys.Rev.Lett.* **43**, 1420 (1979)
50. Huang.C.C, Pindak.R.S and Ho.J.T, *Solid.Stat.Comm.* **25**, 1015 (1978)
51. Agarwal.V.K, Khamis.K.M and Arora.V.P, *Ind.J.Pure.Appl.Phys.* **26**, 614 (1988)
52. Jakli.A, Janossy.I and Vajda.A, *Liq.Cryst.* **8**, 1035 (2000)
53. Hori.K, Koma.Y, Kurosaki.M, Itoh.K, Uekusa.H, Takenaka.Y and Ohashi.Y,
Bull.Chem.Soc.Japan. **69**, 891 (1996)
54. LeGrange.J.D and Mochel.J.M, *Phys.Rev.A*, **23**, 3215 (1981)

Photoacoustic analysis of phase transitions in liquid crystals

Application of photoacoustic technique for the detection of phase transitions in a variety of liquid crystals is discussed in this chapter. Investigations are carried out in 7OCB and 8OCB liquid crystals and in multi-component BL001, BL002, BL032 and BL035 nematic mixtures. The novelty of the present method is that the experiment is performed at a wavelength at which the liquid crystal samples do not absorb the optical radiation. Photoacoustic signal generation is achieved from such a non-absorbing sample by mixing it with a very small amount of an organic dye which absorbs the incident radiation. By employing this approach both first order and second order phase transitions have been detected. A qualitative evaluation of the heat capacity profile during phase transitions is also made by using a simple analysis based on the Rosencwaig-Gersho theory.

5.1 Phase transitions

A phase is a form of matter that is uniform throughout in chemical composition and physical properties and can be distinguished from other phases by these definite properties and composition. A substance in the solid phase has a definite shape and rigidity, but the liquid phase has no definite shape, but has a definite volume. The gaseous phase has no definite shape or volume, but has a shape and volume determined by the shape and size of the container. Usually, phase transitions are associated with a sudden change in the physical properties of the system when temperature, pressure, or other thermodynamic variable changes [1-5]. For a given thermodynamical conditions a phase is said to be stable when its energy called the Gibb's free energy, given by $G = U - TS + PV$, is minimum. During a phase transition, if the Gibb's function varies discontinuously with respect to pressure and temperature, such transitions are said to be of first-order. But, if $\left(\frac{\partial G}{\partial T}\right)_P$ and $\left(\frac{\partial G}{\partial P}\right)_T$ changes continuously and $\left(\frac{\partial^2 G}{\partial T^2}\right)_P$, $\left(\frac{\partial^2 G}{\partial P^2}\right)_T$ and $\left(\frac{\partial^2 G}{\partial P \partial T}\right)$ changes discontinuously during a transition, then it is said to be a second-order phase transition [1-4]. Being a material showing both first order and second order phase transitions, liquid crystals are exploited widely for phase transition studies [5-10].

5.1.1 Phase transitions in liquid crystals

We have seen in *chapter 4* that liquid crystalline materials can exist in a number of mesophases between the crystalline solid and the isotropic liquid state. Consequently, these materials exhibit a rich variety of phase transitions each having its own unique identities. Transition from one mesophase to another state can be brought about by pure thermal processes, *ie.* by changing the temperature of the sample. Liquid crystals belonging to this group are known as *thermotropic* materials [5-8,11]. There is another class of liquid crystals called the *lyotropic* liquid crystals, the details of which are given in the previous chapter. Of these two classes, the former type finds applications in technological devices such as display systems while the latter has great significance in biological systems. The present chapter deals with the studies on thermotropic liquid crystals

Though a detailed description of the different mesophases and their properties are given in *chapter 4*, it would be appropriate to recall the significant properties of the phases that are discussed in this chapter to facilitate the understanding of the results of the investigation. As we know, an essential requirement for mesomorphism to occur is that the molecule must be highly

geometrically anisotropic in shape, like a rod or a disc and on an average their long axis should point in a preferred direction, called the *director*. The nematic phase carries only long-range orientational order of the director and there is no correlation between the centers of gravity of the molecules. Consequently, the molecules are quite mobile in this particular phase. Typically, nematic viscosities are of the order of 0.1 Poise. Smectic liquid crystals are layered systems with varying degrees of order within each layer and with differing angular relations between the director \vec{n} and the normal to the layers. When there is no order within a layer and when \vec{n} is perpendicular to the plane of the layers, we have the case of smectic-A liquid crystal. Compared to nematics, smectics are very viscous and the typical value of viscosity are of the order of 10 Poise. Because of higher symmetry, the nematic phase usually occurs at a higher temperature than the smectic-A phase [5-8]. Apart from these mesophases, all liquid crystals transform to the totally disordered isotropic phase at elevated temperature, *i.e.* after the mesophases. Cooling down to a lower temperature, *i.e.* prior to the mesophases, will result in the crystallisation of these materials. The transition between these phases can be either first order or second order where critical fluctuations play an important role. Regarding the theoretical models used to describe various phases and phase transitions, Maier and Saupe have proposed a molecular theory of the nematic phase in which the alignment of the molecules parallel to a preferred axis is described by an orientational order parameter [12]. Kobayashi and McMillan extended this model to the smectic-A phase by introducing another order parameter, namely, the amplitude of a density wave in the direction of the nematic preferred axis [13-15].

In order to determine the order of different kinds of transitions and to fully characterise the nature of the fluctuations at critical and multi-critical points, different types of high-resolution experimental techniques are usually employed. During the last couple of decades an impressive amount of calorimetric results have been obtained and in many cases a better understanding of several phase transitions in liquid crystals have been reported. These results have been obtained with measuring techniques such as differential scanning calorimetry (DSC), ac calorimetry, steady state calorimetry and the recently introduced photoacoustic and photopyroelectric methods [16-24]. In early days, many of these experimental efforts have largely been devoted to the study of static thermal quantities such as heat capacity and enthalpy. In the last decade, however, a number of high-resolution studies on thermal transport properties during phase transitions are reported. This is achieved by extending ac calorimetry to the high-frequency regime and by applying laser induced photoacoustic or photopyroelectric methods [23-35]. Zammit *et.al* have used the photoacoustic technique for the simultaneous measurement of thermal conductivity, diffusivity and heat capacity during smectic-A to nematic transition in

certain cyanobiphenyl liquid crystals [32]. They are also able to evaluate the critical exponents of these thermal parameters during the phase transition. Apart from these calorimetric studies there exists a number of experimental methods to study the phase transitions in liquid crystals and a few of such methods are light scattering, IR and optical absorption, fluorescence, inelastic neutron scattering, dielectric measurements, electron paramagnetic resonance, ultrasonic studies and x-ray studies [36-47].

Laser induced photoacoustic studies on phase transitions in 4-cyano-4'-heptyloxy biphenyl (7OCB), 4-cyano-4'-octyloxy biphenyl (8OCB) liquid crystals and on certain multi-component nematic liquid crystal mixtures are discussed in the following sections. Regarding 7OCB and 8OCB, phase transition data obtained from investigations using many other methods are available in the literature [48-56]. However, the nematic mixtures investigated here are some of the recently developed compounds by Merck Inc. [57]. BL001, BL002, BL032 and BL035 are the trade names assigned by the manufacturer. Each of these low molecular weight mixtures contains four to nine cyanobiphenyl components. These mixtures possess a wide nematic range around the room temperature and hence they find a lot of applications in display technology.

5.2 Experimental details

Laser induced photoacoustic technique is used to monitor various phase transitions in liquid crystalline materials. A schematic diagram of the experimental set-up is shown in figure 1. The radiation source used to produce the PA signal is a water-cooled argon ion laser (Liconix 5000). The laser emission at 488nm wavelength is used for the investigations. The laser beam having a $1/e^2$ diameter of 1.2mm is intensity modulated at 344Hz using a mechanical chopper (Ithaco HMS 230). The beam is then passed through a convex lens of focal length 5cm. The distance between the lens and the sample surface is adjusted in such a way that the entire surface of the sample gets illuminated. All the measurements are performed at an incident laser power of 20mW. Defocused laser beam at low power level is used to reduce the localised heating at any point in the sample. Investigations are carried out by heating the sample from the room temperature to elevated temperatures. Temperature scanning rate of 0.2 °C per minute is adopted throughout the measurements. The output of the microphone (Knowles BT1834) is recorded at regular intervals of temperatures using a single phase analog lock-in-amplifier (Stanford Research Systems SR 510).

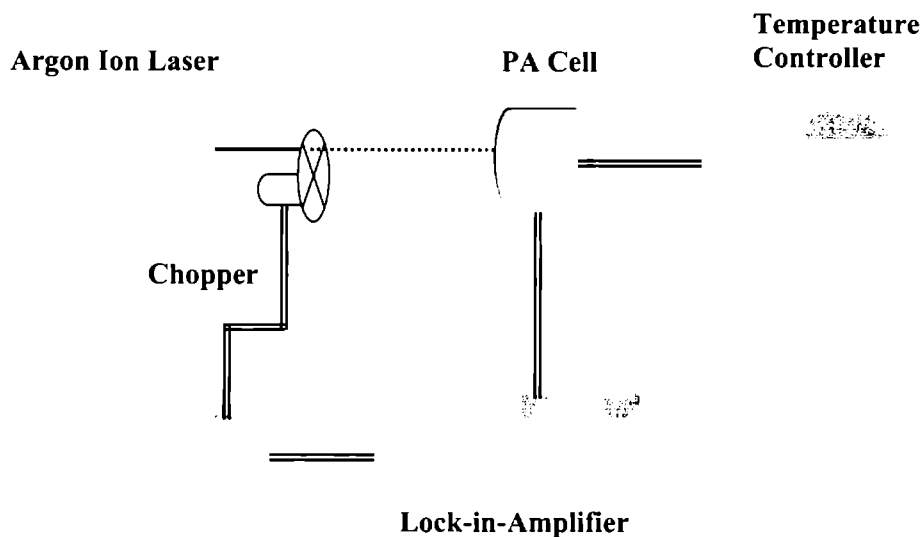


Figure 1: Schematic diagram of the experimental set-up used for the phase transition studies.

Cross-sectional view of the resonant PA cell used for the investigations is shown in figure 2. The sample chamber is 3mm in radius and 6mm in depth. Top of the sample compartment is closed with a glass window which allows the optical radiation to impinge on the sample. In order to protect the microphone from damage due to heating of the sample, the microphone compartment is positioned away from the sample chamber. The two chambers are then acoustically coupled through a thin-walled stainless steel tube of inner diameter 1mm and of length 19cm. This resonant PA cell has an acoustic resonance peak at 440 Hz. The cell has provision to operate in the temperature range from 77K to 400K. For subzero-temperature measurements, liquid nitrogen can be used to cool down the sample temperature. Meanwhile, the heater coil (60W) wound over the sample chamber serves as the heat source for above-room-temperature studies. The heater coil together with a stabilised DC power supply and a chromel-alumel thermocouple forms the temperature controller unit. The thermocouple is inserted into the body of the sample chamber through a narrow bore of diameter 1mm which is drilled from one side of the cell body and ends up very close to the sample in the chamber.

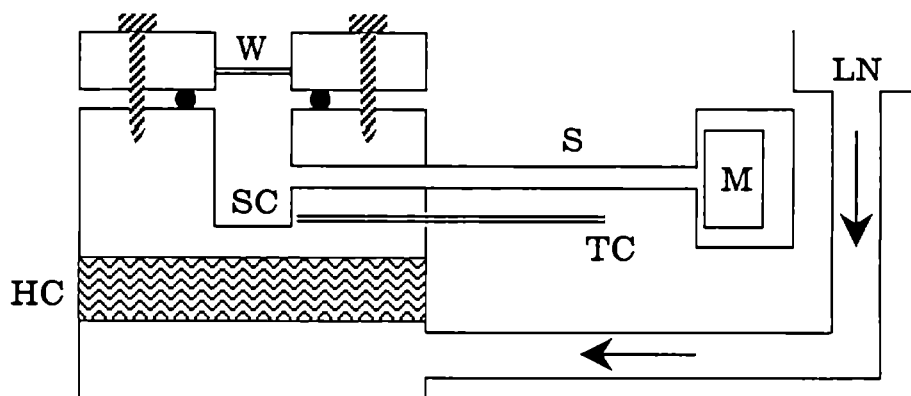


Figure 2: Cross-sectional view of the temperature variable photoacoustic cell. **W** the glass window; **SC** the sample chamber; **HC** the heater coil; **S** the stainless steel tube; **TC** the thermocouple; **M** the microphone and **LN** the provision for pouring liquid nitrogen.

5.3 Results and discussion

5.3.1 Phase transitions in 7OCB and 8OCB

The liquid crystals 7OCB and 8OCB are obtained from Merck Inc. UK and are used without further purification. These compounds are white powder in the crystalline state at room temperature, while in the smectic-A and nematic phases they are white viscous fluids and finally in the isotropic phase they appear like an ordinary, colourless liquid. Similar to most of the other liquid crystals, 7OCB and 8OCB do not absorb the optical radiation in the visible region [5-8,36]. Hence, in order to generate the photoacoustic signal, these materials are mixed with a very small amount (0.5 % weight) of an organic dye Eosin (Merck) which has a very good absorption at the excitation wavelength (488nm). High thermal stability as well as the good photostability of the dye has been taken into account while selecting it as the colouring substance. The liquid crystal sample taken in the photoacoustic cell has a thickness of about 2 millimetre. The photoacoustic signal amplitude is recorded during the heating of the sample, starting from the crystalline phase. Great care is taken in the choice of the laser beam intensity as well as the heating rate to make sure that the photoacoustic signal profile is not affected by too high a laser intensity or by a high heating rate. Though a thick layer of the sample is used for the investigations, the photoacoustic signal is mainly contributed by the light absorbed within the first thermal diffusion length of the material [58]. The thermal diffusion length μ is equal to

$\sqrt{2\alpha/\omega}$, where α is the thermal diffusivity and ω is the modulation frequency. Usually, the

thermal diffusion length is only a few micrometer in liquid crystals [5-8,31,36]. Consequently, the alignment and other properties of the surface layer will reflect in the photoacoustic signal.

Since the PA signal profile varies with pressure and temperature inside the cell and depends on the thermal properties of the gas (air), calibration of the experimental system is necessary. For this purpose, the temperature response of the PA cell is recorded using carbon black as the sample. The observed signal amplitude profile is shown in figure 3. This data is used to normalise the PA signals obtained from the liquid crystal samples.

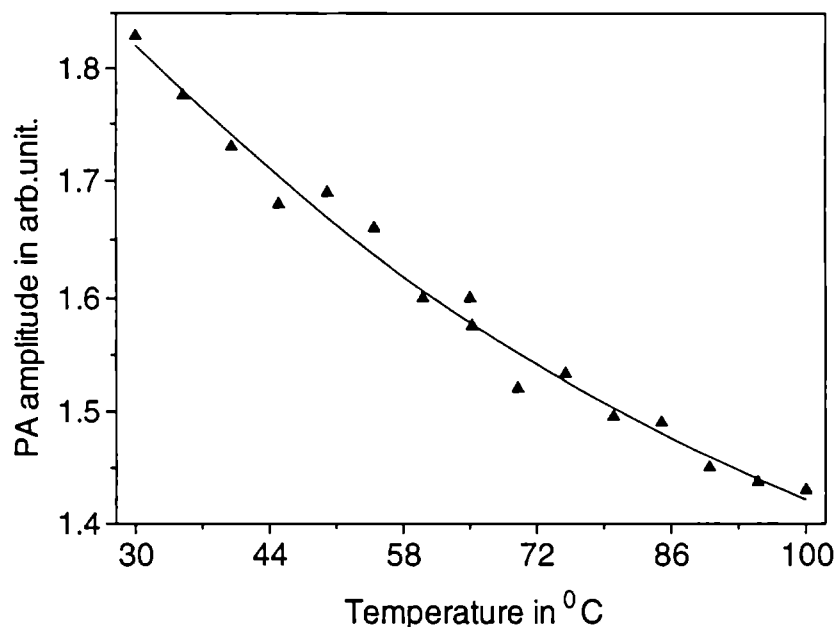


Figure 3: Response of the PA cell with respect to temperature, recorded using carbon black sample.

The normalised PA signal amplitude variation during heating of the liquid crystal 8OCB, starting from the crystalline phase, is shown in figure 4. From this plot it can be seen that there is a remarkable variation in the PA signal amplitude at three distinctly different temperatures. This anomalous behaviour of the signal is obviously due to the sudden changes in the thermal parameters like heat capacity, thermal conductivity etc of the sample. Such changes occur normally during transition from one phase to another phase of the material. In the case of 8OCB, the observed transition temperatures are 54.3 °C, 66.9 °C and 80.8 °C. These values are in agreement with the reported phase transition temperatures 54 °C, 67.2 °C and 80.2 °C of this particular liquid crystal [18,49-52]. These transition temperatures are assigned to crystalline to smectic-A, smectic-A to nematic and nematic to isotropic transitions respectively.

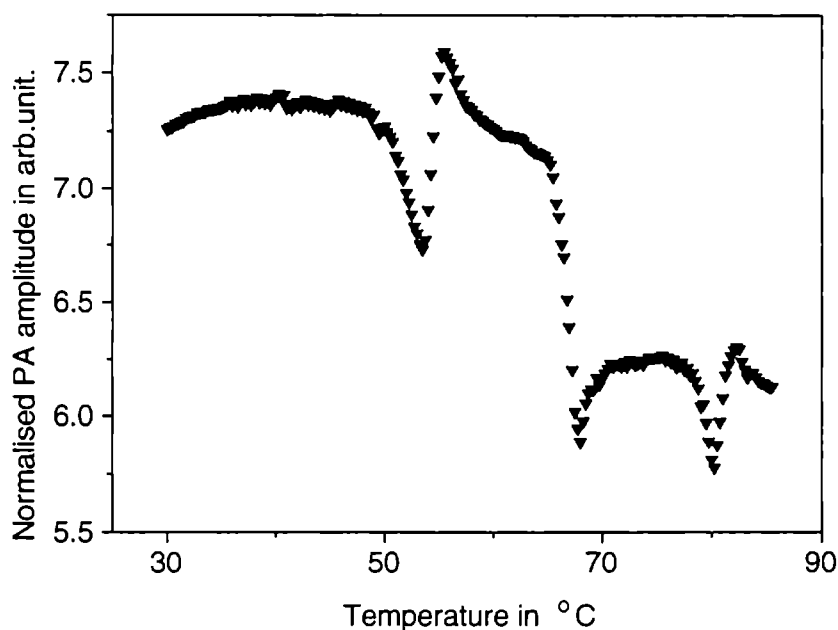


Figure 4: PA signal amplitude versus temperature plot for 8OCB.

From the thermodynamical point of view, the large decrease in the PA signal profile during melting, *i.e.* the crystalline to smectic-A transition, can be explained as follows. During melting, all the available heat is absorbed by the melting process. Or in other words the sample acts a heat sink for the entire heat, including the heat generated by the photoacoustic process. Consequently the PA signal amplitude drops markedly, as visible in figure 4. It is worthwhile to note that, in figure 4, the crystalline to smectic-A and nematic to isotropic transitions are marked by a dip in the PA signal profile followed by a small peak structure. These two transitions are reported to be first order in nature [49-52]. On the other hand, during the smectic-A to nematic transition, the dip in PA signal profile has smaller depth compared to the other two transitions. Also in this case, the PA signal profile does not carry any peak structure in the vicinity of transition temperature. Further more, in the case of smectic-A to nematic transition, the sudden change in PA signal amplitude is restricted to a relatively small temperature range while for the other two transitions the change in the signal amplitude is visible over a much larger temperature range. These facts attributes a different nature for the smectic-A to nematic transition in 8OCB, which is reported to be essentially a second order transition [15,50,51].

Similar results have been observed in the case of the liquid crystal 7OCB as well. The normalised PA signal variation with temperature for 7OCB is shown in figure 5. In this case, only two transitions are observed and the corresponding transition temperatures are 55.6 °C and 74 °C. These values are in agreement with the earlier reported values of 55 °C and 73.5 °C,

which corresponds to crystalline to nematic and nematic to isotropic liquid transitions respectively [48,59,60]. Both the transitions are first order in nature. In the case of both the liquid crystals, no major change in the transition temperatures has been observed in comparison with the earlier reported values. This clearly indicates that the transition temperatures of 7OCB and 8OCB remain almost unaffected by the addition of a small amount of the organic dye. It has already been reported that the very low concentrations of dyes in the liquid crystals will not affect their thermal properties or transition temperatures in any appreciable manner [61].

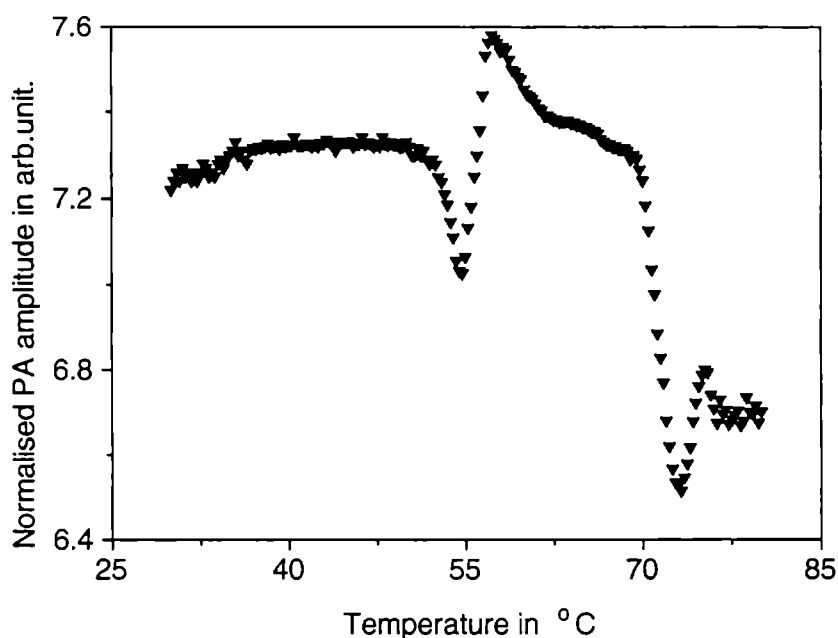


Figure 5: PA signal amplitude versus temperature plot for 7OCB.

5.3.2 Phase transitions in nematic liquid crystal mixtures

The nematic liquid crystal mixtures, namely BL001, BL002, BL032 and BL035, used for the investigations are obtained from Merck Inc. UK [57]. All these compounds are in the nematic phase at room temperature and transform to isotropic liquid phase at elevated temperatures. These mixtures also do not absorb the optical radiation in the visible region and hence as in the case of previous measurements, organic dye Eosin (0.5% by weight) is added to enhance the light absorption at the excitation wavelength (488nm). The liquid crystal samples kept inside the photoacoustic cell have a thickness of around 2mm. The samples are then thermally thick and optically transparent. Again, the measurements are carried out by heating the sample, starting from the nematic phase.

The photoacoustic signal recorded in the case of the liquid crystals BL001 and BL002 during the heating process is shown in figure 6. From these plots it is clear that as the temperature crosses the transition point, the photoacoustic signal amplitude changes from a maximum to a minimum. Similar observations have been made in the case of liquid crystals BL032 and BL035 and the photoacoustic signal profile during the nematic to isotropic transition of these liquid crystals are shown in figure 7. The observed values of transition temperatures are 60.8 °C and 71.8 °C for BL001 and BL002 respectively. The transition temperature of BL032 and BL035 are located at 86.7 °C and 95.7 °C respectively. These values are in good agreement with the thermal data provided by Merck Inc. [57]. According to the manufacturer the nematic to isotropic transition temperatures are 61 °C, 72 °C, 87 °C and 96 °C, respectively, for BL001, BL002, BL032 and BL035. Hence the present observations also confirm that the addition of a trace amount of a dye to the liquid crystals does not affect the transition temperature in any significant manner.

From figures 6 and 7, we can see that there is a gradual increase in photoacoustic signal in the nematic phase as the temperature approaches the transition temperature. It is a well known fact that the elastic properties such as the surface tension and viscosity vary gradually with rise of temperature in the nematic range itself [5-8,31,36]. This may have some influence on the gradual increase of photoacoustic signal in the nematic phase itself as the temperature approaches the transition point. However, this is a special case associated with liquid crystals alone and hence the available general theories for photoacoustic effect are not sufficient to give a satisfactory explanation for this observation.

Another important point that has to be noticed from figures 6 and 7 is that the signal amplitudes in the nematic and isotropic phases differ by a large value. Eventhough the dependence of density on the photoacoustic signal is clearly explained in the Rosencwaig-Gersho theory, the change in volume and hence the change in density during nematic to isotropic transition is less than 0.5% in most of the liquid crystals [5-8,31,36]. Hence density change cannot account for such a large difference in photoacoustic signals in the two phases. But, it is a well-known fact that the nematic phase possesses strong light scattering property compared to the isotropic phase. In the present case, the sample is optically transparent at the excitation wavelength and hence the absorption and scattering processes will take place along the entire thickness of the sample. Under the present experimental condition such a multiple scattering effect in the nematic phase will increase the effective path length of the light beam inside the sample, leading to an increased light absorption and correspondingly an enhanced photoacoustic signal in the nematic phase. In fact this difference in signal amplitudes between

the ordered nematic phase and the isotropic liquid phase is clearly visible in the case of 7OCB also (figure 5), but in the case of 8OCB this difference (figure 4) is not as large as in the other cases. It must be noted here that 8OCB has an additional smectic-A phase and it is not clear whether the presence of this mesophase will influence any of the physical properties in the nematic phase.

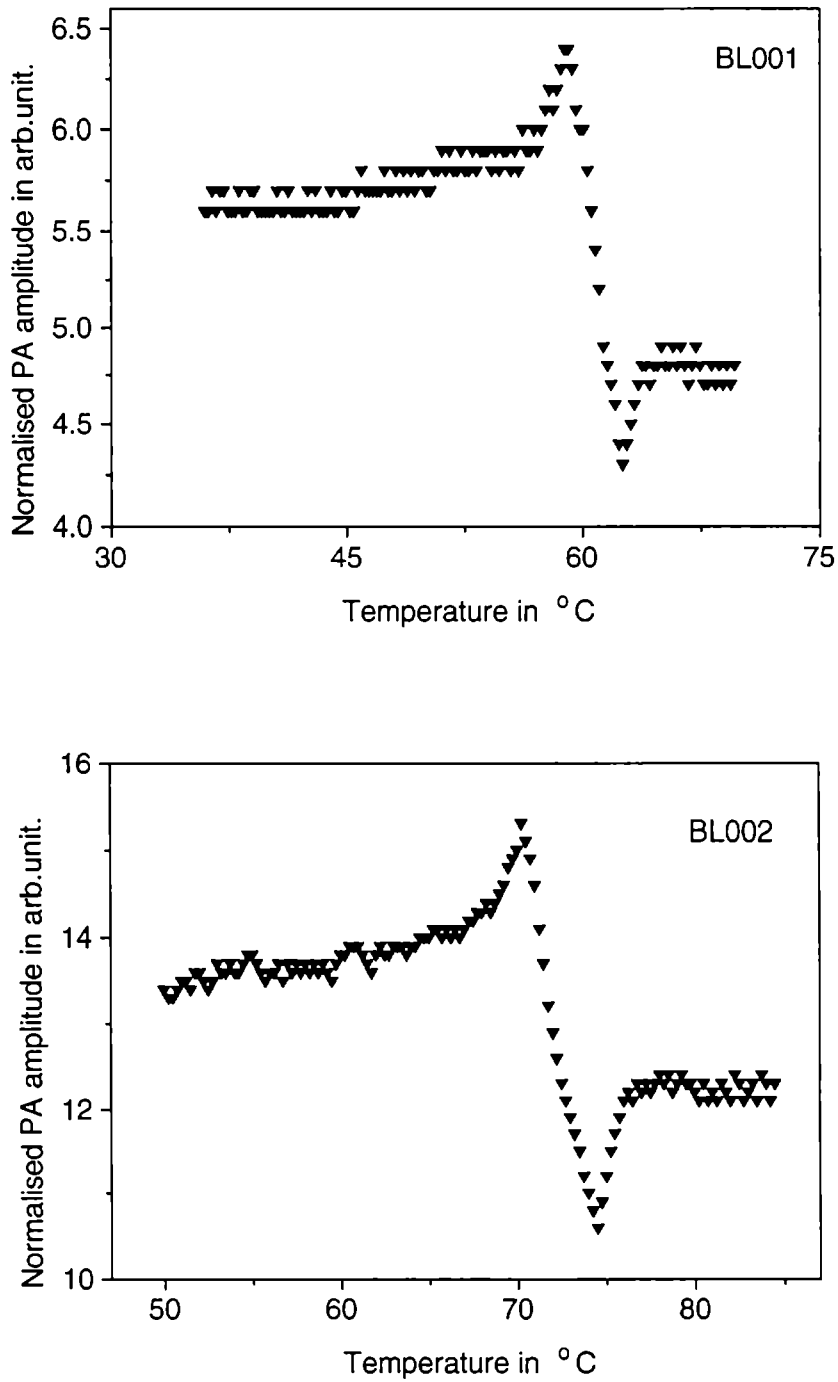


Figure 6: PA signal amplitude versus temperature plot for BL001 and BL002.

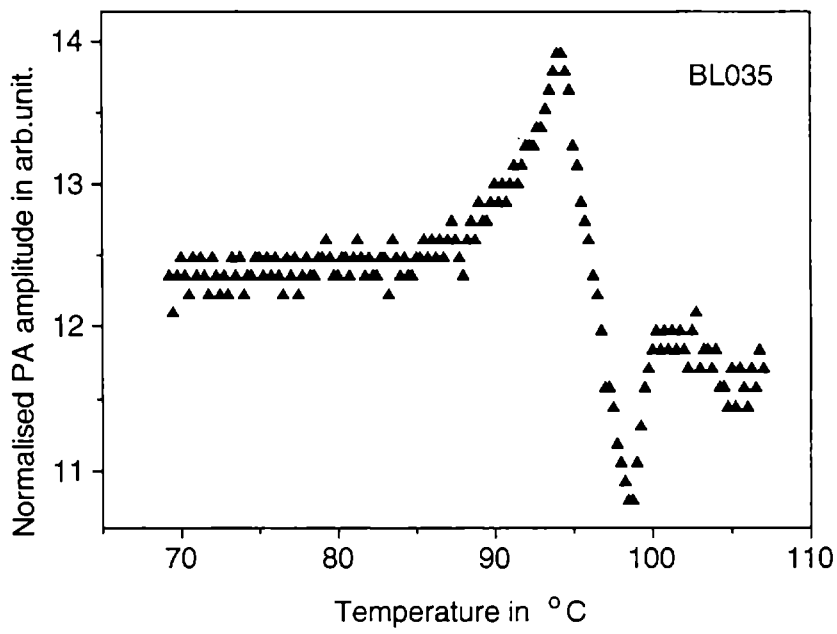
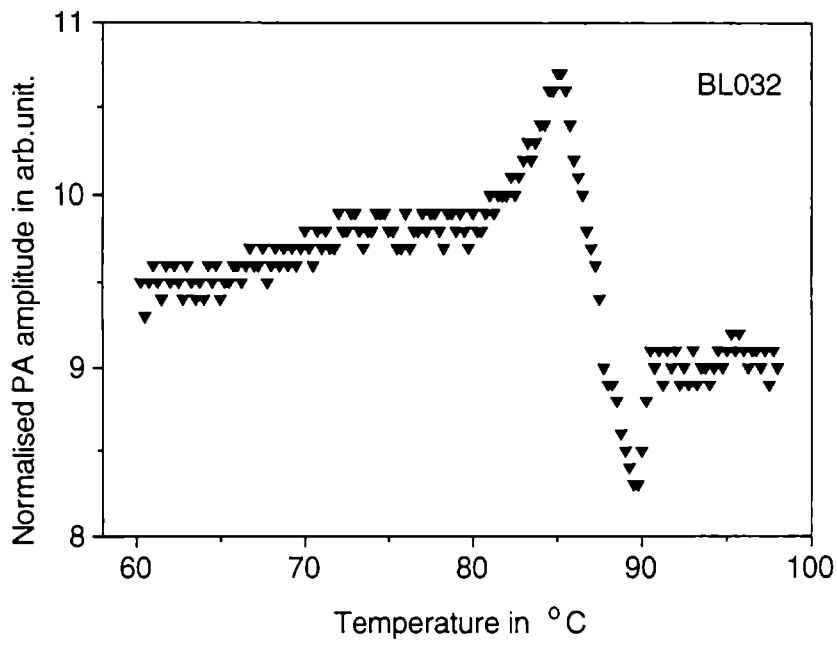


Figure 7: PA signal amplitude versus temperature plot for BL032 and BL035.

5.3.3. Analysis of the PA signal profile using R-G theory

Rosencwaig and Gersho developed the theory for photoacoustic effect in 1976 [58]. This one-dimensional heat flow model is valid in most of the cases and a complete discussion regarding this is given in *chapter 2*. For the complex photoacoustic signal $Q = q \exp(-i\psi)$, with amplitude q and phase ψ (with respect to the incident radiation), the following equation holds:

$$Q = \frac{\eta\beta I_o \gamma_g P_o}{2\sqrt{2}T_o k l_g a_g (\beta^2 - \sigma^2)} \left[\frac{(r-1)(b+1)e^{\sigma l} - (r+1)(b-1)e^{-\sigma l} + 2(b-r)e^{-\beta l}}{(g+1)(b+1)e^{\sigma l} - (g-1)(b-1)e^{-\sigma l}} \right] \quad (1)$$

where, I_o , P_o and T_o are respectively, the incident light intensity, the ambient pressure and temperature; γ_g the ratio of heat capacities of the gas, k and β are the thermal conductivity and optical absorption coefficient of the sample, l the sample thickness, l_g the thickness of the gas column in the cell, and $\sigma = (1+i)a$, with $a = 1/\mu$ the thermal diffusion coefficient. η is the light to heat conversion efficiency. One further has $b = \left(\frac{k_b a_b}{ka} \right)$, $g = \left(\frac{k_g a_g}{ka} \right)$, $r = (1-i)\beta/2a$. Here, the subscripts g and b refer to the gas and the backing material. When the sample is optically transparent and thermally thick, we can set $e^{-\beta l} \cong 1 - \beta l$, $e^{-\sigma l} \cong 0$ and $|r| \ll 1$, then the expression for acoustic signal will reduce to the form,

$$Q \cong \frac{-i\gamma P_o I_o}{4\sqrt{2}T_o l_g} \frac{\beta \mu_s^2}{a_g k_s} \quad (2)$$

In this case, only the light absorbed within the first thermal diffusion length contributes to the signal, in spite of the fact that light is being absorbed throughout the length of the sample. Also, since the thermal diffusion length of the sample is smaller than the sample thickness, the backing material would not have any contribution to the PA signal. The above equation can be written as

$$Q = K \left(\frac{\mu_g}{T_o} \right) \left(\frac{\mu_s^2}{k_s} \right) \quad (3)$$

where the proportionality constant K includes all the constant terms in equation (2). For air, $\left(\mu_g/T_o \right)$ is a slowly varying function of temperature, which can be evaluated from the thermal parameters of air. The term $\left(\mu_s^2/k_s \right)$ is equal to $\left(2/\omega \rho_s C_s \right)$ where ω is the chopping

frequency, ρ_s and C_s are the density and heat capacity of the sample. Hence the reciprocal of the PA signal amplitude multiplied by (μ_g/T_0) will be a quantity proportional to the heat capacity of the sample. The variation of (μ_g/T_0) with temperature is shown in figure 8 [62].

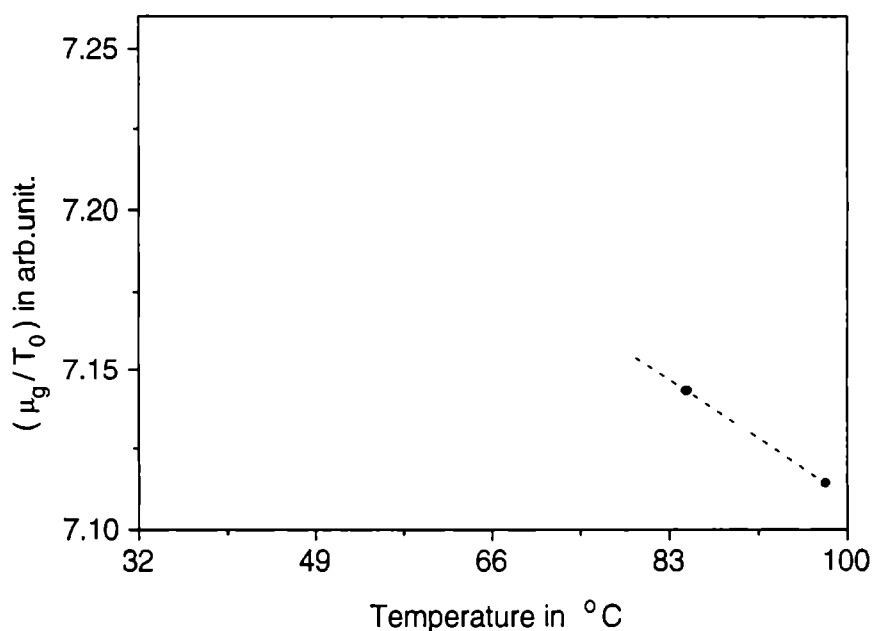


Figure 8: Variation of (μ_g/T_0) of air with temperature.

The behaviour of $[(1 / \text{PA signal}) \times (\mu_g / T_0)]$, which is proportional to specific heat capacity, with respect to temperature is studied for all the liquid crystals. The corresponding plot for the liquid crystals 7OCB and 8OCB are shown in figure 9. From this plot, we can see that the quantity proportional to the heat capacity of both liquid crystals exhibits a sharp peak structure across the transition regions. It is worthwhile to note here that the sharp increase in heat capacity is occurring in a narrow temperature range during the second order smectic-A to nematic transition. But, in the case of the other two first order transitions, namely crystalline to smectic-A and nematic to isotropic transitions, the increase in heat capacity occur in a much broader temperature range. Also, the intensity of the peak during the smectic-A to nematic transition of 8OCB is less than that during nematic to isotropic transition. This is in good agreement with the earlier high-resolution ac calorimetric measurement on 8OCB made by Garland *et.al.* [51].

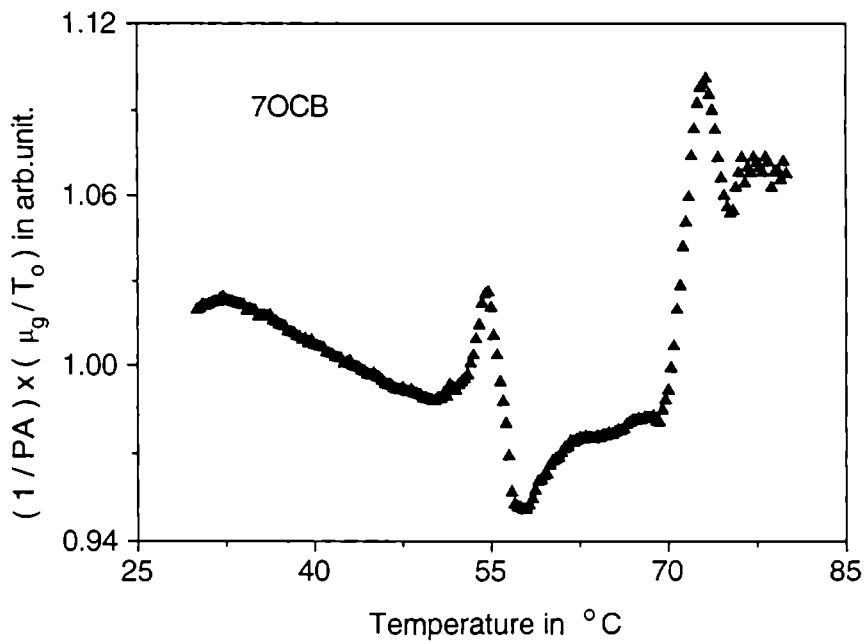
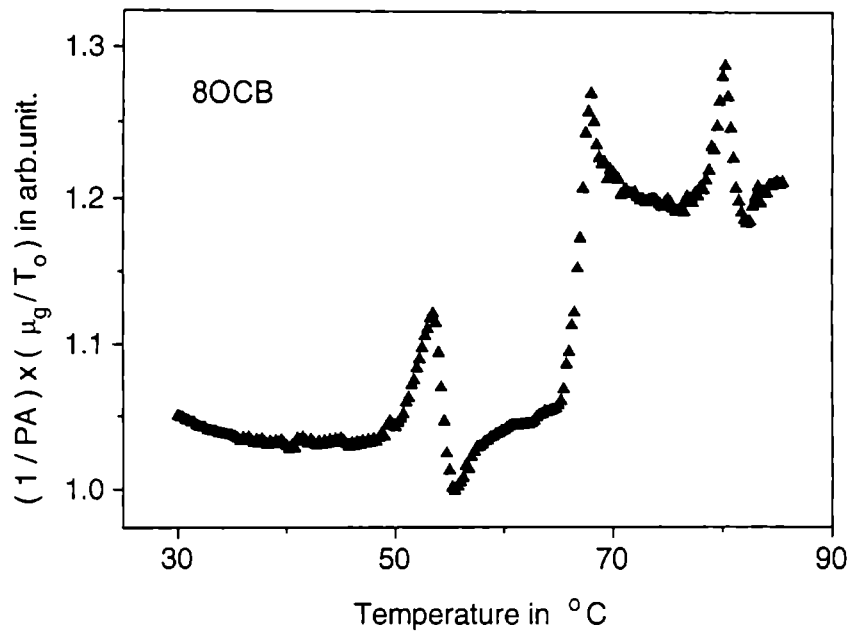


Figure 9: $[(1/PA \text{ signal}) \times (\mu_g/T_0)]$ versus temperature plot for 80CB and 70CB.

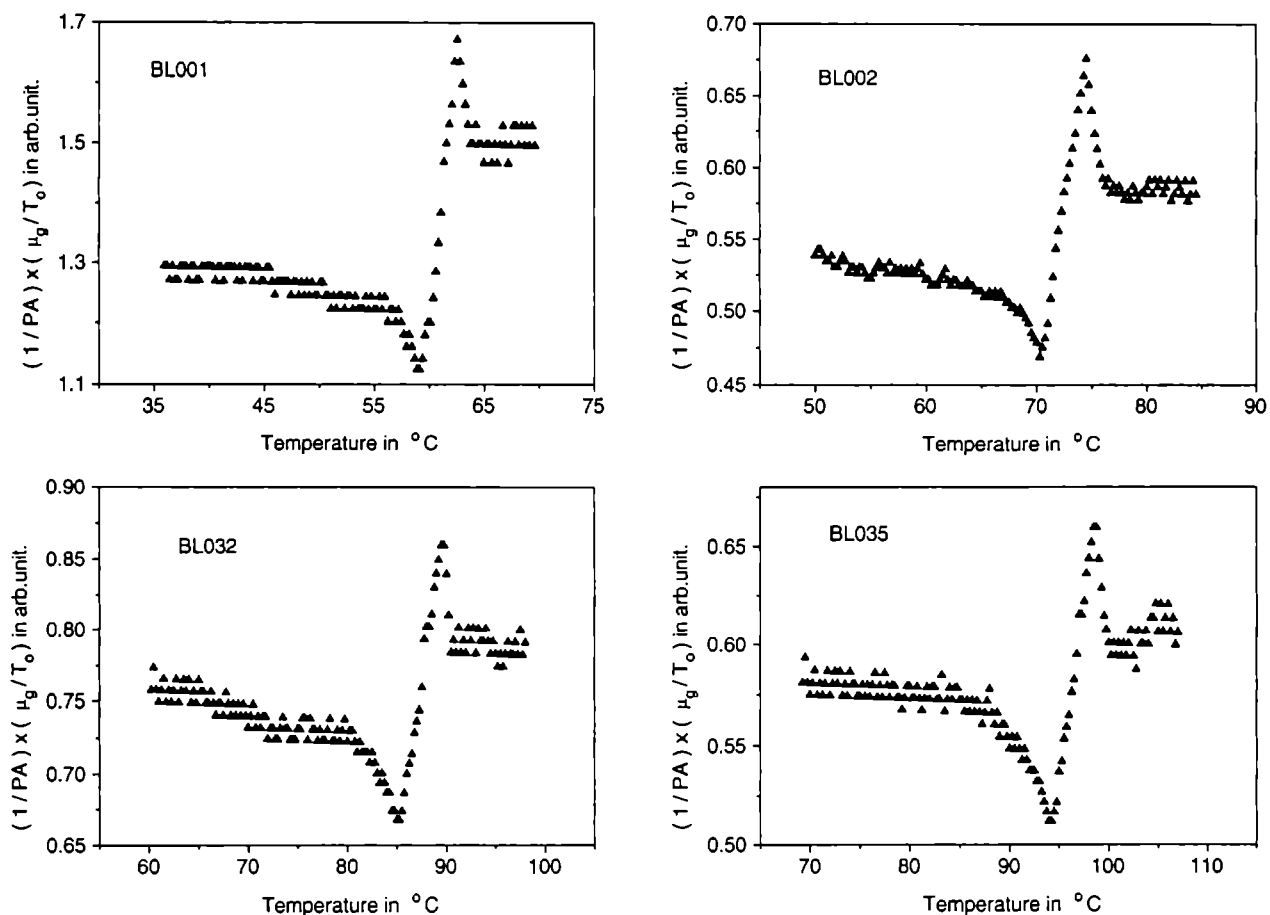


Figure 10: $[(1/PA \text{ signal}) \times (\mu_g/T_0)]$ versus temperature plot for the nematic mixtures BL001, BL002, BL032 and BL035.

The typical behaviour of $[(1/PA \text{ signal}) \times (\mu_g/T_0)]$ with respect to the temperature, for the nematic liquid crystal mixtures is shown in Figure 10. Typically, the specific heat capacity of liquid crystals shows only a sharp peak structure across the transition temperature [5-8,31,36,48-56]. The present observation of a dip structure prior to the transition peak is resulting from the gradual increase in the PA signal in the nematic phase as the temperature approaches the transition temperature. This dip in the heat capacity profile may be due to some surface effects as discussed in the previous section. Again, the difference in the signal amplitudes in the nematic and isotropic phases are attributed to the difference in bulk light scattering properties in these two phases. However, any reports regarding the phase transition studies on these nematic liquid crystal mixtures are not available in the literature for a comparative study. Though, the present measurement is only a qualitative one, the same method can be used to evaluate the absolute values of static and dynamic thermal parameters of the liquid crystals if the material under investigation is optically opaque at the excitation wavelength [32].

5.4 Conclusions

The application and advantages of photoacoustic technique for determining the phase transition temperatures in a variety of liquid crystals are discussed. First order as well as a near second order phase transition in two alkoxy-cyanobiphenyl liquid crystals, 7OCB and 8OCB, have been studied using a gas-microphone photoacoustic technique. The observed phase transition temperatures are found to be in good agreement with the earlier reported values. It is confirmed that the addition of a very small quantity of an organic dye to the liquid crystals will not affect the transition temperatures in any significant manner. Results obtained from the nematic liquid crystal mixtures are also very promising. The difference in the measured signal amplitude in the nematic and isotropic phases is attributed to the difference in the light scattering properties associated with the degree of order of these phases. Decrease in signal amplitude during phase transitions is mainly due to the increase in the heat capacity of the liquid crystal.

Present investigations show that the PA technique is a powerful analytical tool for the study of variations in thermal parameters associated with phase transitions in liquid crystals and in the identification of the order of transition. This method is very simple, less time consuming and can be performed using an optical radiation at any wavelength by properly selecting the dye and hence is a very promising tool for the thermal characterisation of liquid crystals.

References

1. Stanley.H.E, *Introduction to phase transitions and critical phenomena*, (Oxford University Press, New York) (1987)
2. Domb.C and Green.M.S (Eds.), *Phase transitions and critical phenomena*, **Vol. 2**, (Academic Press, New York) (1976)
3. Domb.C and Lebowitz.J.L (Eds.), *Phase transitions and critical phenomena*, **Vol. 14**, (Academic Press, New York) (1989)
4. Chaikin.P.M and Lubensky.T.C, *Principles of condensed matter physics*, (Cambridge University Press, Cambridge) (1995)
5. Chandrasekhar.S, *Liquid crystals*, (Cambridge University Press, Cambridge) (1992)
6. De Gennes.P.G, *The physics of liquid crystals*, (Oxford University Press, New York) (1974)
7. Saeva.F.D (Edit.), *Liquid crystals, the fourth state of matter*, (Marcel Dekker, New York) (1979)
8. Gray.G (Edit.), *Physical properties of liquid crystalline materials*, (Gordon and Breach) (1980)
9. Poniewierski.A and Sluckin.T.J, *Phys. Rev. Lett.* **55**, 2907 (1985)
10. Cladis.P.E, *Phys. Rev. Lett.* **35**, 48 (1975)
11. Vertogen.G, De Jeu.W.H, *Thermotropic liquid crystals: fundamentals*, (Springer-Verlag, Berlin) (1993)
12. Maier.W and Saupe.A, *Z.Naturforsch*, **A14**, 882 (1959)
13. Kobayashi.K.K, *Phys.Lett.A*, **31**, 125 (1970)
14. Kobayashi.K.K,*J.Phys.Soc.Japan.* **29**, 101 (1970)
15. McMillan.W.L, *Phys.rev.A*, **4**, 1238 (1971)
16. Iannacchione.G and Finotello.D, *Phys.Rev.Lett.* **69**, 2094 (1992)
17. Geer.R, Stoebe.T, Pitchford.T and Huang.C.C, *Rev.Sci.Instrum.* **62**, 415 (1991)
18. Cladis.P.E, Bogardus.R.K and Aadsen.D, *Phys.Rev.A*, **18**, 2922 (1978)
19. Thoen.J, Marynissen.H and dael.W.V, *Phys.Rev.A*, **26**, 2886 (1982)
20. Birgeneau.R.J, Garland.C.W, Kasting.G.B and Ocko.B.M, *Phys.Rev.A*, **24**, 2624 (1981)
21. Das.P, Nounesis.G, Garland.C.W, Sigaud.G and tinh.N.H, *Liq.Cryst.* **7**, 883 (1990)
22. Cladis.P.E, Guillon.D, Bouchet.F.R and Finn.P.L, *Phys.Rev.A*, **23**, 2594 (1981)
23. Mandelis.A, Schobus.E, Paralta.S.B and Thoen.J, *J.Appl.Phys.* **70**, 1771 (1991)
24. Thoen.J, Glorieux.C, Schoubs.E and Lauriks.W, *Mol.Cryst.Liq.Cryst.* **191**, 29 (1991)

25. Zammit.U, Marinelli.M, Pizzoferrato.R, Scudieri.F and Martellucci.S, *J.Phys.E: Sci.Instrum.* **21**, 935 (1988)
26. Mityurich.G.S, Zelenyi.V.P, Semchenko.I.V and Serdyukov.A.N, *Opt.Spectroscop. (USSR)*, **72**, 233 (1992)
27. Puccetti.G and Leblanc.R.M, *J.Chem.Phys.* **108**, 7258 (1998)
28. Glorieux.C, Bozoki.Z, Fizez.J and Thoen.J, *J.Appl.Phys.* **78**, 3096 (1995)
29. Glorieux.C, Schoubs.E and Thoen.J, *Mater.Sci.Eng.* **A122**, 87 (1989)
30. Zammit.U, Marinelli.M, Pizzoferrato.R, Scudieri.F and Martellucci.S, *Liq.Cryst.* **4**, 619 (1989)
31. Martellucci.S and Chester.A.N (Eds.), *Phase transitions in liquid crystals*, (Plenum Press, New York) (1992)
32. Zammit.U, Marinelli.M, Pizzoferrato.R, Scudieri.F and Martellucci.S, *Phys.Rev.A*, **41**, 1153 (1990)
33. Mercuri.F, Ghosh.A.K and Marinelli.M, *Phys.Rev.E*, **60**, R6309 (1999)
34. Marinelli.M, Mercuri.F, Zammit.U and Scudieri.F, *Phys.Rev.E*, **58**, 5860 (1998)
35. Sahraou.A.H, Louis.G, Mangeot.B, Peretti.P and Billards.J, *Liq.Cryst.* **5**, 579 (1989)
36. Collings.P.J and Patel.J.S (Eds.), *Handbook of Liquid Crystal Research*, (Oxford University Press) (1997)
37. Ozbek.H, Yildiz.S and Pekcan.O, *Phys.Rev.E*, **59**, 6798 (1999)
38. Siny.I.G, Tu.C.S and Schmidt.V.H, *Mol.Cryst.Liq.Cryst.*, **269**, 125(1995)
39. Booth.K.M and Coles.H.J, *Liq. Cryst.* **13**, 677 (1993)
40. Monval.MO, Coles.H.J, Lalanne.J.R, Marcerou.J.P and Philip.J, *J. Chem. Phys.* **101**, 6301 (1994)
41. Chen.D.H and Luckhurst.G.R, *Trans. Faraday Soc.* **65**, 656 (1969)
42. Heeks.S.K and Luckhurst.G.R, *J. Chem. Soc. Faraday Trans.* **89**, 3783 (1993)
43. Panarin.Y.P, Aliev.F.M, and Rosenblatt.C, *Phys. Rev. Lett.* **81**, 2699 (1998)
44. George.A.K, *Acustica*, **73**, 287 (1991)
45. Eden.D, Garland.C.E and Williamson.R.C, *J.Chem.Phys.* **58**, 1861 (1973)
46. Mohandas.K.P and George.A.K, *J.Chem.Phys.* **96**, 4779 (1992)
47. Reiker.T.P, Clark.N.A, Smith.G.S, Parmar.D.S, Sirota.E.B and Safinya.C.R, *Phys.Rev.Lett.* **59**, 2658 (1987)
48. Agarwal.V.K, Khamis.K.M and Arora.V.P, *Ind.J.Pure.Appl.Phys.* **26**, 614 (1988)
49. Viner.J.M and Huang.C.C, *Solid.Stat.Comm.* **39**, 789 (1981)
50. Kasting.G.B, Lushington.K.J and Garland.C.W, *Phys.Rev.B.* **22**, 321 (1980)

51. Garland.C.W, Kasting.G.B and Lushington.K.J, *Phys.Rev.Lett.* **43**, 1420 (1979)
52. Huang.C.C, Pindak.R.S and Ho.J.T, *Solid.Stat.Comm.* **25**, 1015 (1978)
53. Johnson.D.L, Hayes.C.F, deHoff.R.J and Schants.C.A, *Phys.Rev.B.* **18**, 4902 (1978)
54. Beaubois.F, Claverie.T, Marcerou.P, Rouillon.J.C and Nguyen.H.T, *Phys.Rev.E.* **56**, 5566 (1997)
55. Cox.R.J, Barrall.E.M, Doelman.A, Clecak.N.J, Logan.J.A, Diller.R.D and Greggs.A.R, *Annal.Calorimetry.* **4**, 37 (1977)
56. Orwoll.R.A, Sullivan.V.J and Campbell.G.C, *Mol.Cryst.Liq.Cryst.* **149**, 121 (1987)
57. *Liquid Crystal Data Sheet*, (Merck. Inc., England) (1995)
58. Rosencwaig.A and Gersho.A, *J.Appl.Phys*, **47**, 64 (1976)
59. Jakli.A, Janossy.I and Vajda.A, *Liq.Cryst.* **8**, 1035 (2000)
60. Hori.K, Koma.Y, Kurosaki.M, Itoh.K, Uekusa.H, Takenaka.Y and Ohashi.Y, *Bull.Chem.Soc.Japan.* **69**, 891 (1996)
61. Scudieri..F, Marinelli.M and Martellucci.S, *J.Phys.D:Appl.Phys.* **20**, 1045 (1987)
62. *CRC Handbook of physics and chemistry* (Boca Raton) (1999)

Photoacoustic investigations on photostability of Rhodamine 6G doped PMMA

Synthesis of rhodamine 6G doped poly (methyl methacrylate) samples and their photostability studies using a laser induced photoacoustic technique are discussed in this chapter. The linear dependence of photoacoustic signal amplitude on the optical absorption coefficient of the sample is made use of in these measurements. rhodamine 6G doped PMMA samples are prepared using conventional free-radical polymerization method. Investigations are carried out at different incident light intensities, wavelengths, dye concentrations and modulation frequencies. The photobleaching rate is found to increase monotonically with increase in pump power and decrease with increase in dye concentration. Various aspects of the mechanisms of the photodegradation of the dye molecules and the role of different externally influencing parameters such as wavelength, modulation frequency etc. are discussed in detail.

6.1 Importance of dye doped polymers

Conventional laser systems employing solutions of organic dyes have been in existence for many years and are widely used as tunable lasers, from the ultraviolet to the near infrared range [1-10]. However, the need of complex and bulky laser designs, requirement of large volumes of the organic solvents and handling problems have limited their use in many applications. Consequently, from the early days of the development of liquid state dye lasers, people are looking for an alternative, a solid state strategy, to employ these organic chromophores. In fact a direct employment of the dye materials as solid-state cast films is not feasible because of increased luminescence quenching resulting from a strong interaction of excited-state molecules [7-10]. This molecular quenching mechanism leads to a complete suppression of stimulated emission in pure dye films. A strategy to circumvent this concentration quenching due to molecular interaction is, therefore, to spatially separate the dye molecules by incorporating them as guests in host materials [11-14].

As a result of the search for new laser materials in the last decade there has been a renewed interest in the use of solid matrices containing laser dyes to produce tunable solid-state dye lasers [13-27]. A solid host for lasing dyes is an attractive alternative to the liquid-phase dye lasers with obvious advantages such as compactness, manageability, lack of toxicity and flammability, suppression of flow fluctuations, solvent evaporation etc. In the dye doped solid matrix systems, the dye molecules are dispersed in a solid host medium which is either chosen to be polymers or sol-gel materials. Soffer and McFarland in 1967 [11] and Peterson and Snavely in 1968 [12] independently reported stimulated emission from polymer matrices doped with organic dyes. Since then a number of solid organic and inorganic polymer matrices have been described, where the laser dyes have been in most cases merely dispersed. Although this approach is very attractive, the first results are not very encouraging, with low lasing efficiencies, fast dye photodegradation and low laser damage threshold of the solid host. Consequently, the research on solid-state dye lasers remained almost dormant for more than a decade. During the past two decades new and optimized approaches have led to significant advances in these systems with respect to laser efficiency and damage threshold. Late 1980's have witnessed the development of improved host materials with higher laser damage resistance, which gave a new interest in this field [15,16,28,29]. Also, in the past decade the synthesis of new high-performance dyes and the implementation of new ways of incorporating the organic molecules into the solid matrix have resulted in significant advances towards the development of practical tunable solid-state dye lasers [30-36].

Even though the recently reported works with silica gels [37-41] have indicated that the sol-gel materials might show higher photostability and better lasing properties than those based on organic polymers, the polymeric matrix approach offers various advantages. Most frequently used polymeric materials are based on methyl methacrylate (MMA), such as poly methyl methacrylate (PMMA) or compositions of methacrylate copolymers like HEMA: MMA etc. [16-21,27,30]. The advantages of these synthetic polymer hosts are better optical transparency, homogeneity of refractive index, good compatibility with the organic dye, inexpensive fabrication techniques, lightweight etc. In addition to these, chemical control of the polarity in the visible range and the modification of viscoelasticity are possible in polymers. Furthermore, new modified polymeric organic materials have been developed with a laser radiation threshold that is comparable to or higher than those of most laser-damage-resistant inorganic glasses and crystals [18,42].

Though the polymers possess a large number of advantages over the conventional dye lasers, the finite lifetime for stable operation of the dye incorporated into the solid host still persists as a limitation to the commercial exploitation of this kind of active laser materials. One of the important parameters to reduce the photodegradation of the dye is to optimize the rigidity of the host. Dissipation of the excess energy of photoexcitation can be favoured by a more efficient phononic coupling of the dye molecule to the host media. This can be achieved by using optimized copolymer mixtures as matrix materials or by covalent linkage of the dye molecules to the polymeric chain [15,20,43].

Apart from the use as active laser media, dye doped polymers find many other applications in the modern photonic technology. Though the photodegradation of the dyes is a disadvantage when these materials are used as a laser medium, the dye degradation can be made use of in many other applications such as holographic recording [44,45]. Several studies on photo-induced bleaching of organic dyes impregnated in solid matrices have been reported during the past few decades [46-49]. Such studies have great importance due to various applications of these materials such as active laser elements, passive Q-switches, optical data storage, photonic displays, optical wave-guides etc. Suitable materials for different applications can be prepared by properly selecting the type of solid matrix and the dye incorporated into it. For example, dye doped polymer can be used as an active laser medium, phthalocyanines doped polymers can be used as Q-switches and dye-sensitized gelatin or poly(vinyl alcohol) can be used as holographic recording media [18,35,49].

In all the applications discussed above, a thorough knowledge of the photostability of the dyes incorporated in a solid matrix is necessary. Several theoretical models have been

developed to explain photobleaching of the dye under pulsed and continuous-wave (cw) irradiation. Dyumaev *et.al.* have studied the dye photodegradation in a polymer matrix under high power pulsed irradiation [18]. They have also developed a theoretical model for the photodestruction of lasing dyes by correlating the dye concentration, pump power, pulse duration and number of pump pulses. Newell *et.al.* have developed a model to explain their observations on dye photobleaching using transmission studies under cw laser irradiation [50]. Filho *et.al.* have studied the laser-induced iodine desorption from polystyrene and compared the results with the theoretical model developed by them [51]. However, these models for cw laser irradiation are generally found to be valid only at low pump powers.

6.2 Methods to measure dye photodegradation

The photodegradation of organic dyes in a solid matrix is essentially due to a photoinduced reaction. Since the primary photo-process is absorption of a photon to create a photoexcited molecule, photochemistry and spectroscopy are intimately related. In a quantitative study, therefore, a radiation source of known intensity and wavelength and an appropriate detector are necessary to detect a photochemical reaction or any other photoinduced changes.

A molecule excited to a higher energy state must return to the ground state, unless it gets involved in a photochemical reaction and loses its identity. In condensed systems there exist a number of ways for the excited molecule to dissipate the excitation energy. Out of these different paths, commonly occurring and most important channels are radiative relaxation (fluorescence or phosphorescence), nonradiative relaxation (usually thermal relaxation) and excited state chemical reaction [52-57].

In the case of a photoexcited dye molecule, any of the above mentioned relaxation mechanisms are possible. Irrespective of whether the dye molecules are in a solution form or embedded in a solid matrix, the amount of energy liberated via radiative or nonradiative relaxation mechanisms is determined by the number of original dye molecules in the ground state as well as those in the excited state. Any kind of a photochemical reaction will result in a change in the number density of the original dye molecules. Consequently, the optical absorption as well as the amount of energy liberated through the radiative or nonradiative channels may change. Hence, by measuring either of these two quantities or both, one can easily make a quantitative evaluation of the photochemical processes that the sample (dye) undergoes. Another way to monitor a photochemical change is the analysis of the resultant products.

In order to induce a photochemical process as well as for its detection one can use either a steady state light source or a pulsed optical radiation. In its broadest sense, we can divide the detection methods into two categories. The first one is purely optical methods in which the radiative relaxation or the optical absorption (or transmission) is investigated. The second method is the photothermal techniques in which the sample is excited using an optical radiation and the quantity detected is the energy released through nonradiative relaxation processes.

6.2.1 Optical methods

Pure optical methods are the oldest and the simplest techniques to study the photodegradation of organic dyes in a solution form or when they are impregnated in a solid matrix [45-50]. Optical transmission studies, fluorescence or phosphorescence methods are some of the major optical methods that can be used for the dye photostability studies. The basic theory applied in the optical transmission studies is the Beer-Lambert law, expressed as

$$I = I_o \exp(-\alpha_\nu \cdot C \cdot l) \quad (1)$$

where I_o and I are the incident and transmitted intensities of the light beam with a frequency ν . α_ν is the optical absorption coefficient which is a function of the frequency (wavelength) of radiation. C and l are the concentration of the absorbing species and the optical path length, respectively. Hence, a change in the number density of the absorbing species (say, the organic dye in the solution or solid matrix) can be detected very easily by simply measuring the transmitted light intensity. This can be done either as a function of time or as a function of wavelength of the incident light, depending on the experimental situation. If the photochemical reaction takes place in a faster time scale, then the time dependent measurements are more suitable; whereas, if it is a very slow process then the wavelength scanning (optical absorption spectrum) is ideal [45]. The advantage of wavelength scanning is that it not only carries the signals of the degradation of the original molecules but also the signatures of the creation of new products and their absorption properties will be visible in the spectrum. Usually a single source of light is used for inducing a photochemical change and for detecting it. Since most of the dyes absorb in the ultraviolet or visible region, lasers and arc lamps are the most suitable sources for this kind of studies. A large number of reports are available in the literature where this simple photon transmission method is used for the photobleaching studies of different dyes in solid matrices [46, 48-50]. The experimental set up usually used for the optical transmission studies is very simple and is shown below.

However, the necessary requirements for employing this method are the need of a good surface optical quality for the sample and it should not be optically opaque. Apart from these, the methods discussed above suffer from many other constraints and hence its application in a detailed study of the different mechanisms responsible for the photodegradation is strictly limited.

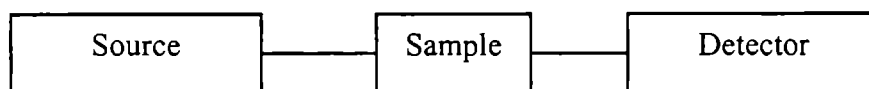


Figure 1. Block diagram of a typical optical transmission set-up for the photostability studies.

In the case of a luminescent dye such as a laser dye, a still better approach is to study the radiative relaxation (fluorescence or phosphorescence). In this approach, the sample is excited using a suitable optical radiation and the variation in the radiative emission during a photochemical change is detected. This method has been employed in many of the photostability studies on dye doped polymers [15,19]. Apart from mere fluorescent studies to investigate the photostability of the dyes, people have also used the decay of laser output when these materials are used as an active laser media [16,20,24,27,30]. If the excitation radiation has sufficiently high energy, then multi-photon absorption may take place and hence the photochemical process will become more complicated [58,59]. In such situations pure optical methods are not sufficient to understand the intricate intermediate steps as well as a complete quantitative evaluation of the photochemical process. The major reason for this is that many of the intermediate steps are associated with nonradiative relaxation processes and this cannot be effectively detected using an all-optical method. In such situations the photothermal methods play a vital role.

6.2.2 Photothermal methods

Photothermal methods are a group of highly sensitive techniques used to measure optical absorption and thermal characteristics of a sample. The fundamental principle of a photothermal method is the *photo*-induced change in the *thermal* state of a sample. Measurements of the temperature, pressure or density changes that occur due to optical absorption form the basis of the photothermal spectroscopic method [60-63]. Sample heating is a direct consequence of optical absorption and hence the photothermal signal is directly dependent on the quantity of the light absorbed. Scattering and reflection losses do not produce photothermal signals. Subsequently, photothermal spectroscopy more accurately measures optical absorption in scattering solutions, solids and at interfaces.

In a photochemical process, generally, intermediate species (radicals) are created and eventually the free radicals convert into some other products. Usually these intermediate steps are associated with nonradiative energy transfer which in turn produces the thermal effects. Hence, photothermal methods are more suitable for detecting these ultrafast processes [64-71]. They can also be used to detect the photochemical changes that occur during a steady state excitation of the molecules. As in the case of thermal and optical characterisation of materials, almost all the photothermal methods can be employed to investigate the photochemical processes. Though many of the photothermal methods are used in the photochemical study of gases or liquids, they are not yet widely employed in solid samples such as dye doped polymers. Photothermal interferometry, photoacoustics, thermal lens, photothermal beam deflection, transient grating etc. are some of the most useful photothermal methods that can be used to investigate photodegradation of organic materials.

6.3 Experimental details

6.3.1 Preparation of rhodamine 6G doped PMMA samples

Rhodamine dyes, belonging to the Xanthene family, with fluorescence emission in the yellow-red region of the spectrum are well known for their excellent laser performance in liquid solutions as well as in solid matrices [7-9]. For the present investigation rhodamine 6G chloride (Loba Chemie Wien) is used as received. Initially, the monomer methyl methacrylate (CDH Chemicals) is mixed with ethyl alcohol (Merck) in the ratio 4:1. Reasons for using ethyl alcohol as an additive to MMA are discussed in the next section. Solutions of monomer - alcohol mixture at three different dye concentrations namely, 1×10^{-3} mol/l, 5×10^{-4} mol/l and 1×10^{-4} mol/l are used for polymerisation. Benzoylperoxide (CDH chemicals) is used as the polymerisation initiator (1% by weight). The monomer-alcohol mixture containing the dye and the initiator held in thin glass test tubes is kept in a constant temperature bath maintained at 50 (± 0.5) °C for polymerisation. Completely polymerised samples obtained after 48 hours is then kept at room temperature for one week for drying. Perfect drying is necessary to avoid shrinkage of the sample. Careful examination (including the absorption spectra) of the polymerised samples confirmed that the dye is homogeneously dispersed in the polymer matrix. Plane undoped PMMA samples are also prepared under the same experimental conditions for using it as a reference sample in optical absorption recording. The dried samples are then cut into small disc like pieces of thickness 1.2 mm and their faces are polished using fine emery paper and finally with woolen cloth. Polishing is done only to reduce the scattering losses.

6.3.2 Recording of photoacoustic spectra

The linear dependence of the PA signal amplitude on the absorption coefficient of the sample is used to record the PA spectrum, which is essentially the optical absorption spectrum, of the dye doped PMMA matrix. For this purpose a 1000W Xe arc lamp (Oriel 6269) is used as the excitation source and a 0.1m monochromator (Oriel 7250) to select the desired wavelength. The block diagram of the experimental setup is shown in figure 2. To protect the monochromator from thermal damage due to the large infrared emission from the arc lamp, a water cell (5cm long) is used in front of the monochromator. The water will effectively filter out the infrared portion of the spectrum. In order to achieve a large signal to noise ratio, the entrance and exit slits of the monochromator are adjusted to get maximum signal (bandwidth 10nm). Light coming out of the monochromator is intensity modulated using a mechanical chopper (Ithaco HMS 230) and the PA signal is processed using a lock-in-amplifier (Stanford Research Systems SR 510).

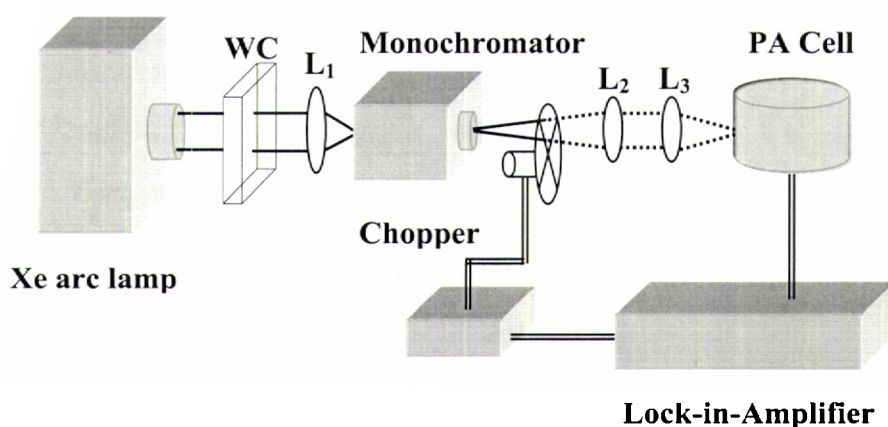


Figure 2. Schematic diagram of the experimental setup used to record the photoacoustic spectra. WC, the water column; L₁, L₂ and L₃, the focusing lenses.

Though the xenon arc emission spectrum is a continuum, its intensity varies from wavelength to wavelength and hence, an intensity normalisation procedure is required. For this purpose carbon black thin film coated on a glass plate is used as the sample. Being a perfectly black body, the absorption and emission of carbon black throughout the spectral region of interest is uniform and hence the PA spectrum recorded using this sample will be essentially the emission spectrum of the arc. The emission spectrum of Xe arc recorded using PA method is shown in figure 3. This spectrum is used to normalise the PA spectrum of the dye doped PMMA samples and the photodegraded samples. In addition to the PA spectrum, optical absorption spectra of the samples are also recorded using a spectrophotometer (Milton Roy, Genesys 5).

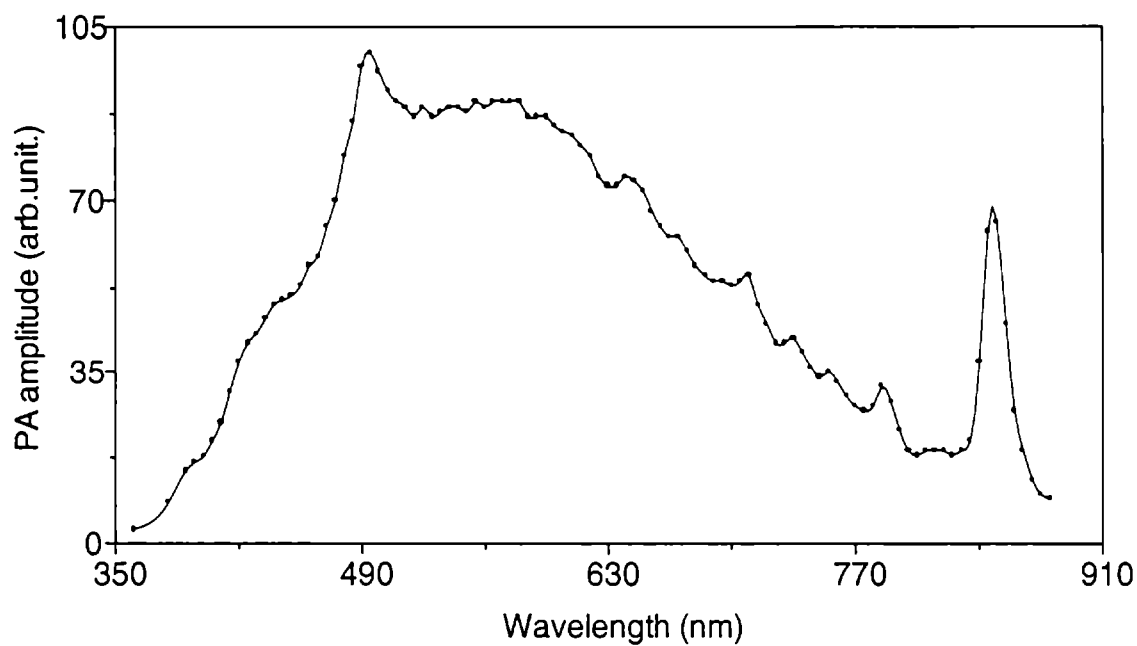


Figure 3. The emission spectrum of Xe arc recorded using PA method

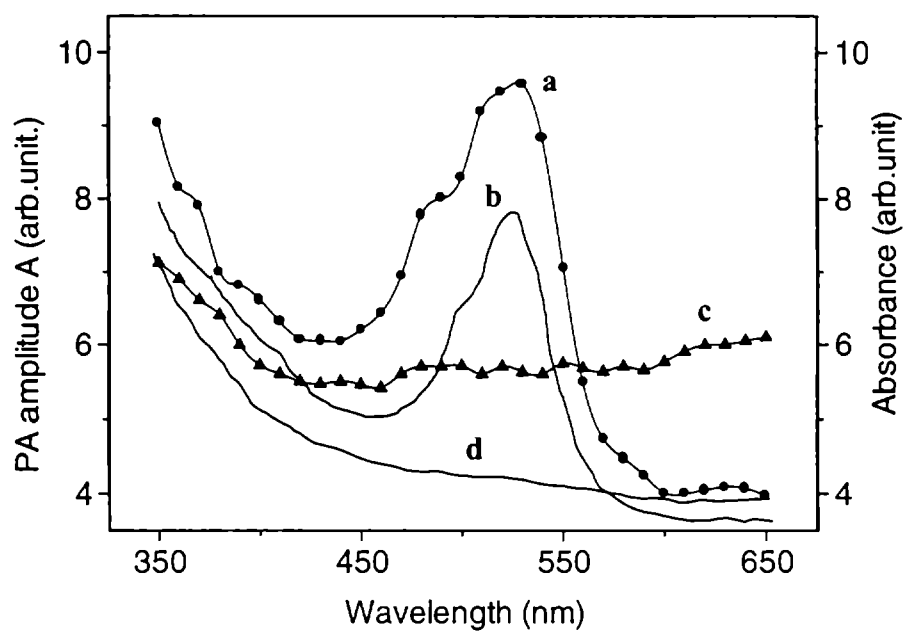


Figure 4. PA spectra and optical absorption spectra of rhodamine 6G samples before and after bleaching (dye concentration: 1×10^{-3} mol/l). (a,c) PA spectrum before and after bleaching, (b,d) optical absorption spectrum before and after bleaching.

6.3.3 Experimental setup used to study the dye photodegradation

A continuous wave (cw) laser induced photoacoustic technique is employed to investigate the photo-induced degradation of the laser dye rhodamine 6G doped in PMMA. The experimental setup used for the present investigation is schematically shown in figure 5. The excitation source used is a highly stabilised argon ion laser (Liconix 5000) and its different emission lines are used for the study. The cw laser emission is intensity modulated using a mechanical chopper (Ithaco HMS 230). The modulated light beam at specific power levels is then allowed to fall on the sample kept in a home-built non-resonant PA cell. The details of the cell are given in the next paragraph. A highly sensitive electret microphone (Knowles BT 1834) is used to detect the PA signal. Finally, the PA signal is processed using a single phase, analog lock-in-amplifier (Stanford Research Systems SR 510). Laser lines at 476nm, 488nm, 506nm and 514.5nm wavelengths are used for the investigations. Influence of the excitation light intensity on the rate of dye photodegradation is studied at 50mW, 100mw, 150mW, 200mW and 250mW. Other parameters that are varied are the dye concentration and the laser modulation frequency.

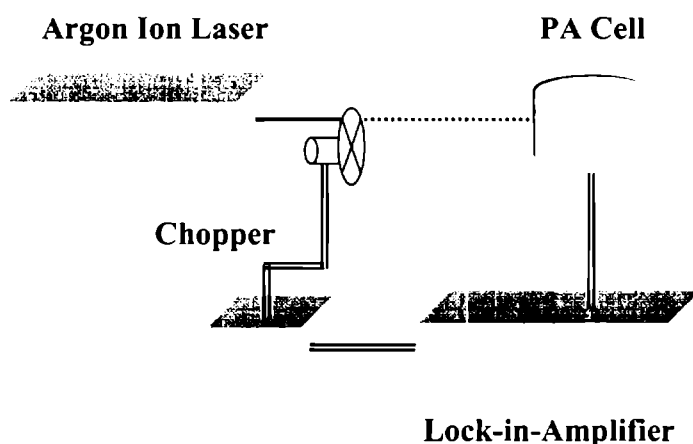


Figure 5. Schematic diagram of the photoacoustic set-up for the photostability studies

The photoacoustic cell used for the present investigation is made of a heavy stainless steel block which effectively protects the PA signal from the ambient noises. The cross-sectional view of the cell is shown in figure 6. The cell is designed in such a way that it can be used either in the front illumination configuration or in the rear side illumination configuration. W_1 and W_2 are two glass windows and M is the microphone. The sample chamber is 5mm long and 4mm in

diameter. The microphone is kept 3mm away from the sample chamber and is coupled to the sample compartment through a bore of 3mm diameter. For the photostability studies, thin disk like sample is kept in the space between the window (W_2) and the PA cavity. Laser irradiation is made through the other window W_1 (front illumination).

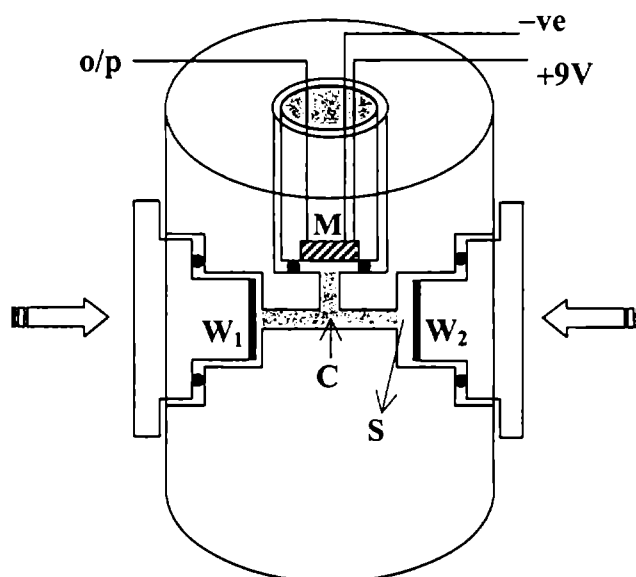


Figure 6. Cross-sectional view of the photoacoustic cell. W_1 and W_2 are the glass windows, M is the microphone, C is the PA cavity and S is the position to keep the sample.

6.4 Results and discussion

In *chapter 2* we have discussed the Rosencwaig-Gersho theory (R-G theory) which gives a satisfactory explanation to the generation of photoacoustic effect in condensed media. The dye doped PMMA samples are optically transparent and thermally thick, as the thermal diffusion length in PMMA is only a few tens of microns in the frequency range of investigations. Then, the complex amplitude of the PA signal produced is given by

$$Q = \frac{-i\beta\mu^2\gamma P_o I_o}{4\sqrt{2}T_o l_g a_g k} \quad (2)$$

where β is the optical absorption coefficient of the sample and μ is the thermal diffusion length in the solid material; γ is the ratio of specific heat capacities of air; P_o and T_o are the ambient pressure and temperature, respectively; I_o is the incident light intensity; l_g and a_g are the length of the gas column inside the cavity and the thermal diffusion length in the gas, respectively and k is the thermal conductivity of the sample. Hence, by any means, if the β value changes, then the PA signal amplitude will also vary accordingly. Any kind of photochemical reaction will

result in a change in the number density or concentration of the original species and this, in turn, will result in a change in the optical absorption properties of the sample. Equation (2) is not only valid for optically transparent samples but also for opaque samples, provided the sample is thermally thick. Moreover, doping of an organic dye in a solid matrix will not alter the thermal properties of the host. Therefore, in the present case photodecomposition of the dye (and hence a change in its concentration) will not alter the thermal parameters of the host material. The above discussed facts clearly indicate that when a dye doped PMMA sample is investigated using PA method, any change in the PA signal amplitude is essentially a measure of the rate of photodecomposition of the dye.

Before going to the details of the experimental results, let us discuss the reasons for choosing ethyl alcohol as an additive to the monomer (and hence the polymer). One of the major reasons is that it combines good solubility for xanthene dyes and enhancement of the host laser-damage resistance [17,18]. Another reason, from the point of view of the use of dye doped PMMA as an active laser medium, is that polymerisation causes a decrease in the dielectric constant ($\epsilon_{\text{MMA}} \cong 4$ and $\epsilon_{\text{PMMA}} \cong 2.9$). This results in a shift of equilibrium between the dye monomer molecules and their aggregates towards the latter and consequently, the conversion efficiency decreases. Introduction of ethyl alcohol into MMA and PMMA causes ϵ to increase and results in a reduction of the interaction between the cation and the anion in a dye ionic pair. This leads to expansion of the tight ionic pairs and shifts the equilibrium between the monomer and the dimer configurations toward the former; thereby increasing the quantum yield and the conversion efficiency of rhodamine 6G chloride [17]. This increase in quantum yield and the conversion efficiency on going from tight ionic pair to the expanded one is due to a decrease in the luminescence quenching of the dye-cation excited state that is associated with electron transfer from the anion to the cation.

The effect of laser power on photobleaching rate of the dye molecules is investigated at different pump powers ranging from 50mW to 250mW. The variation of PA signal amplitude as a function of time for different pump powers is shown in figure 7. From this plot it is clear that the PA signal amplitude decreases quickly during the initial stage followed by a saturation. This obviously corresponds to a decrease in the absorption coefficient of the sample at 488nm. The saturation in the PA signal corresponds to the complete photodegradation of the dye molecules from their original state. The PA spectrum as well as the optical absorption spectrum of the sample shown in figure 4 also confirms this observation.

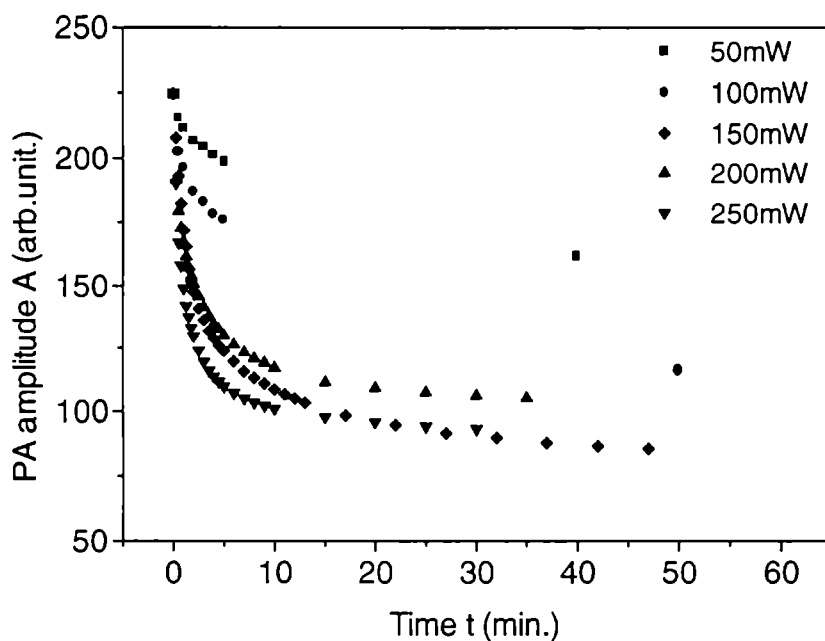


Figure 7. PA signal amplitude versus time plot for rhodamine 6G doped PMMA at different incident laser intensities ($\lambda = 488\text{nm}$, dye concentration $1 \times 10^{-3} \text{ mol/l}$).

From the spectra it is clear that the long-wavelength absorption band of rhodamine 6G in PMMA matrix falls in the blue-green region with the peak at 530nm. However, the photodecomposition of the dye completely wipes out this long-wavelength band. This indicates that on irradiating the dye doped PMMA sample with strong laser beam, photodegradation of the dye molecules takes place and the resultant product does not absorb in the spectral region where the original dye molecules absorb. Therefore the observed decrease in PA signal amplitude is purely due to the gradual photodecomposition of the dye molecules. The finite value of the PA signal even after complete degradation of the dye molecules is the contribution of the solid PMMA matrix. The bleaching of the dye molecules causes a colour change of the sample from yellowish-orange to a colourless one. It is also clear from figure 6 that as the pump power increases the plot becomes steeper or the dye degradation takes place at a faster rate. This is more clearly displayed in a logarithmic plot connecting PA signal and time as given in figure 8.

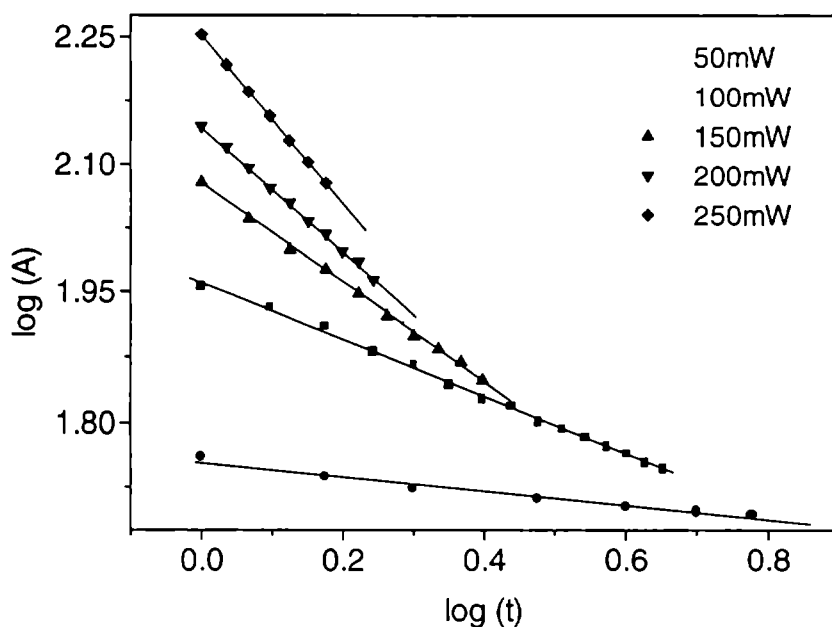


Figure 8. Log-Log plot connecting the PA signal amplitude and time for different pump powers ($\lambda = 488\text{nm}$).

The slope of the plot, which gives the rate of bleaching, is found to monotonically increase with the increase in laser power. Figure 9 shows the plot connecting the rate of bleaching (in arbitrary units) and pump power. This observation is in accordance with many of the earlier reported studies on photodegradation of dyes in solutions and in polymer matrices [18]. This plot indicates that the photobleaching rate varies linearly with the pump power within the range studied. The plot also indicates that there exists a threshold power level below which there is no appreciable degradation of the dye molecules for a reasonable time duration.

The variation of photobleaching with concentration of the dye molecules is studied at three different concentration values namely $1 \times 10^{-3} \text{ mol/l}$, $5 \times 10^{-4} \text{ mol/l}$ and $1 \times 10^{-4} \text{ mol/l}$. In all these measurements the laser power is kept fixed at 100mW and the wavelength used is 488nm. The observed PA signal variation with time for these dye concentration values is shown in figure 10. From this figure it can be seen that there is a considerable increase in the photobleaching rate with decrease in dye concentration. This observation is in good agreement with the earlier reported results based on the lasing studies on rhodamine 6G doped PMMA [17]. The rate of bleaching at a concentration of $1 \times 10^{-4} \text{ mol/l}$ is found to be 2.61 times greater than that at a concentration of $1 \times 10^{-3} \text{ mol/l}$ and for a concentration of $5 \times 10^{-4} \text{ mol/l}$, it is 1.77 times greater than that at a concentration of $1 \times 10^{-3} \text{ mol/l}$. Also, the photobleaching of

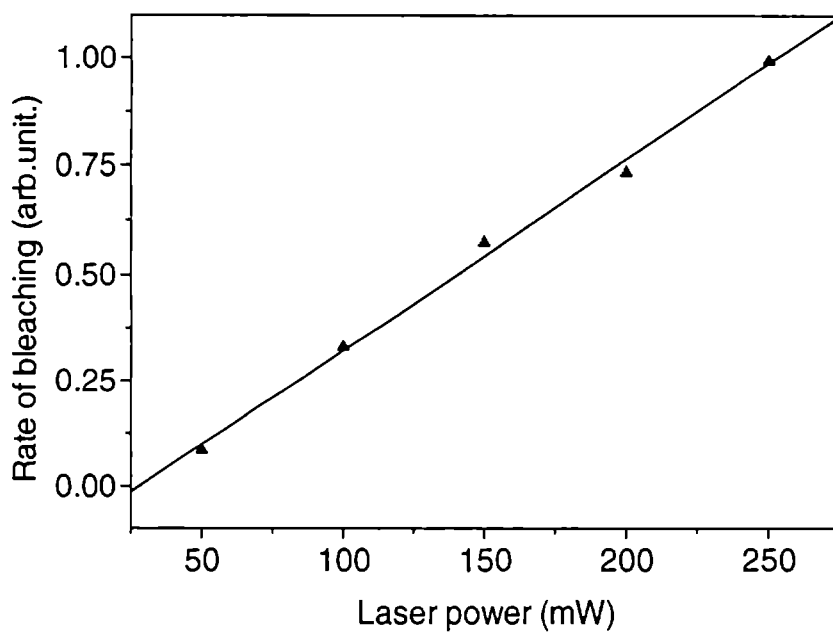


Figure 9. Variation of the rate of bleaching of rhodamine 6G doped PMMA with incident laser power ($\lambda = 488\text{nm}$, dye concentration $1 \times 10^{-3} \text{ mol/l}$).

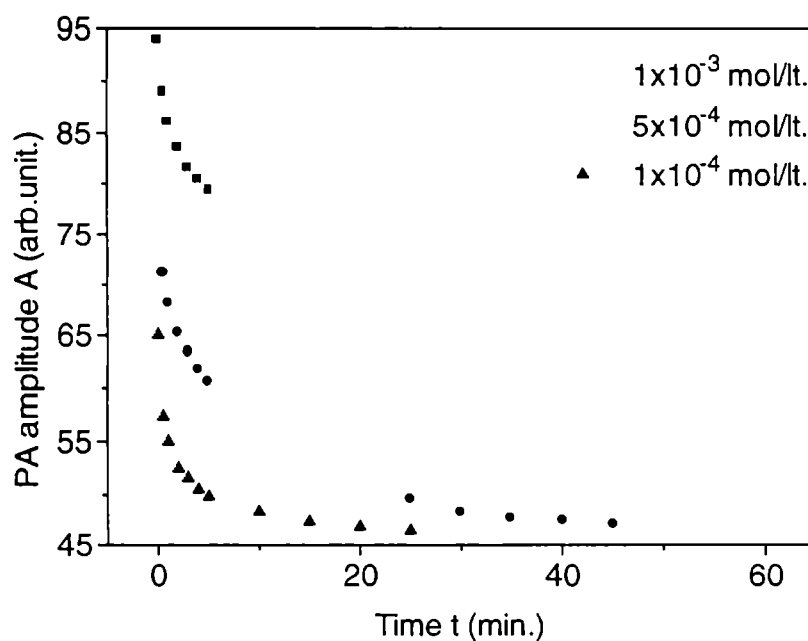


Figure 10. PA signal versus time plot for three different dye concentrations ($\lambda = 514.5\text{nm}$, laser power 100mW).

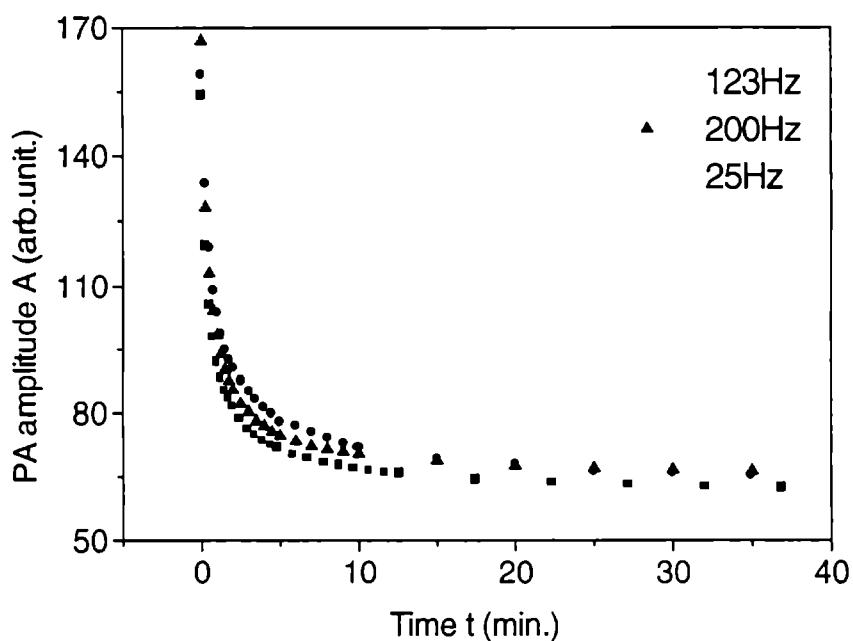


Figure 11. PA signal versus time plot for three different modulation frequencies ($\lambda = 488\text{nm}$, laser power 200mW).

rhodamine 6G in PMMA is observed to be an irreversible process. The PMMA matrix is found to be very stable and it can neatly withstand an intensity modulated laser radiation at a power level of 250mW. Also, the unbleached sample does not show any noticeable degradation even after its storage for two months at room temperature.

Another possible parameter that may influence the rate of photodegradation is the excitation pulse duration or the modulation frequency. The effect of modulation frequency on photobleaching rate of the dye is investigated at three distinct frequencies namely, 25Hz, 123 Hz and 200Hz. The PA signal variations at these chopping frequencies are given in figure 11. It can be seen from this figure that within the range selected, the chopping frequency does not have any noticeable dependence on the photobleaching rate of the dye molecules. This implies that the photodestruction of rhodamine 6G in PMMA matrix depends only on the total incident energy per unit time on the sample, which is same for all the chopping frequencies. However, for certain other dyes doped in certain other polymers, a dependence of chopping frequency on photobleaching has been noticed earlier [72].

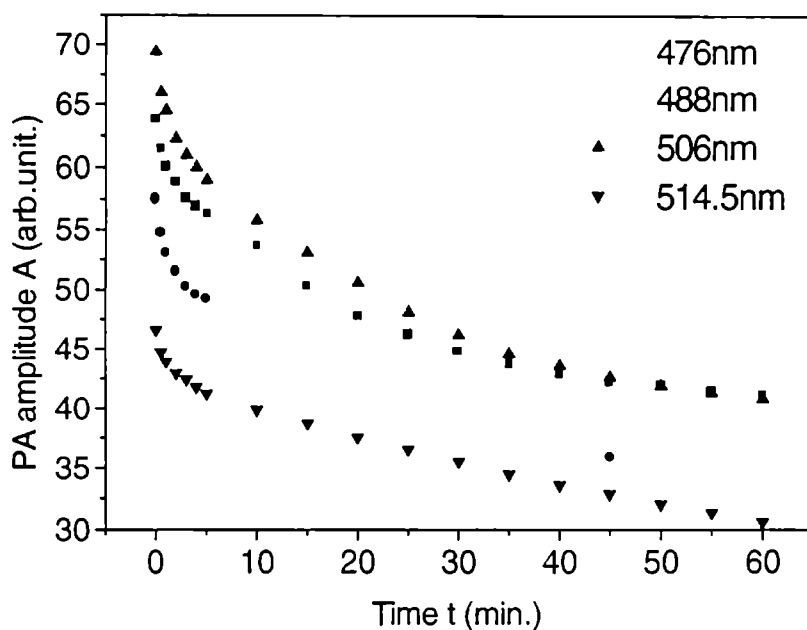


Figure 12. PA signal versus time plot for different wavelengths (laser power used is 50mW, concentration of the dye is 1×10^{-3} mol/l). Plots corresponding to different wavelengths are shifted from each other for the sake of clarity.

Generally, laser dyes have two broad absorption bands, one in the short-wavelength region (usually in UV) and the other in the long-wavelength region [8,9]. Even in a particular band, one can use different wavelengths for pumping a dye laser. In the case of rhodamine 6G, different emission lines of an argon ion laser come under the long-wavelength absorption band of the dye. In order to investigate whether these distinct lines have any influence on the photodegradation rate of the dye, four different wavelengths namely 476nm, 488nm, 506nm and 514nm are employed. The laser power is kept constant at 50mW for all the wavelengths. The time evolution of the PA signal amplitude for different excitation wavelengths are shown in figure 12. From this plot it is clear that the selected wavelengths have no significant influence on the photobleaching rate of the dye.

Even though a large number of studies have been reported in the field of dye doped polymers, the exact mechanism responsible for photodegradation of laser dyes in polymers is not yet fully brought out. There exist a large number of channels for the photochemical reaction processes. The reaction will take place only when the molecules are in the excited state. Most of the analyses available in the literature are based on the pulsed laser excitation. Under such high energy ($> 10^7$ W/cm²) excitation, multi-photon absorption process is possible and the dye

photodecomposition mechanism becomes very complex as the reaction may happen from any of the excited states. In a recent paper published by Ferrer *et.al*, it is pointed out that the dyes undergo a thermal degradation due to the poor thermal conductivity of the polymer matrix [32]. However, this explanation does not seem to be reasonable as temperatures as high as 80 °C are used for the polymerisation of the dye doped samples. Also, considering the very high fluorescence quantum yield of laser dyes such as rhodamine 6G, the thermal energy liberated will be very small. However, a more reasonable and genuine explanation is given by Dyumaev *et.al*. They have recently reported that the excitation of the dye molecules can give rise to electron energy transfer from the dye molecules to the polymer macromolecules. Subsequently vibrational relaxation of the first excited state of the polymer macromolecules results in the formation of radicals by a mechanism similar to that for UV or γ irradiation of polymers[18]. These radicals interact efficiently with the dye molecules in any of the excited state, resulting in their destruction. If this is the major mechanism responsible for the photobleaching of the dye, then the addition of a low molecular weight additive such as ethyl alcohol may improve the photostability of the dye to some extent. The addition of a low molecular weight additive may significantly improve the dye photoresistance through resonance vibrational cross relaxation, which hampers the formation of macroradicals.

It is a clearly established fact that at relatively low radiation intensities ($< 10^6$ W/cm²) the dye destruction occurs from the first excited (singlet or triplet) electronic states and the photobleaching rate is linearly dependent on the radiation intensity [18]. The laser intensities used for the present investigations falls in this range and hence the dye destruction takes place while the system is either in the first excited singlet-state or lowest triplet state. Also, a linear dependence of dye degradation rate on the incident intensity is observed as reported earlier. It is expected that in the present case the dye degradation is due to the excited state reactions with the polymer macromolecules or with the free radicals formed in the matrix during polymerisation.

6.5 Conclusions

The photoacoustic technique has been implemented successfully to investigate the bleaching of organic dye molecules embedded in PMMA matrix. Based on the experimental observations using the PA technique, the following conclusions have been made. In the case of Rh 6G doped in the solid matrix PMMA, the rate of photobleaching is directly proportional to the incident laser power and it decreases with increase in concentration of the dye molecules. Moreover, it is found that the photobleaching rate of the dye is insensitive to modulation

frequency when the dye is irradiated with an intensity modulated cw laser. This means that the time scale of photo-induced reaction is shorter than milliseconds, as the investigated time scales are in the millisecond regime. Hence in the present case the rate of photodegradation depends only on the total energy incident on the sample. Also, no noticeable change in the bleaching rate is observed for the four different irradiation wavelengths used.

It is obvious that an increase in dye concentration increases the optical density of the sample. The present observation indicates that by increasing the optical density of the sample one can decrease the photobleaching rate. Therefore, if we use a dye-doped polymeric material as a laser active element, the lifetime for stable operation can be increased by increasing the dye concentration. However, in this case care should be taken to ensure that the selected concentration values do not bring them to the range of fluorescence quenching. Alternatively, if one uses such a material as a medium for optical data storage, then by decreasing the dye concentration one can decrease the time for recording.

References

1. Sorokin.P.P and Lankard.J.R, *IBM J.Res.Develop.* **10**, 162 (1966)
2. Schafer.F.P, Schmidt.W and Volze.J, *Appl.Phys.Lett.* **9**, 309 (1966)
3. Shank.C.V, *Rev.Mod.Phys.* **47**, 649 (1975)
4. Hansch.T.W Shahin.I.S and Schawlow.A.L, *Nature*, **235**, 63 (1972)
5. Penzkofer.A and Falkenstein.W, *Opt.Quant.Electron.* **10**, 399 (1978)
6. Sperber.P, Spangler.W, Meier.B and Penzkofer.A, *Opt.Quant.Electron.* **20**, 395 (1988)
7. Duarte.F.J and Hillman.L.W, *Dye laser principles*, (Academic Press, New York) (1990)
8. Maeda.M, *Laser dyes*, (Academic Press, New York) (1984)
9. Schafer.F.P (Edit.), *Dye lasers*, (Springer, Berlin) (1977)
10. Kneubuchl.Sigrist.M.W, *Laser* (Stuttgart, Teubner) (1995)
11. Soffer.B.H and McFarland.B.B, *Appl.Phys.Lett.* **10**, 266 (1967)
12. Peterson.O.G and Snavely.B.B, *Appl.Phys.Lett.* **12**, 238 (1968)
13. Kranzelbinder.G and Leising.G, *Rep.Prog.Phys.* **63**, 729 (2000)
14. Rodriguez.M, Costela.A, Moreno.I.G, Florido.F, Figuera.J.M and Sastre.R, *Meas.Sci.Technol.* **6**, 971 (1995)
15. Arbeloa.E.L, Arbeloa.T.L, Arbeloa.L, Costela.A, Moreno.I.G, Figuera.J.M, Guerri.F.A and Sastre.R, *Appl.Phys.B: Las.Opt.* **64**, 651 (1997)
16. Sastre.R and Costela.A, *Adv.Mater.* **7**, 198 (1995)
17. Gromov.D.A, Dyumaev.K.M, Manenkov.A.A, Maslyukov.A.P, Matyushin.G.A, Nechitailo.V.S and Prokhorov.A.M, *J.Opt.Soc.Am.B.* **2**, 1028 (1985)
18. Dyumaev.K.M, Manenkov.A.A, Maslyukov.A.P, Matyushin.G.A, Nechitailo.V.S and Prokhorov.A.M, *J.Opt.Soc.Am.B.* **9**, 143 (1992)
19. Costela.A, Moreno.I.G, Barroso.J and Sastre.R, *J.Appl.Phys.* **83**, 650 (1998)
20. Costela.A, Florido.F, Moreno.I.G, Duchowicz.R, Guerri.F.A, Figuera.J.M and Sastre.R, *Appl.Phys.B: Las.Opt.* **60**, 383 (1995)
21. Duarte.F.J, Costela.A and Moreno.I.G, Sastre.R, Ehrlich.J.J and Taylor.S, *Opt.Quant.Electron.* **29**, 461 (1997)
22. Costela.A, Moreno.I.G, Figuera.J.M, Guerri.F.A, Barroso.J and Sastre.R, *Opt.Comm.* **130**, 44 (1996)
23. Costela.A, Moreno.I.G, Tian.H, Su.J, Chen.K, Guerri.F.A, Carrascoso.M, Barroso.J and Sastre.R, *Chem.Phys.Lett.* **277**, 392 (1997)
24. Costela.A, Moreno.I.G, Barroso.J and Sastre.R, *Appl.Phys.B: Las.Opt.* **607**, 167 (1998)

25. Balachandran.R.M, Pacheco.D.P and Lawandy.N.M, *Appl.Opt.* **35**, 640 (1996)
26. Raju.R.R and Varadarajan.T.S, *Appl.Phys.B: Las.Opt.* **59**, 83 (1994)
27. Maslyukov.A, Sokolov.S, Kaivola.M, Nyholam.K and Popov.S, *Appl.Opt.* **34**, 1516 (1995)
28. Salin.F, Le Saux.G, Georges.P, Brum.A, Bagnall.C and Zarzycki.J, *Opt.Lett.* **14**, 785 (1989)
29. Knobbe.E.T, Dunn.B, Fuqua.P.D and Nishida.F, *Appl.Opt.* **29**, 27279 (1990)
30. Costela.A, Moreno.I.G, Figuera.J.M, Guerri.F.A, Mallavia.R, Maria.m.D.S and Sastre.R, *J.Appl.Phys.* **80**, 3167 (1996)
31. Guerri.F.A, Costela.A, Figuera.J.M, Florido.F and Sastre.R, *Chem.Phys.Lett.* **269**, 352 (1993)
32. Ferrer.M.L, Acuna.A.U, Guerri.F.A, Costela.A, Figuera.J.M, Florido.F and Sastre.R, *Appl.Opt.* **33**, 2266 (1994)
33. Rahn.M.D, King.T.A, Gorman.A.A and Hamblett.I, *Appl.Opt.* **36**, 5862 (1997)
34. Calderon.O.G, Guerra.J.M, Costela.A, Moreno.I.G and Sastre.R, *Appl.Phys.Lett.* **70**, 25 (1997)
35. He.G.S, Bhawalkar.D, Zhao.C and Prasad.P.N, *IEEE J.Quant.Electron.* **32**, 749 (1996)
36. Chandra.S, Allik.T.H, Hutchinson.J.A, Fox.J and Swim.C, *Opt.Lett.* **15**, 209 (1997)
37. Hu.L and Jiang.Z, *Opt.Comm.* **148**, 275 (1998)
38. Canva.M, Georges.P, Perelgritz.J.F, Brum.A, Chapuo.F and Boilot.J.P, *Appl.Opt.* **34**,428 (1995)
39. Ammer.F, Penzkofer.A and Weidner.P, *Chem.Phys.* **192**, 325 (1995)
40. Weidner.P and Penzkofer.A, *Chem.Phys.* **191**, 303 (1995)
41. Lo.D, Parris.J.E and Lawless.J.L, *Appl.Phys.B*, **56**, 385 (1993)
42. Hermes.R.E, Allik.T.H, Chandra.S and Hutchinson.J.A, *Appl.Phys.Lett.* **63**, 877 (1993)
43. Costela.A, Moreno.I.G, Figuera.J.M, Guerri.F.A and Sastre.R, *Laser.Chem.* **18**, 63 (1998)
44. Franke.H, *Appl.Opt.* **23**, 2729 (1984)
45. Nakanishi.M, Sugihara.O, Okamoto.N and Hirota.K, *Appl.Opt.* **37**, 1068 (1998)
46. Kaminow.I.P, Stulz.L.W, Chandross.E.A and Pryde.C.A, *Appl.Opt.* **11**, 1563 (1972)
47. Kinoshita.K, Horie.K, Morino.S and Nishikubo.T, *Appl.Phys.Lett.* **70**, 2940 (1997)
48. Okabe.H, *Appl.Opt.* **20**, 4054 (1981)
49. Capolla.N and Lessard.R, *Appl.Opt.* **30**, 1196 (1991)
50. Newell.J.C, Solymar.L and Ward.A.A, *Appl.Opt.* **24**, 4460 (1985)
51. Filho.A.T, Leite.N.F, Miranda.L.C.M and Stempniak.R.A, *J.Appl.Phys.* **66**, 407 (1989)

52. Kliger.D.S (Edit.), *Ultrasensitive laser spectroscopy*, (Academic Press, New York) (1983)
53. Mukherjee.K.K.R, *Fundamentals of photochemistry*, (New Age International Publishers, New Delhi) (1978)
54. Winefordner.J.D (Edit.), *Chemical analysis: A series of monographs on analytical chemistry and its applications*, (John Wiley & Sons, Inc.) (1996)
55. Hieftje.G.M, Travis.J.C and Lytle.F.E (Eds.), *Lasers in chemical analysis*, (Humana: Clifton, New Jersey) (1981)
56. West.W (Edit.), *Chemical applications of spectroscopy*, Vol. IX, Part I (John Wiley & Sons, New York) (1968)
57. Bindhu.C.V, *Studies on laser induced photothermal phenomena in selected organic compounds and fullerenes*, (Ph.D. thesis, Cochin University of Science and Technology) (1998)
58. Shen.Y.R, *The principles of nonlinear optics*, (John Wiley, New York) (1984)
59. Boyd.R.W, *Nonlinear optics*, (Academic Press, New York) (1992)
60. Hess.P (Edit.), *Photoacoustic, photothermal and photochemical processes in Gases*, (Springer-Verlag, Berlin) (1989)
61. Hess.P and Pelzl.J (Eds.), *Photoacoustic and photothermal phenomena*, (Springer-Verlag, Berlin) (1988)
62. Winefordner.J.D (Edit.), *Chemical analysis: A series of monographs on analytical chemistry and its applications*, (John Wiley & Sons, Inc.) (1996)
63. Sell.J.A, *Photothermal investigations of solids and fluids*, (Academic Press, Boston) (1989)
64. Okamoto.K, Hirota.N, Terazima.M, *J.Chem.Soc.Farad.Trans.* **94**, 185 (1998)
65. Simon.J.D and Peters.K.S, *J.Am.Chem.Soc.* **105**, 5156 (1983)
66. Okamoto.K, Hirota.N, Terazima.M, *J.Phys.Chem.A*, **102**, 3447 (1998)
67. Yamaguchi.S, Hirota.N and Terazima.M, *Chem.Phys.Lett.* **286** 284 (1998)
68. Ooe.H, Kimura.Y, Terazima.M and Hirota.N, *J.Phys.ChemA*, **103**, 7730 (1999)
69. Neckers.D, Volman.D.H and Bunau.G (Eds.), *Advances in photochemistry*, (John Wiley, New York) (1998)
70. Terazima.M, *J.Phys.Chem.A*, **103**, 7401 (1999)
71. Okazaki.T, Hirota.N and Terazima.M, *J.Chem.Phys.* **110**, 11399 (1999)
72. Philip.A, Radhakrishnan.P, Nampoori.V.P.N and Vallabhan.C.P.G, *Int.J.Optoelect.* **8**, 501 (1993)

Summary and conclusions

A detailed account of the investigations carried out by the author on certain selected photonic materials of current importance, such as III-V semiconductors, liquid crystals and dye doped polymers are given in this thesis. Photoacoustic and photothermal deflection effects arising as a result of modulated continuous-wave laser excitation is made use of in these studies. A variety of measurements included in this monograph points out the versatility as well as the potential of photothermal based techniques in material characterization.

The origin of photothermal effects is based on nonradiative transitions which transform a part of the absorbed radiation energy into thermal energy of the medium. Consequently, the optical absorption properties and static and dynamic thermal properties of the sample play a vital role in the photothermal signal generation. Since both photoacoustic and photothermal deflection techniques are based on the thermal wave propagation through the sample, these methods can be effectively utilized for the evaluation of thermal transport properties such as thermal diffusivity of materials.

In recent years, interest in research on electronic and photonic properties of semiconductor materials, especially compound semiconductors, has captured special attention of the research community across the whole world. In semiconductor materials, in addition to the electronic and phononic contribution to the heat conduction, free carrier recombination is a major contributing factor. Photoacoustic signal phase measurement is an excellent approach for the evaluation of thermal diffusivity and identification of heat transport mechanism in semiconductor materials. The thermal diffusivity of a moderately doped n-type indium phosphide evaluated by photoacoustic measurements is found to be less than that of an undoped sample. This leads to the conclusion that free carrier recombinations, either bulk or surface, do not contribute to the heat diffusion and the subsequent photoacoustic signal generation. Studies with samples of different surface polishness also confirm this aspect, since the surface quality of semiconductor materials has a pronounced effect on the carrier recombination at the surface. Further analysis of the photoacoustic phase data obtained from an open photoacoustic cell measurement suggests that thermoelastic bending is absent in this sample. In photothermal based measurements the thermoelastic bending is usually observed in optically opaque and thin

disc-like solid materials, resulting from the temperature gradient existing along the thickness of the sample. But, moderately high value of thermal diffusivity of indium phosphide results in the distribution of thermal energy in a rather enhanced rate, which reduces the temperature gradient existing along the thickness and hence there is no bending of the sample.

The photothermal deflection technique has certain advantages over photoacoustic technique, especially in the study of thin film samples coated on bulk substrates. When a solid sample is irradiated with a focused laser beam, thermal waves generated from this point source will propagate in all directions, the characteristics of which are determined by the thermal properties of the sample. The profile of refractive index gradient generated in a coupling fluid in contact with the heated surface of the solid sample is ultimately decided by these thermal waves. A probe-beam propagating through this gradient gets deflected. The phase of the deflection signal as a function of the distance between the point source and the probe-beam holds a linear relationship and the slope of the plot determines the thermal diffusivity of the solid sample. The thermal diffusivity of n-type and p-type GaAs thin films of few hundred microns thick is measured using this approach and the results show a decrease in the thermal diffusivity values compared to bulk samples. The thermal wave scattering as well as reflection at the boundaries may have some influence in this observation.

The fact that photoacoustic technique can be performed over a wide range of temperature is an added advantage of this method in material characterisation. Consequently, this approach has a special importance in the study of liquid crystals, different phases of which are lying in different temperature ranges. Being long rod-shaped molecules oriented in different directions in different phases, each mesophase of liquid crystals show totally different thermal, optical and physical properties. Thermal diffusivity values in different phases of a variety of liquid crystalline materials reported in this thesis clearly show the variation of thermal properties in different phases. From the diffusivity values of 7OCB and 8OCB measured using an open photoacoustic cell, it is concluded that thermal diffusivity increases with increase in molecular chain length. This observation, in fact, is in agreement with the previously reported thermal conductivity studies on identical liquid crystals. Measurements carried out in the isotropic phase of different side chain liquid crystalline polymers leads to the conclusion that, not only the main chain but the side chains also have a significant role in determining the thermal transport properties of these materials. Results obtained from the investigations of nematic liquid crystal mixtures are also very promising. Even though the structure and composition of liquid crystal mixtures are unknown, the thermal diffusivity measurements can be made use in the identification of materials which possess almost similar thermal properties.

Another use of photoacoustic technique in the study of liquid crystalline materials is for the investigation of transition between different phases. From the thermodynamical point of view, these transitions will be associated with a drastic change in the static and dynamic thermal parameters of the sample. Since the photoacoustic signal strength is determined by the thermal properties of the sample, any change in these parameters will be reflected in the signal. From the phase transition studies included in this thesis, it can be seen that the photoacoustic technique can be easily employed for the precise determination of transition temperatures in liquid crystals. A simple analysis of the signal amplitude data using the R-G theory leads to a qualitative evaluation of the specific heat capacity profile during first order or second order phase transitions. Difference in bulk light scattering properties in the liquid crystalline and isotropic phases of liquid crystal materials are also visible in the photoacoustic signal.

Various difficulties in the handling of complex and bulky structured conventional liquid phase dye lasers pointed out the need for a compact design, which finally resulted in the development of dye doped solid matrices. However, right from the beginning to this date, photodecomposition of organic dyes in solid matrices has been a subject of detailed investigations. In most of the previously reported measurements, pulsed laser excitation is used and the photostability studies are performed by making use of the radiative emission. Continuous wave photoacoustic study of photobleaching of rhodamine 6G doped poly methyl methacrylate samples show that the photobleaching rate is directly proportional to the incident laser intensity. Also, it is observed that there is decrease in photobleaching rate with increase in dye concentration. These observations are in perfect accordance with the earlier reported radiative emission studies. Since the pump laser beam is modulated in the millisecond time scales, the observation of identical photobleaching behaviour at different modulation frequencies implies that the pulse duration has negligible influence on the photochemical reaction rate. A well-defined and strong photoacoustic signal profile obtained from such a highly fluorescing sample shows the high sensitivity of photoacoustic technique.

In general, the author believes that the application of photoacoustic and photothermal deflection techniques in the characterisation of certain photonic materials such as semiconductors, liquid crystals and dye-doped polymers are highlighted in this thesis. The potentialities of photothermal effects are not yet fully exploited and hence the scope of its numerous applications in different fields of science and technology can be widened.

